Phase transitions on complex networks

Mariana Krasnytska

Collegium Sciences et Techniques
École Doctorale Energie Mécanique
et Matériaux (EMMA)

Institute for Condensed Matter Physics
of the National Academy of
Sciences of Ukraine

Thèse présentée pour l'obtention du titre de
Docteur de l'Université de Lorraine
en Physique
par **Mariana KRASNYTSKA**

Transitions de phase dans les réseaux complexes
Phase transitions on complex networks

Membres du jury:

Rapporteurs:	Victor Dotsenko	Professeur, LPTMC, Université Paris VI
	Volodymyr Tkachuk	Professeur, Ivan Franko National University of Lviv
Examinateurs:	Thierry Platini	Doctor, AMRC, Coventry University
Co-directeurs:	Bertrand Berche	Professeur, Université de Lorraine
	Yurij Holovatch	Professeur, Institute for Condensed Matter Physics NASU

Institut Jean Lamour - Groupe de Physique Statistique
Faculté des Sciences & Technologies - 54500 Vandœuvre-l'es-Nancy

Phase Transitions on complex networks

by

Krasnytska Mariana

A thesis submitted for the award of
Doctor of Philosophy

Institute for Condensed Matter Physics of the
National Academy of Sciences of Ukraine

Institut Jean Lamour - Groupe de Physique Statistique

Faculté des Sciences & Technologies - 54500 Vandœuvre-l'es-Nancy

September 7, 2016

To my FAMILY

Ab imo pectore

I would like to express my special gratitude to two of my mother research institutions, the Institute for Condensed Matter Physics of the National Academy of Sciences of Ukraine and the Groupe de Physique Statistique, Institut Jean Lamour, Université de Lorraine (Nancy, France).

This work would have been impossible without constant help and support from my supervisors. That is why I would like to give my special thanks to Yurij Holovatch and Bertrand Berche. They helped me not only in learning, allowing to complete thesis, but provided an opportunity to study in an international graduate school. Their capture of unsolved problems and positive research spirit gave me a strong desire and effort in learning.

I am grateful for the support from the international graduate college " Doctoral College for the Statistical Physics of Complex Systems" Leipzig-Lorraine-Lviv-Coventry ($\mathbb{L}^4$), École Doctorale (EMMA) and projects FP7 EU IRSES, as well as people who have committed themselves to the existence of such cooperation, including my supervisors.

I would also like to thank the scientific groups, whose guest I was, and the people that helped me to adjust to the new environment.

I thank my friends and colleagues, for interesting discussions (scientific and not only), and for working days being filled with positive emotions.

I would especially like to thank my family that supported me in a distance. They added me faith and strength to cope with difficulties and inspired with confidence.

I am sincerely grateful to all who helped and contributed interest in my work.

Thank YOU!

Contents

Introduction

The whole is greater than the sum of its parts.

(Aristotle)

Contents

The complex network science became the subject of an intensive analysis during the last decades of XXth century. The complex network as set of nodes and links is nothing else than a random graph. The graph theory originates from the famous work of Leonard Euler on a solution of the seven bridges problem [1] and is one of the parts of a discrete mathematics [2]. It was shown that a large number of natural and man-made systems are much better described by the topology of networks than lattices. Among them are the food web networks, ecological systems, internet, www, transport systems, social networks, networks of citations and so on (se e.g. [3–7]). Furthermore the properties of such networks differ from those of a classical random graph [8]. Usually they are correlated structures at small size (small-world effect [9, 10]), not sensitive to random attacks but sensitive to the directed ones [11, 12]. Their inherent features often include self-organization and governing power-laws (so called scale-free networks [13, 14]). Namely such properties are common for a large number of complex systems. Application of statistical physics methods made possible to understand the reasons of such type of behaviour.

Among different problems on complex networks the investigation of phase transitions on complex networks can be distinguished as an independent trend. Those investigations play an important role for the description of processes on networks. It is known that for the lattice structures, one of the global characteristic determining the type of phase transition is space dimensionality. Euclidean dimension is ill-defined for networks. From that fact it is possible to expect different features of phase transitions for models on networks. In particular, this will be demonstrated in the thesis.

Subject actuality

The problems on critical behaviour and phase transitions on complex networks became a subject of analysis only recently. Possible applications of models of phase transition on complex networks can be found in different branches of physics. In sociophysics the different states of social network are considered [15], when the different social states of individuals are considered as localized on the nodes of a social network. The appearance of ordered state for such systems is considered as a phase transition. Another examples is given by nanophysics, where the structure better corresponds to those of networks or fractals [16]. Moreover, recently it was observed that phase transitions on complex networks differ from those on lattices and are characterized by novel effects. Recently, the experiment allowing to measure the physical characheristics of quantum systems which correspond to the complex physical parameter of classical many-body system had been made [17]. That is why the investigation of complex partition function zeros for a spin system on scale-free networks is an important task.

Goals and tasks of the research

Spin models (Ising and Potts models) on graphs (complete graph, configurational graph model and an uncorrelated annealed scale free network) are chosen as the main *objects of the research.* An investigation of the critical behaviour for those models is *the subject of the research. The goal* consists in obtaining the thermodynamic functions, constructing the phase diagram, searching the critical exponents and other universal characteristics in the case of second order phase transitions. We use two main *methods* to investigate the critical behaviour: an inhomogeneous mean field approach and Lee-Yang-Fisher formalism for the partition function zeros in the case of complex magnetic field or complex temperature.

Scientific novelty of the research

For the q-state Potts model on a scale-free network (with a power law node degree distribution decay exponent λ) in the mean-field approach, we have obtained: the phase diagram, critical exponents, logarithmic corrections exponents. For the $q = 1$-state Potts model (percolation) it was shown, that at $\lambda = 4$ percolation on a scale-free network is enhanced by a set of logarithmic corrections to scaling. Those corrections weaken the singularities of the observables near the percolation point [18]. For the Potts model on a scale-free network in the second order regime we obtained the expressions for the scaling functions and critical amplitude ratios [19]. Investigating the heat capacity jump for the Ising model on an annealed scale-free network we found that the jump remains λ-dependent even at $\lambda > 5$ and tends to the mean-field value in the limit $\lambda \to \infty$ [20].

The Lee-Yang-Fisher formalism has been applied for the first time to phase transition analysis for a spin model on scale-free networks. The partition function zeros in complex temperature and complex magnetic field plane for the Ising model on an annealed scale-free network have been analyzed. In this way the description of critical behaviour of many-particle system on scale-free networks in terms of conformal invariant angles of zeros location has been done at the first time. The connection between these angles and scaling exponent of Lee-Yang zeros edge singularity is used. The angles of zeros location as well as critical exponents appear to be λ-dependent, which signals that the principle of universality on scale-free networks becomes wider. For the Lee-Yang zeros of the Ising model on an annealed scale-free network it was found that Lee-Yang circle theorem is violated in the region $3 < \lambda < 5$ [21, 22].

Practical value of the results

The obtained results can be used as the base of ordering processes modeling for interacting systems on complex networks. Our results can be used to describe models of opinion formation in sociophysics. Similarly, they are relevant for the analysis of phase transitions in nanosystems with network topology. Recently the experimental realization of partition function complex zeros detection has been proposed. The coordinates of purely imaginary Lee-Yang zeros of the partition function are connected with times of quantum coherence of a probe spin in spin bath [17]. Such demonstration of experimental realization of Lee-Yang zeros is important at a fundamental level and points to new ways of studying zeros in complex, many-bodied materials. Our results

could help in the study of real systems in which the zeros can't easily be calculated giving access to new quantum phenomena that would otherwise remain hidden if one were to restrict attention to real, physical parameters.

Personal contribution of the researcher

In the papers written with co-authors the contribution of the author includes:

- the expressions for the free energy for the q-state Potts model on an uncorrelated scale-free network in the mean-field approximation and their analysis [18];
- the formula of the heat capacity jump for the Ising model on an annealed scale-free network at $\lambda > 5$. The comparison of the heat capacity on lattices and networks is discussed [20];
- the exact integral representation for the partition function of the Ising model on a complete graph and on an annealed scale-free network in the case of complex external field; the numerical solutions for the Lee-Yang and Fisher zeros [21, 22];
- the values for the logarithmic corrections to scaling for the size dependence of Fisher and Lee-Yang zeros coordinates at $\lambda = 5$ [21, 22];
- the violation of Lee-Yang circle theorem for the Ising model on an annealed scale-free network in the region $3<\lambda<5$ was found. The numerical analysis and analytical description of the Lee-Yang zeros was given [21, 22].

Research connection with scientific programs, plans, themes

The thesis is prepared in the Institute for Condensed Matter Physics of the National Academy of Sciences of Ukraine (Lviv, Ukraine) and in the Groupe de Physique Statistique, Institut Jean Lamour, Université de Lorraine, Nancy 1 under support of the following projects: 0112U007763 "Development of the theoretical methods to the description of fluids, lattices and complex systems near phase transition points"; PhD program Collège Doctoral "Statistical Physics of Complex Systems" Leipzig-Lorraine-Lviv-Coventry ($\mathbb{L}^4$), grants FP7 EU IRSES 269139 (DCP-PhysBio), 295302 "Statistical Physics in Diverse Realizations", 612707 "Dynamics of and in Complex Systems", 612669 "Structure and Evolution of Complex Systems with Applications in Physics and Life Sciences", and scholarship of the French Embassy in Ukraine for short-term internships in a French university).

Thesis approbation

The results of the thesis have been reported and discussed at the following scientific meetings: "Christmas discussions -2013" (Lviv, 3th-4th January 2013); XIII Ukrainian School of young scientists in Statistical Physics and Condensed Matter theory (Lviv, 5th-7th June 2013); VI International conference "Physics of disordered systems" (Lviv, Ukraine, 14th-16th October 2013); conference of young scientists on theoretical physics 2013 (Kyiv, 24th-27th December 2013); conference "MECO-39" (Coventry, UK, 8th-10th April 2014); conference "CompPhys" (Leipzig, Germany, 27th-29th November 2014); "Christmas discussions-2015" (Lviv, Ukraine 7th-8th January 2015); XV Ukrainian School of young scientists in Statistical Physics and Condensed Matter theory (Lviv, Ukraine, 4th-5th June 2015), "Jordan discussions - 2016" (Lviv, 20th-21th January 2016), conference "MECO-41" (Vienna, Austria, 15th-17th February 2016). And also of numerous seminars: seminar at GPS, Institut Jean Lamour (Nancy, France, 20th January 13, 25th November 14); DCP-PhysBio Steering Committee Meeting (Lviv, Ukraine, 28th-30th May 2013); seminar in AMRC group in Coventry university (Coventry, UK, 12th July 2013); seminar at Computational quantum field theory group, Leipzig university of theoretical physics (Leipzig, Germany, 7th November 2013); poster presentation at annual Ècole Doctorale seminar (Nancy, France, 12th June 14); seminar of the Department of applied mathematics of Maria Sklodovska-Curie university (Lublin, Poland, 22 October 15); DIONICOS and STREVCOMS Steering Committee Meeting (Lviv, Ukraine, 17th-19th May 2016); and fifteen seminars of the Laboratory for Statistical Physics of Complex Systems (ICMP, Lviv, Ukraine).

Publications

Five papers in journals [18–22], one paper in conference proceedings [23] and nine conference abstracts [24–32] have been published on the material of the thesis.

Thesis structure

The thesis consists of four chapters of the main text (literature review and three chapters with the original results), conclusions, Appendices and the bibliography. In the 1st chapter an overview of the main literature and main definitions is given; in the next 2nd chapter the critical behaviour of the Potts model on a scale-free network in terms of the mean-field approximation is analyzed; 3d and 4th chapters contain results on the analysis of the partition function zeros for the Ising model on a complete graph

and on an annealed scale-free network correspondingly; in conclusions the main results and perspectives are presented.

Chapter 1 | LITERATURE REVIEW

Contents

In this chapter we provide an overview of the major works devoted to investigation of the critical behavior of spin models on complex networks. Firstly, (subsection 1.1) we consider the models of complex networks and introduce the main definitions that describe this quantitative characteristics. Particular attention will be paid to the so-called scale-free networks, which are characterized by a power-law node-degree distribution decay. In the next subsection 1.2 the results of the analysis of the critical behavior of many-particle-interacting systems on complex networks are given. Besides the Ising model and Potts model, we will consider the behavior of other models, percolation phenomenon being one of them. Comparing the critical behavior of these models on latices and on complex networks, we will focus on such changes in critical behavior, which lead to the small-world effects and scale-free properties. Since a major part of the thesis (chapters 3-4) is made by using the method of partition zeros analysis in a complex plane we will make a brief review of works devoted to this method in section 1.3.

1.1 Complex networks: models and observables

Recently the concept of complex network became widely used in physical studies. Networks or random graphs are sets of vertices and edges connecting them. The graph theory is a part of mathematics [33, 34] and originates in XVIIIth century [1]. However, the modern network science began to develop in 90ies of the last century, when

powerful computers appeared and it became possible to store and analyze big data sets [35–38]. At the same time the structure of numerous man-made and natural networks had been analysed. It was shown that they cannot be described in terms of regular lattices or regular graphs. Thus the basis of modern network science had been built (see, reviews [4–7]).

Random graph has the structure of a set of vertices and randomly distributed edges. For a graph with a given number of vertices N and edges the adjacency matrix is one of the characteristics. The matrix elements can take two possible values: $a_{ij} = 1$ if nodes i and j are connected, or $a_{ij} = 0$ if the link between nodes does not exist. In case of undirected networks $a_{ij} = a_{ji}$, $a_{ii} = 0$ and for a node degree k_i we obtain $k_i = \sum_j a_{ij}$.

There are a large number of other quantities to describe graphs and networks properties [5], some of then are the following:

- the mean shortest path length:

$$\langle l \rangle = \frac{2}{N(N-1)} \sum_{i>j} l(ij), \tag{1.1}$$

  where the summation is taken over connected components of the network and $l(ij)$ is a shortest path length between nodes;

- the clustering coefficient is a local node characteristic which for a given node i with a degree k_i corresponds to the ratio of number of links between nearest neighours E_i to all possible number of links between the nodes:

$$C_i = \frac{2E_i}{k_i(k_i-1)}. \tag{1.2}$$

  Using the definition of the adjacency matrix we can rewrite the clustering coefficient as folllows:

$$C_i = \frac{\sum_i (\hat{A}^3)_{ii}}{\sum_{i \neq j} (\hat{A}^2)_{ij}}. \tag{1.3}$$

  The clustering coefficient is a special measure of network nodes correlation and gives for a given node the number of nearest neighours which are connected with each other;

- the clique is the number of interrelated groups in network;

- the betweenness centrality is a local node characteristic. It is correspond to the number of shortest pass lengths pass through it. Betweenness centrality of a node

m is defined as the ratio of all shortest path which pass through a node m to the general number of shortest paths:

$$\sigma(m) = \sum_{i \neq j} \frac{l(i,m,j)}{l(i,j)}. \tag{1.4}$$

Another important characteristics of a network is the node degree distribution function $P(k)$. This is a probability that randomly chosen node i has a degree (number of nearest neighbors) $k_i = k$. For complex networks the most typical node degree distributions are:

- Poisson distribution

$$P(k) = e^{-\langle k \rangle} \frac{\langle k \rangle^k}{k!}, \tag{1.5}$$

- exponentially decaying distribution

$$P(k) \sim e^{-k/\langle k \rangle}, \quad k \to \infty \tag{1.6}$$

- power law decaying distribution

$$P(k) \sim 1/k^{\gamma}, \quad k \to \infty. \tag{1.7}$$

The first two distributions contain typical scale, but this is not the case of the third one. In the case of an infinite network, all moments $\langle k^{\alpha} \rangle$ for the distributions (1.5)-(1.6) exist, while for (1.7) only a few first moments with $\alpha < \gamma - 1$ are not divergent. Networks with a power-law node degree distribution decay are called scale-free networks [13]. The name follows from the definition of the distribution function, which does not have a typical scale.

Scale-free networks are used to describe a wide class of natural and artificial systems. For example, the Internet scale free structure was found [14, 35, 36, 39–41], where the nodes correspond to web-pages and links correspond to hyper-links. This discovery attracted the special attention to study the systems on networks. Previously the network theory notions have been used to study social processes, with nodes corresponding to members or groups of society [42, 43] and links describing the different social relations. An examples of a social network is a scientific collaboration network [42, 44],

where the nodes correspond to the authors and links correspond for example to existence of a common publication. The study of links distribution in such networks shows that it is governed by a power law with exponential cut-off [42, 45] caused by a limited time interval. Another interesting example to investigate is a transport network, when the nodes are stations (stops) and links are route lines. In such a way the scale-free structure of airports [46–51], railways [52], and public transports [53–58] was studied.

For the complex networks description, different models have been proposed, the most well-known are:

- **Classical random graph**

  Using the probabilistic methods A. Rényi and P. Erdös described in detail the properties of graph being called Erdös-Rényi random graph [8], now the classical random graph. There are different ways to build the classical random graph. One of the possible procedures is to fix the probability of a link between two nodes in an ensemble with given number of vertices. Otherwise the links are randomly and independently distributed between all vertices.

- **Small world network**

  The small world network is a network for which a characteristic size l decays with a system size N slower than a power law. For the so called Watts-Strogatz small world model $l \sim \ln N$ [9]. Social networks revealed to be small world networks. Watts-Strogatz network can be constructed from a regular structure (for example, one-dimensional chain) using the rewiring procedure [9]: each link is removed with a probability p and then it is rewired with another node. In such a way the small world network allows to interpolate between a regular structure and random a graph changing the parameter p. The local properties of a regular lattice as well as global ones for a random graph are realized for small world networks [10].

- **Albert-Barabási model (preferential attachment)**

  A possible ways to construct a scale-free network is a Albert-Barabási scenario [13, 14]. This model is characterized by the following node degree distribution function: $P(k) \sim 1/k^3$. The network is constructed using two main principles: increasing and preferential attachment [13, 14]. At the beginning the system contains fixed number of nodes n_0, a new node with $n < n_0$ links is attached to them at every next step. The probability to create the link between the new node and the old node i is proportional to the node degree k_i.

Further we will consider papers where the behaviour of classical statistical physics models, in particular spin models, on complex networks has been analyzed. In this case one has to deal with structural disorder as well with disorder connected with the distribution of individual states of particles. In turn that leads to different models, similarly as quenched and annealed structural disorder in the theory of structurally-disordered systems is considered [59]. The configurational model [60] and the annealed network model are widely used to describe uncorrelated networks [61,62]. Configurational model is a maximally random graph with a given node degree distribution. In graph theory such graph is called labeled random graph with a given nodes sequence [60, 63, 64]. In the case of an annealed network, link configurations fluctuate on the same time scales as spin variables. That leads to averaging the partition function, but not its logarithms as in the previous case [59]. Such a property of annealed network allows to obtain the exact results for a large number of spin models [61, 62], in particular the partition function for an uncorrelated annealed network can be written in the similar form as for the model on a complete graph with separable interactions [61].

1.2 Spin models on complex networks

During the last decades critical phenomena on complex networks have been widely discussed in the context of statistical physics and condensed matter physics [64]. Different problems have been considered: appearance of scale-free network structure, percolation phenomena, an epidemic spreading, phase transitions and cooperative behaviour many-particles system localized on the nodes of random graph. In this subsection we give a short overview of analysis of the critical behaviour of spin models on complex networks. Such kind of research has a wide number of interesting applications, ranging from physics of nanosystems to sociophysics. It happens that nanosystems architecture is much better described by the topology of network rather than lattices [16]. On the other hand numerous models of opinion formation are based on an analysis of interacting agents in social networks [3]. Respectively, the question of existence of an ordered state for a spin system on a complex network can be reformulated as a problem of reaching common opinion in opinion formation models [65, 66]. The motivations to study phase transitions on complex networks mentioned above can be complemented by another reason: the behaviour of many-particles statistical physics models on complex networks fundamentally differs from their behaviour on d-dimensional lattices.

The critical behaviour of Potts model depends not only on the dimensionality of a

lattice but it is also determined by the value of Potts variable q [67]. Similarly as for the Ising model [68, 69] the Potts model on a Cayley tree is characterized by a long-range order [70], with a new type of a phase transition, the so called phase transition of continuous order [71]. Depending on the value of temperature-dependent constant of interactions the order of lowest singular derivative decreases from the first to the infinite one.

For lattice systems, the dimensionality plays the role of a global parameter. The fact that the concept of Euclidian dimensionality is ill-defined for graphs allows to expect non-trivial critical behaviours of spin models on complex networks. In the case of random networks the situation becomes more complicated by the presence of node-degree distribution disorder. In contrast to structural disorder for the lattice systems [75, 76] in the case of complex networks one deals with a strong disorder often characterized by a divergent variance. The presence of such kind of disorder together with a small-world effect (see previous subsection) are the main factors determining the features of the critical behaviour of models on complex networks. For the Ising model and for the XY model on a small-world network built on 1-dimensional regular chain the mean-field-like second order phase transition occurs [77, 78]. The similar mean-field-like phase transition for small-world networks constructed on a $d = 2$ and $d = 3$ lattices is observed [79, 80]. In the case of an antiferromagnetic Ising model on a small-world network built on 2-dimensional lattice the phase transition paramagnet-spin glass happens [81].

The critical behaviour on complex networks depends in an essential way on a presence of correlations between node degrees. The results obtained in the thesis concern uncorrelated networks. The short overview of the critical behaviour of such models will be presented below. Firstly, we should notice that correlations between node degrees play an important role. It is known [82] that the nodes with high number of links (hubs) in social networks have a tendency to join each other. Such property of networks is called the assortativity. On the other hand, for a large number of biological networks, undirected www network [83, 84] the anticorrelations for hubs are observed and such networks are called disassortative networks. Consideration of the influence of assortativity and disassortativity effects on the critical behaviour of many-particles systems is an actual problem of the theory of phase transitions [85, 86].

For uncorrelated complex networks the critical behaviour is influenced by convergent moments of the node degree distribution function $P(k)$. For networks with a convergent moment $\langle k^4 \rangle$ a typical mean-field behaviour is observed. When the moment

$\langle k^4 \rangle$ diverges and $\langle k^2 \rangle$ is convergent the universal characteristics of critical bahaviour depend on assymptotics of the function $P(k)$ at large k. Correspondingly, the spin systems on complex networks with convergent $\langle k \rangle$ and divergent $\langle k^2 \rangle$ remain ordered at any finite temperature. For a ferromagnetic Ising model on an uncorrelated network these results have been obtained by exact recurrent method [63] and replicas method [87].

In particular, the exponent λ determines the collective behaviour and plays a role similar to that of the space dimension d for lattice systems; there are lower and upper critical values of λ for networks, analogous to lower and upper critical dimensions for lattices. At upper critical value $\lambda = \lambda_{\rm uc}$ and $d = d_{\rm uc}$ the scaling behaviour is modified by multiplicative logarithmic corrections [63,87–89], while above them, critical exponents attain their mean-field values. The above analogy has limitations; e.g., for $d \leq d_{\rm lc}$ lattice systems remain disordered at any finite temperature T whereas systems on networks are always ordered at $\lambda \leq \lambda_{\rm lc}$. Being a global parameter, λ determines universal properties of critical behaviour. For the Ising model $\lambda_{\rm lc} = 3$, $\lambda_{\rm uc} = 5$ while $d_{\rm lc} = 1$ and $d_{\rm uc} = 4$. The main features of logarithmic corrections for the Potts model as studied in Chapter 2.

It is known that the critical behaviour of the XY-model on lattices significantly differs from that of the Ising model. So in two dimensions (d=2) the special phase transition between two phases occurs [90]: low-temperature phase is characterized by a power law decay of spin-spin correlation function (however, spontaneous magnetization being equal zero) and non-ordered high-temperature phase with an exponential correlation function decay. For the XY-model on a scale-free network the critical behaviour appears to be similar to that of the Ising model: the obtained critical exponents for XY-model coincide with corresponding critical exponents for the Ising model [91].

Some exact results for the 3-state Potts model with competing interactions on Bethe lattice are given in [72] and the phase diagram of the 3-state Potts model with next nearest neighbour interactions on the Bethe lattice is discussed in [73]. Potts model on the Apollonian network (an undirected graph constructed using the procedure of recursive subdivision) was considered in [92]. So far, not too much is known about the critical properties of the model on scale-free networks of different types.

Two pioneering papers [93,94] (the latter paper was further elaborated in [95]) used the generalized mean field approach and recurrent relations in the tree-like approximation, respectively. Although they agree in principle about the suppression of first order phase transition in this model for the fat-tailed node degree distribution, they differ in

the description of the phase diagram. Moreover, besides the value of q the order of the phase transition is determined by a node degree distribution decay exponent λ [93,94]. Several MC simulations also show evidence of the changes in the behaviour of the Potts model on a scale-free network in comparison with its $2d$ counterpart [95, 96]. For the Potts model on an uncorrelated scale-free network first or second order phase transition were observed.

In the limit $q \to 1$ the Potts model describes the percolation phenomenon. The percolation cluster which is observed for lattice systems [97] corresponds to the giant connected component (GCC) in the case of network [98]. The last is a connected part of the network nodes that remains finite if the system size $N \to \infty$. For an uncorrelated network the percolation threshold c_{perc} (nodes concentration at which GCC appears) is determined by the ratio of the second and first moments of node degree distribution function: $\langle k^2 \rangle / \langle k \rangle = 2$ at c_{perc}. This assertion is known as Molloy-Reed criterion [11, 99, 100]. Taking into account the above considerations about convergence of distribution function moments (1.7) one can conclude that percolation on scale-free networks depends in an essential way on the value of the parameter λ. In particular, at $\lambda \leq 3$, GCC exists at any non-zero concentration of nodes. The analysis of percolation phenomenon on complex networks enables one to find the robustness of networks to attacks of different typesand search the best ways for their protection. It was established that a real-world scale-free network is resistent to random attacks, while it is extremely sensitive to targeted ones. The examples are given by Internet [101, 102], metabolic network [37, 104], food webs [103]. Removing the high-degree nodes influences the system effectivness, for example in case of Internet the removal of 1% of hubs leads to network‘s productivity decrease in two times [101]. However, hubs do not always play the main role for a network resistance to attacks. So, for airport network it was found that nodes with large betweeness are more important than nodes with high degree [47, 48]. The natural application of resistance of networks to attacks is an investigation of computer viruses spreading in Internet or epidemic spreading in social networks [13, 82, 105–107].

The phenomenological Landau theory has been also used for the analysis of phase transitions on uncorrelated networks [88,108]. In such analysis Landau energy is dependent, besides the order parameter, on the node degree distribution function as well. For a model with scalar order parameter Landau theory was formulated by [108]. The model of connected scalar fields with local anisotropy was analyzed in [88].

Many real structures can be described as several interacting networks being called

multilayer networks [86]. One of examples is the network of networks, when different sets of nodes are connected. Another example is multiplex networks where links of different types for a given node set exist. Social networks with different types of social interactions (different links) being one of them. In particular, papers [109–111] (percolation phenomenon had been studied) and [112–114] were dedicated to the analysis of the critical phenomena on multilayer networks.

Any real or artificial system with a large number of components is finite at the end. That is why it is important to analyze how the critical behaviour of many-particle systems on a network depend on the system size N (finite size effect) [115, 116]. For a scale-free networks the second moment of a node degree distribution function $\langle k^2 \rangle$ diverges at $2 < \lambda \leq 3$ only in the limit $N \to \infty$. However, for a finite size system that divergency does not emerge. Finite size effect leads to the finite maximal number of link in a system, and it is impossible to have nodes with an infinite degree k. For a finite system the maximal node degree k_{max} is called cut-off. It depends on network size N, see Appendix I. So that for the case of percolation in the region $2 < \lambda \leq 3$ considering $k_{max} \sim \sqrt{N}$, it is possible to obtain the following dependencies for percolation threshold p_c on system size [64]: $p_c(N, 2 < \lambda < 3) \sim N^{\frac{\lambda-3}{2}}$, $p_c(N, \lambda = 3) \sim 1/\ln N$. The finite size scaling methods [115, 116] has been used for the investigation of the critical behaviour on networks [117] too.

1.3 Partition function zeros analysis in the complex plane

The work by Lee and Yang [118, 119], as well as by Fisher [120], created the basis for a new method of critical bahaviour analysis in terms of partition function zeros in the complex external field and temperature plane. This analysis has become a standard tool to study properties of phase transitions in various systems [121, 122], lattice spin models being one of them.

The Lee-Yang zeros are calculated at (real) temperature T in the complex magnetic field H plane whereas Fisher zeros (usually in the absence of a magnetic field) are located in the complex temperature plane. In the thermodynamic limit when the system size N approaches infinity, the Lee-Yang and Fisher zeros form curves on the complex (H- or T-) plane. By analysing the location and scaling of these zeros, an alternative description of critical phenomena is achieved involving angles formed by these curves [123–127]. In this way the angles may be considered to be conjugate

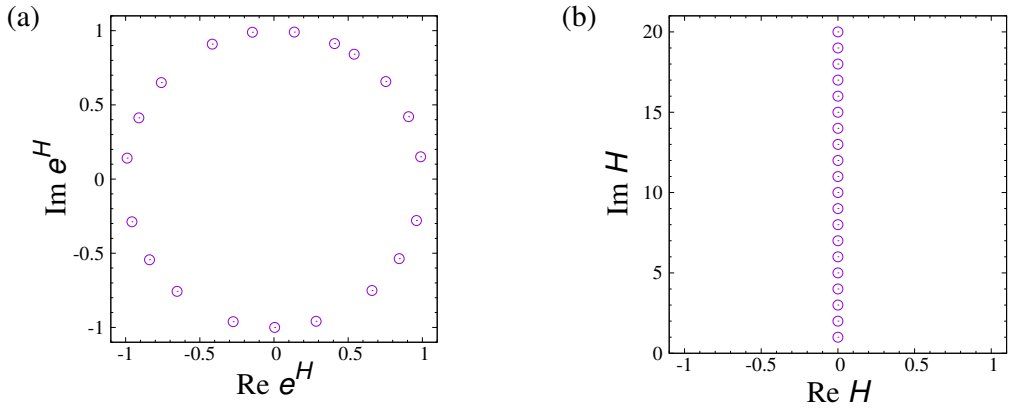

Fig. 1.1: The schematically represented Lee-Yang zeros for the ferromagnetic Ising model on a two-dimensional lattice **(a)** in a complex e^H-plane and **(b)** complex H-plane. Accordingly to the Lee-Yang circle theorem all zeros lie on a unit circle or are purely imaginary in a complex e^H and H-plane correspondingly.

to the set of critical exponents and critical amplitudes ratios. Of special interest are the finite-size scaling properties of zeros, which also encode universal features of the underlying phase transition [124].

In Fig. 1.1 we schematically represent Lee-Yang zeros coordinates for the partition function of the ferromagnetic Ising model on a two-dimensional lattice $Z(T_c, H)$ at critical temperature $T = T_c$ in complex field plane. Let us write $H = \mathrm{Re}\, H + i\, \mathrm{Im}\, H$ and define the Lee-Yang zeros coordinates $H = H_j$ for the partition function $Z(T_c, H)$, resulting from a numerically solved system of equations $\mathrm{Re}\, Z(T_c, H) = 0$ and $\mathrm{Im}\, Z(T_c, H) = 0$ in the complex field plane. Accordingly to the Lee-Yang circle theorem [118, 119] all Lee-Yang zeros for a two-dimensional ferromagnetic Ising model lie on an unit circle in e^H-plane or zeros contain only imaginary part of the coordinate $H = i\, \mathrm{Im}\, H$ in complex $H = H_j$-plane, see Fig. 1.1**a** and **b** correspondingly. In the thermodynamic limit the first zero with purely imaginary coordinate (Lee-Yang edge) touches to the real axis [128, 129].

The Lee-Yang theorem holds for the ferromagnetic Ising model on a regular lattice [118, 119] as well as for a wider class of Ising-like models on regular lattices. Besides such classical lattice discrete spin models [130], the theorem also holds for continuous spin systems [131]; for quantum systems such as an ideal pseudospin $-1/2$ Bose gas in an external field and arbitrary external potential [132]; for nonequilibrium systems [133], which relate with the collective phenomena and biophysics processes [134, 135]. Our example of the violation of the circle theorem is not unique. The Lee-Yang theorem does not hold for Ising models with antiferromagnetic interactions [136, 137]; with degenerated spins [138, 139]; with multi-spin interactions at

sufficiently high temperature [140, 141]; and van der Waals gases [142, 143]. It also fails for the high q-Potts model and the Blume-Capel model [144,145]. The theorem is violated for some quantum many-particle systems such as the quantum isotropic Ising chain and certain quantum many-body systems [146,147]. See [122] for a more detailed review.

For a detailed explanation of a connection between lines of zeros location and universal characteristics in complex temperature plane we rewrite $T = \mathrm{Re}\, T + i\, \mathrm{Im}\, T = T_c(1+t)$, where T_c is the (real) critical temperature in zero field and $t = \rho e^{i\Phi}$ ($t = (T - T_c)/T_c$) parametrises the location in the complex plane relative to T_c [148]. To determine the Fisher zeros, we search for intersections of $\mathrm{Re}\, Z(T, 0) = 0$ and $\mathrm{Im}\, Z(T, 0) = 0$ (for better understanding see Appendix II). These Fisher zeros accumulate in the vicinity of the critical point T_c along a line and tend to pinch the positive real axis with the angle $\Phi(t \to 0) = \varphi$ [123, 127, 148]. Consider the locus of Fisher zeros in the complex temperature plane depicted in Fig. 1.2. Fisher zeros are represented as light blue discs the black one being the critical point position. The critical temperature is real, so the critical point is located on the real axis. Applying a real magnetic field to the system, we observe that Fisher zeros move in the complex $T-$plane along a curve which defines an angle ψ wrt the positive real axis [124].

A useful relation connects the impact angle φ with the exponent α of the specific heat and with the specific heat universal amplitude ratio A_-/A_+, where A_+, A_- are scaling amplitudes at $t > 0$, $t < 0$ respectively [115, 149]. The idea of explanation of this relation is a following [124]. On the real axis, the singular part of the free energy in the vicinity of critical point in the absence of magnetic field can be written as $f \simeq F_\pm |t|^{2-\alpha}$. In the high-temperature phase given by $t > 0$, this is $f \simeq F_\pm t^{2-\alpha}$. In the low-temperature phase for which $t < 0$ it is $f \simeq F_\pm (-t)^{2-\alpha}$. In the complex plane, the free energy is analytic everywhere except along the lines of zeros of the partition function. that line separates the two regions (high and low temperatures) in Fig. 1.2. By analytic continuation from the high temperature real axis, the region on the right of the line of zeros (the "high temperature phase") has

$$f_+(t) \simeq F_+(\rho e^{i\Phi})^{2-\alpha} + f_+^{reg}, \quad 0 \le \Phi < \pi - \varphi. \tag{1.8}$$

On the other hand, continuing the region to the left of the line of zeros (the "low temperature phase"), one has

$$f_-(t) \simeq F_-(-\rho e^{i\Phi})^{2-\alpha} + f_-^{reg}, \quad \pi - \varphi < \Phi \le \pi. \tag{1.9}$$

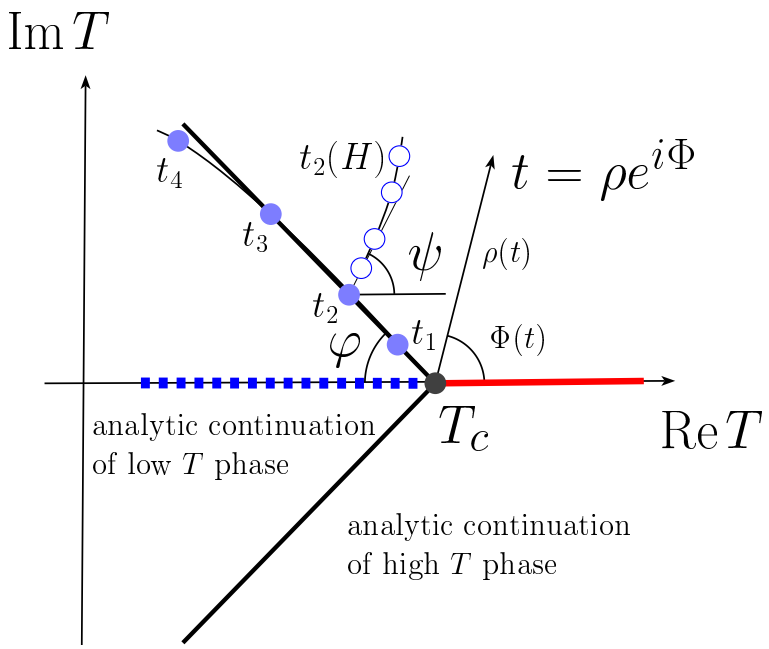

Fig. 1.2: Plot of the distribution of zeros in the complex T-plane: the angle φ corresponds to the impact angle of Fisher zeros on the real axis, and the angle ψ describes the motion of the Fisher zeros in presence of a real magnetic field.

At the transition along the line of Fisher zeros, $\Phi = \pi - \varphi$, the real parts of the free energies of both phases are equal [123, 124]. Substituting $\Phi = \pi - \varphi$ into (1.8)-(1.9) and using the fact that $F_-/F_+ = A_-/A_+$ we arrive at the formula [124, 126, 127]:

$$\tan[(2-\alpha)\varphi] = \frac{\cos(\pi\alpha) - A_-/A_+}{\sin(\pi\alpha)}. \tag{1.10}$$

The scaling of the zeros follows from general arguments. Replacing the volume L^d of a regular lattice by the number of sites N on a complete graph the partition function in terms of complex reduced temperature t and magnetic field H, $Z(t, H)$, can be written as a generalized homogenous function [124]:

$$Z(t, H) = e^{\epsilon_0} Z(tN^{1/(2-\alpha)}, HN^{\beta\delta/(2-\alpha)}), \tag{1.11}$$

where β and δ are critical exponents of order parameter. The constant e^{ϵ_0} takes only real values and can be neglected:

$$Z(t, H) = Z(tN^{1/(2-\alpha)}, HN^{\beta\delta/(2-\alpha)}) = 0. \tag{1.12}$$

Let us find the solution of Eq.(1.4). The partition function is an even function of H so

that the previous scaling relation may be written either as

$$H^2 N^{2\beta\delta/(2-\alpha)} = f(tN^{1/(2-\alpha)}), \tag{1.13}$$

or as

$$tN^{1/(2-\alpha)} = g(HN^{\beta\delta/(2-\alpha)}), \tag{1.14}$$

where $f(x)$, $g(x)$ are some analytical functions of x. At $H = 0$ equation (1.14) gives the scaling of Fisher zeros:

$$t_j = N^{-1/(2-\alpha)} g_j(0), \tag{1.15}$$

where $g_j(0)$ is in general a complex number. Extending to scaling with the label index j [124] we generalize from (1.13) and (1.14) to the Lee-Yang and Fisher zeros scaling as

$$H_j(N, t = 0) \sim \left(\frac{j}{N}\right)^{\frac{\beta\delta}{2-\alpha}}, \tag{1.16}$$

$$t_j(N, H = 0) \sim \left(\frac{j}{N}\right)^{\frac{1}{2-\alpha}}. \tag{1.17}$$

Setting $t = 0$ in (1.13) leads for the Lee-Yang zeros to [124]:

$$H_j^2 = N^{-2\beta\delta/(2-\alpha)} f_j(0)\,. \tag{1.18}$$

In general, $f_j(0)$ is a complex number. However, for models that obey the Lee-Yang theorem (all zeros are purely imaginary $h_j \sim i\,\mathrm{Im}\,H_j$ [118,119]) $f_j(0)$ is a negative real number. Using this property one can derive from the scaling properties of the partition function [124] an angle ψ of Fisher zeros motion in real magnetic field. At fixed t and for the $N \to \infty$, the variable H_j tends to the Lee-Yang edge, hence, substituting $N^{-1/(2-\alpha)}$ from (1.15) into (1.18) we parametrise:

$$t_j \sim H_j^{1/(\beta\delta)} \exp(\pm i\psi), \tag{1.19}$$

to obtain [124]

$$\psi = \frac{\pi}{2\beta\delta}. \tag{1.20}$$

Besides being of fundamental interest, and being useful for theory, the zeroes attract attention due to their experimental observation too. The first step to connect zeros to experimental data was made in Ref. [150]. The density of zeros on the Lee-Yang circle was determined by analyzing isothermal magnetization data of the Ising ferromagnets.

Recently Peng et al. related imaginary magnetic fields associated with a bath of Ising spins to the quantum coherence [151] of a probe spin [17,152,153]. For the experimental study the trimethylphosphite (TMP) molecule was used. It contains nine equivalent 1H nuclear spins (spins bath) and one 31P nuclear spin (probe spin). Investigating the interaction of the probe spin with spins bath the function of quantum decoherence $L(t)$ was measured. At some moment of time $L(t_n) = 0$. The experimentally obtained times t_n, when the quantum decoherence disappears, can be interpreted as coordinates of purely imaginary Lee-Yang zeros [152]:

$$t_n = \Theta_n/(4\lambda). \tag{1.21}$$

where Θ_n corresponds to the Lee-Yang zeros coordinates $u_n \equiv e^{i\Theta_n}$, and λ is the coupling constant of the interaction of the probe spin with spins bath. The approach could help in the study of real systems in which the zeros cannot easily be calculated, giving access to new quantum phenomena that would otherwise remain hidden if one were to restrict one's attention to real, physical parameters. The experiments also confirm a profound connection between a static entity – the complex magnetic field in thermodynamics – and dynamical properties of quantum systems – coherence.

1.4 Conclusions

In this section we gave a brief description of complex networks and examples of spin models on networks. There is a large number of previous studies with a critical behavior of spin models on lattices or regular graphs, that is why the research of critical behavior of spin models on complex networks contains many unresolved problems. While for the Ising model on a scale-free network a set of scaling functions and amplitude ratios [88] had been found, such studies have not been done so far for many other spin models, including the Potts model. It is known that in the limit $q \to 1$ the Potts model describes bond percolation. Therefore the consideration of percolation on complex networks associated with the emergence of a giant connected component is useful for a study of a large number of phenomena on networks. The examples are reaction of networks to targeted and random attacks, epidemic spreading in social networks and others. However, the role of logarithmic corrections to the quantitative description of percolation phenomena on a scale-free network is still not clear.

An application of complex zeros analysis for the partition function led to a significant progress in the qualitative understanding and quantitative description of phase

transitions in many systems. It is surprising, that this method had not been used to describe phase transitions and critical phenomena in scale-free network yet. In frames of the method, the description of thermodynamics of the system is carried out not in terms of partition function moments but in terms of its zeros. In this case the universal characteristics are not sets of critical exponents and critical amplitude ratios but the angles describing localization of the partition function zeros in the complex field or temperature plane. The values of these angles for spin systems on a scale-free network is unknown. The validation of the classic statements such as a Lee-Yang unit circle theorem for the case where the spin system on scale-free network had not been investigated yet.

The thesis will be devoted to clarification of the above questions.

Chapter 2 | PHASE TRANSITION IN THE POTTS MODEL ON A SCALE-FREE NETWORK

Contents

In this chapter, we discuss a q-state Potts model on an uncorrelated scale-free network. Applying an inhomogeneous mean-field method (see subsection 2.2) we analyze the phase diagram (subsections 2.3, 2.4) and obtain thermodynamic functions (subsections 2.5, 2.6). In particular, we show that the

critical behavior of the model essentially depends on the number of Potts states q and the distribution decay exponent λ. First and second order phase transitions occur, and for small values of λ (so called fat tails distributions) the system is ordered at any finite temperature. Contrary to the previous studies our research is based on the analysis of the free energy expression. In particular, it allows us to present all thermodynamic functions in universal scaling forms. Other quantitative universal characteristics are found: critical parameters and critical amplitudes. It was shown that the logarithmic corrections to scaling appear and the logarithmic corrections exponents were calculated. For percolation phenomena these exponents are found for the first time. The main conclusions of our research is given in section 2.7.

The main results of this chapter were published in [18–20].

2.1 Hamiltonian of the Potts model on a scale-free network

Being one of possible generalizations of the Ising model, the Potts model possesses a richer phase diagram. In particular, either first or second order phase transitions occur depending on specific values of q and d for d-dimensional lattice systems [67]. It is well established by now that this picture is changed by introducing structural disorder, see e.g. [154] and references therein for 2d lattices and [155] for 3d lattices. The Hamiltonian of the Potts model that we are going to consider in this paper reads:

$$-\mathcal{H} = \frac{1}{2}\sum_{i,j} J_{ij}\delta_{n_i,n_j} + \sum_i H_i\delta_{n_i,0}, \tag{2.1}$$

here, $n_i = 0, 1, ...q-1$, where $q \geq 1$ is the number of Potts states, H_i is a local external magnetic field chosen to favour the 0-th component of the Potts spin variable n_i. The main difference with respect to the usual lattice Potts Hamiltonian is that the summation in (2.1) is performed over all pairs i, j of N nodes of the network, J_{ij} being proportional to the elements of an adjacency matrix of the network. For a given network, J_{ij} equals J if nodes i and j are linked and it equals 0 otherwise.

Possible applications of spin models on complex networks can be found in various segments of physics, starting from problems of sociophysics [15] to physics of nanosystems [16], where the structure is often much better described not by the geometry of a lattice but by a network. In turn, the Potts model, being of interest also for purely academic reasons, it has numerous realizations, see e.g. [67] for some of them. Besides the Ising model at $q = 2$ it also describes percolation at $q \to 1$ [156,157]. Spanning treelike

percolation with a geometric phase transition is described by a zero-state $q = 0$ Potts model [158]. Subsequently, it has been shown the equivalence between zero-state Potts model and Abelian sandpile models in case of an arbitrary finite graphs [159]. Sandpile models describe processes in neural networks, fracture, hydrogen bonding in liquid water. Other particular case of Potts model at $q = 1/2$ is a spin glass model [160,161]. The case of $0 \leq q < 1$ is used to describe gelation and vulcanization processes in branched polymers [162]. Other examples concern application of the Potts model for larger values of q. Three-component $q = 3$ Potts model is used to describe a cubic ferromagnet with three axes in a diagonal magnetic field [163], an adsorption of 4He atoms on graphite in two dimensions [164], transition of helium films on graphite substrate [165], etc. The 4-state Potts model also describes the effect of absorbtion on surfaces [166]. The Potts model at large q is used to simulate the processes of intercellular adhesion and cancer invasion [167], see also [168].

Here, we will analyze the impact of changes in the topology of the underlying structure on thermodynamics of this model, when Potts spins reside on the nodes of an uncorrelated scale-free network, as explained in more details below.

2.2 Non-homogenous mean-field approach

In the following we will use the mean field approach to analyze thermodynamics of the Potts model (2.1) on an uncorrelated scale-free network, that is, a network that is maximally random under the constraint of a power-law node degree distribution:

$$P(k) = c_\lambda k^{-\lambda}, \tag{2.2}$$

where $P(k)$ is the probability that any given node has degree k and c_λ can be readily found from the normalization condition $\sum_{k=k_\star}^{k^\star} P(k) = 1$, with $k_\star$ and $k^\star$ being the minimal and maximal node degree, correspondingly. For an infinite network, $\lim_{N\to\infty} k^\star \to \infty$. A model of uncorrelated network with a given node-degree (called also configuration model, see e.g. [60]) provides a natural generalization of the classical Erdös-Rényi random graph and is an undirected graph maximally random under the constraint that its degree distribution is a given one. It has been shown, that for such networks the mean field approach leads in many cases to asymptotically exact results. In particular, this has been verified for the Ising model using recurrence relations [63] and replica method [87] and further applied to $O(m)$-symmetric and anisotropic cubic models [88], mutually interacting Ising models [112, 169] as well as to percolation [93].

For the Potts model however, two approximation schemes, the mean field treatment [93] and an effective medium Bethe lattice approach [94] were shown to lead to different results.

To define the order parameter and to carry out the mean field approximation in the Hamiltonian (2.1), let us introduce local thermodynamic averages:

$$\mu_i = \overline{\delta_{n_i,0}}\,, \qquad \nu_i = \overline{\delta_{n_i,\alpha\neq 0}}, \tag{2.3}$$

where the averaging means:

$$\overline{(\ldots)} = \frac{\mathrm{Sp}(\ldots)\exp(-H/T)}{\mathcal{Z}}, \tag{2.4}$$

T is the temperature and we choose units such that the Boltzmann constant $k_\mathrm{B} = 1$. The partition function

$$\mathcal{Z} = \mathrm{Sp}\exp(-H/T), \tag{2.5}$$

and the trace is defined by:

$$\mathrm{Sp}(\ldots) = \prod_{i=1}^{N}\sum_{n_i=0}^{q-1}(\ldots). \tag{2.6}$$

The two quantities defined in (2.3) can be related using the normalization condition $\delta_{n_i,0} + \sum_{\alpha=1}^{q-1}\delta_{n_i,\alpha} = 1$, leading to:

$$\nu_i = (1-\mu_i)/(q-1). \tag{2.7}$$

Observing the behaviour of averages (2.3) calculated with the Hamiltonian (2.1) in the low- and high-temperature limits: $\mu_i(T\to\infty) = \nu_i(T\to\infty) = 1/q$, and $\mu_i(T\to 0) = 1$, $\nu_i(T\to 0) = 0$ the local order parameter (local magnetization), $0 \le m_i \le 1$, can be written as:

$$m_i = \frac{q\overline{\delta_{n_i 0}} - 1}{q-1}. \tag{2.8}$$

Now, neglecting the second-order contributions from the fluctuations $\delta_{n_i,n_j} - \overline{\delta_{n_i,n_j}}$ one gets the Hamiltonian (2.1) in the mean field approximation:

$$\begin{aligned} -\mathcal{H}^{mfa} &= \sum_{i,j} J_{ij}\delta_{n_i,0}m_j + \frac{1}{q}\sum_{i,j} J_{ij}(1-m_j \\ &\quad +(1-q)m_i m_j) + \sum_i H_i\delta_{n_i,0}. \end{aligned} \tag{2.9}$$

2.3 Free energy of the Potts model on uncorrelated scale-free network

The free energy in the mean field approximation, $-g = T \ln \mathrm{Sp} e^{-\mathcal{H}^{mfa}/T}$, readily follows:

$$\begin{aligned} -g &= \frac{1}{q}\sum_{i,j} J_{ij}(1 - m_j + (1-q)m_i m_j) \\ &\quad + T\sum_i \ln\left[\exp\left(\frac{\sum_j J_{ij}m_j + H_i}{T}\right) + q - 1\right]. \end{aligned} \tag{2.10}$$

As usual within the mean field scheme, the free energy (2.10) depends, besides the temperature, both on magnetic field and magnetization. The latter dependence is eliminated by the free energy minimization, leading in its turn to the equation of state. For the Potts model on uncorrelated scale-free networks the equation of state, that follows from (2.9) was analyzed in Ref. [93]. Here, we aim to further analyze temperature and field dependencies of the thermodynamic functions. Opposite to the mean field approximation for lattice models, where one assumes homogeneity of the local order parameter (putting $m_i = m$ for lattices), intrinsic heterogeneity of a network, where different nodes may have in principle very different degrees, does not allow to make such an assumption. One can rather assume within the mean field approximation that the nodes with the same degree are characterized by the same magnetization. Therefore, the global order parameter for spin models on network is introduced via weighted local order parameters (see e.g. [170]). Following [93] let us define the global order parameter by:

$$m = \frac{\sum_i k_i m_i}{\sum_i k_i}. \tag{2.11}$$

Within the mean field approach, we substitute the matrix elements J_{ij} in (2.10) by the probability p_{ij} of nodes i, j to be connected. The last for the uncorrelated network depends only on the node degrees k_i, k_j:

$$J_{ij} = J p_{ij} = J\frac{k_i k_j}{N\langle k\rangle}, \tag{2.12}$$

where J is an interaction constant, $\langle k\rangle = 1/N\sum_{i=1}^{N} k_i$ is the mean node degree per node.[1] The free energy (2.10), being expressed in terms of (2.11), (2.12), contains sums

[1]Such approximation makes the model alike the Hopfield model used in the description of spin

of unary functions over all network nodes. Using the node degree distribution function, these sums can be written as sums over node degrees: $\frac{1}{N}\sum_{i=1}^{N} f(k_i) = \sum_{k=k_\star}^{k^\star} P(k)f(k)$. In the infinite network limit, $N \to \infty$, $k^\star \to \infty$, passing from sums to integrals and assuming homogeneous external magnetic field $H_i = H$ we get for the free energy of the Potts model on an uncorrelated scale-free network:

$$\begin{aligned} g &= \int_{k_\star}^{\infty} [-\frac{Jk}{q} + \frac{Jk}{q}m + \frac{Jk(q-1)}{q}m^2 \\ &\quad -T\ln(e^{\frac{mJk+H}{T}} + q - 1)]P(k)dk\,, \end{aligned} \tag{2.13}$$

where the node-degree distribution function is given by (2.2). For small external magnetic field H, keeping in (2.13) the lowest order contributions in H, Hm and absorbing the m-independent terms into the free energy shift we obtain:

$$\begin{aligned} g &= \frac{J\langle k\rangle}{q}m + \frac{J\langle k\rangle(q-1)}{q}m^2 \\ &\quad -T\int_{k_\star}^{\infty} \ln(e^{mJk/T} + q - 1)P(k)dk - \frac{(q-1)\langle k\rangle J}{q^2 T}mH\,. \end{aligned} \tag{2.14}$$

Free energy (2.14) is the central expression to be further analyzed. In spirit of the Landau theory, expanding (2.14) at small m and first keeping terms $\sim m^2$ one gets for the above expression at zero external magnetic field:

$$g \simeq -\ln q + \frac{J\langle k\rangle(q-1)}{qT}(T - T_0)m^2\,, \tag{2.15}$$

where $T_0 = \frac{J\langle k^2\rangle}{2q\langle k\rangle}$. Provided that the second moment $\langle k^2\rangle$ of the distribution (2.2) exists, one observes that depending on temperature T, the coefficient at m^2 changes its sign at T_0. This temperature will be further related to the transition temperature. Another observation, usual for spin models on scale-free networks [64] is, that the system remains ordered at any finite temperature when $\langle k^2\rangle$ diverges (since $T_0 \to \infty$). For distribution (2.2) this happens at $\lambda \leq 3$. Therefore, we will be primarily interested in temperature and magnetic field behaviours of the Potts model at $\lambda > 3$.[2] The expansion of the function under the logarithm in (2.14) at small order parameter m involves both the small and the large values of its argument, mJk. To further analyze

glasses and autoassociative memory [66, 171–175].

[2]Scale-free networks with $k_\star = 1$ do not possess a spanning cluster for $\lambda > \lambda_c$ ($\lambda_c = 4$ for continuous node degree distribution and $\lambda_c \simeq 3.48$ for the discrete one [176]). We can avoid this restriction by a proper choice of $k_\star > 1$.

(2.14), let us rewrite it singling out the contribution (2.15)[3] and introducing a new integration variable $x = mJk/T$:

$$g = \frac{J\langle k\rangle(q-1)}{qT}(T-T_0)m^2 + \frac{c_\lambda (mJ)^{\lambda-1}}{T^{\lambda-2}}\int_{x_\star}^{\infty}\varphi(x)dx - \frac{(q-1)\langle k\rangle J}{q^2T}mH\,, \tag{2.16}$$

where $x_\star = mJk_\star/T$ and

$$\varphi(x) = [-\ln(e^x+q-1) + \ln q + \frac{x}{q} + \frac{q-1}{2q^2}x^2]\frac{1}{x^\lambda}. \tag{2.17}$$

Note that the Taylor expansion of the expression in square brackets in (2.17) at small x starts from x^3, whereas at large x the function $\varphi(x)$ behaves as $x^{2-\lambda}$ and therefore the integral in (2.16) is bounded at the upper integration limit for $\lambda > 3$. To analyze the behaviour of the integral at the lower integration limit when $m \to 0$ we proceed as follows.

2.3.1 Non-integer λ

Let us first consider the case when λ is non-integer. Then we represent $\varphi(x)$ for small x as:[4]

$$\varphi(x) = \sum_{i=3}^{[\lambda-1]}\frac{a_i}{x^{\lambda-i}} + \sum_{i=[\lambda]}^{\infty}\frac{a_i}{x^{\lambda-i}}\,, \tag{2.18}$$

where $[\ell]$ is the integer part of ℓ, $a_i \equiv a_i(q)$ are the coefficients of the Taylor expansion:

$$-\ln(e^x+q-1) = \sum_{i=0}^{\infty}a_i x^i\,. \tag{2.19}$$

The first coefficients are as follows:

$$a_0 = -\ln q, \qquad a_1 = -1/q, \qquad a_2 = -\frac{q-1}{2q^2},$$

$$a_3 = -\frac{(q-1)(q-2)}{6q^3}, \qquad a_4 = -\frac{(q-1)(q^2-6q+6)}{24q^4}.$$

[3] Again, we absorb the constant $-\ln q$ into the free energy shift.

[4] It is meant in (2.18) and afterwards, that the first sum is equal to zero if the upper summation limit is smaller than the lower one, i.e. for $\lambda < 4$.

Integration of the first sum in (2.18) leads to initial terms that diverge at $x \to 0$. Let us extract these from the integrand and evaluate the integral in (2.16) as follows:

$$\begin{aligned} \lim_{x_\star \to 0} \int_{x_\star}^{\infty} \varphi(x) dx &= \lim_{x_\star \to 0} \int_{x_\star}^{\infty} \Big[\varphi(x) - \sum_{i=3}^{[\lambda-1]} \frac{a_i}{x^{\lambda-i}} \Big] dx \\ &+ \lim_{x_\star \to 0} \sum_{i=3}^{[\lambda-1]} \int_{x_\star}^{\infty} \frac{a_i}{x^{\lambda-i}} dx \,. \end{aligned} \tag{2.20}$$

For the reasons explained above, the first term in (2.20) does not diverge at small m, neither does it diverges at large x, so one can evaluate this integral at $m = 0$ numerically. We will in the following denote it as:

$$c(q, \lambda) \equiv \int_0^{\infty} \Big[\varphi(x) - \sum_{i=3}^{[\lambda-1]} \frac{a_i}{x^{\lambda-i}} \Big] dx \,. \tag{2.21}$$

Numerical values of $c(q, \lambda)$ at different q and λ are given in Table 3.1. Integration of the second term in (2.20) leads to:

$$\sum_{i=3}^{[\lambda-1]} \int_{x_\star}^{\infty} \frac{a_i}{x^{\lambda-i}} dx = \sum_{i=3}^{[\lambda-1]} \frac{a_i (x_\star)^{-\lambda+i+1}}{\lambda - 1 - i} \,. \tag{2.22}$$

Finally, substituting (2.21) and (2.22) into (2.16) we arrive at the following expression for the first leading terms of the free energy at *non-integer* λ:

$$\begin{aligned} g &= \frac{J\langle k \rangle (q-1)}{qT} (T - T_0) m^2 + \frac{c_\lambda c(q, \lambda)}{T^{\lambda-2}} (mJ)^{\lambda-1} \\ &+ c_\lambda \sum_{i=3}^{[\lambda-1]} \frac{a_i (mJk_\star)^i}{\lambda - 1 - i} T^{1-i} - \frac{J\langle k \rangle (q-1)}{q^2 T} mH + O(m^{[\lambda]}) \,. \end{aligned} \tag{2.23}$$

2.3.2 Integer λ

Let us consider now the case of integer λ. To single out the logarithmic singularity in the integral of Eq. (2.16) let us proceed as follows [177]. Denoting

$$K(y) = \int_y^{\infty} \varphi(x) dx \tag{2.24}$$

Table 2.1: Normalized numerical values of the coefficient $c(q,\lambda)/(q-1)$, Eq. (2.21), for different q and λ.

$\lambda \setminus q$	1	2	3	4	6	8
5.4	−3.0692	−0.0079	−0.0002	0.0013	0.0011	0.0007
5.1	−5.9318	−0.0454	−0.0106	−0.0006	0.0028	0.0025
4.8	−0.1686	0.0352	0.0148	0.0058	0.0005	−0.0005
4.5	−0.2439	0.0237	0.0154	0.0085	0.0030	0.0012
4.2	−0.6809	0.0275	0.0344	0.0240	0.0119	0.0067
3.9	0.5975	0.0420	−0.0540	−0.0528	−0.0346	−0.0231
3.6	0.7240	0.0830	0.0065	−0.0076	−0.0102	−0.0085
3.3	1.4001	0.2469	0.0790	0.0315	0.0052	−0.0010

we take the derivative with respect to y:

$$\frac{dK(y)}{dy} = -\varphi(y)\,. \tag{2.25}$$

Now, $K(y)$ can be obtained expanding the expression in square brackets in (2.17) at small y and integrating Eq. (2.25):

$$K(y) = -\int \varphi(y)dy \;=\; \sum_{i=3,i\neq\lambda-1}^{\infty} \frac{a_i y^{i+1-\lambda}}{\lambda-i-1} - a_{\lambda-1}\ln(y) + C(q,\lambda), \tag{2.26}$$

with an integration constant $C(q,\lambda)$ and coefficients a_i given by (2.19). Numerical values of $C(q,\lambda)$ at different q and λ are given in Table 2.2.

Substituting $K(mJk_\star)$, cf. Eq. (2.24), into (2.16) we arrive at the following expression for the free energy at *integer* λ:

$$\begin{aligned} g \;=\; & \frac{J\langle k\rangle(q-1)}{qT}(T-T_0)m^2 - \frac{c_\lambda a_{\lambda-1}}{T^{\lambda-2}}(mJ)^{\lambda-1}\ln m + c_\lambda[C(q,\lambda) \\ & -a_{\lambda-1}\ln(Jk_\star/T)]\frac{(mJ)^{\lambda-1}}{T^{\lambda-2}} + c_\lambda\sum_{i=3}^{\lambda-2}\frac{a_i(mJk_\star)^i}{\lambda-i-1}T^{1-i} \\ & -\frac{J\langle k\rangle(q-1)}{q^2T}mH + O(m^{[\lambda]})\,. \end{aligned} \tag{2.27}$$

Expressions (2.23), (2.27) for the free energy of the Potts model will be analyzed in the subsequent sections in different regions of q and λ.

Table 2.2: Normalized numerical values of the coefficient $C(q,\lambda)/(q-1)$ for different q and λ.

$\lambda \setminus q$	1	2	3	4	6	8
4	0.9810	0.0355	−0.0085	−0.0134	−0.0109	−0.0079
5	0.4853	0.0194	−0.0527	−0.0483	−0.0303	−0.0197

2.4 The phase diagram

Towards an analysis of the Potts model also in the percolation limit $q = 1$, let us re-scale the free energy by the factor $(q-1)$: $g^{'mfa} = g/(q-1)$ and absorb it by re-defining the free energy scale. Then, each term in (2.23), (2.27) is also to be divided by $(q-1)$. Let us use the following notations for several first coefficients at different powers of m in (2.23), (2.27):

$$A = \frac{2J\langle k\rangle}{q}\,, \tag{2.28}$$

$$B = -\frac{c_\lambda (Jk_\star)^3(q-2)}{2q^3(\lambda-4)}\,, \quad B' = -\frac{c_\lambda J^3(q-2)}{2q^3}\,, \tag{2.29}$$

$$C = -\frac{c_\lambda (Jk_\star)^4(q^2-6q+6)}{6q^4(\lambda-5)}\,, \quad C' = -\frac{c_\lambda J^4(q^2-6q+6)}{6q^4}\,, \tag{2.30}$$

$$K = \frac{c_\lambda J^{\lambda-1} c(q,\lambda)}{(q-1)}\,, \tag{2.31}$$

$$D = \frac{J\langle k\rangle}{q^2}\,. \tag{2.32}$$

Below, we will start the analysis of the thermodynamic properties of the Potts model by determining its phase diagram in different regions of q and λ.

To analyze the phase diagram, let us write down the expressions of the free energy at small values of m, keeping in (2.23), (2.27) only the contributions that, on the one hand, allow to describe non-trivial behaviour, and, on the other hand, ensure thermodynamic stability. Since the coefficients at different powers of m are functions of q and λ, cf. (2.28)–(2.32), the form of the free energy will differ for different q and λ as well.

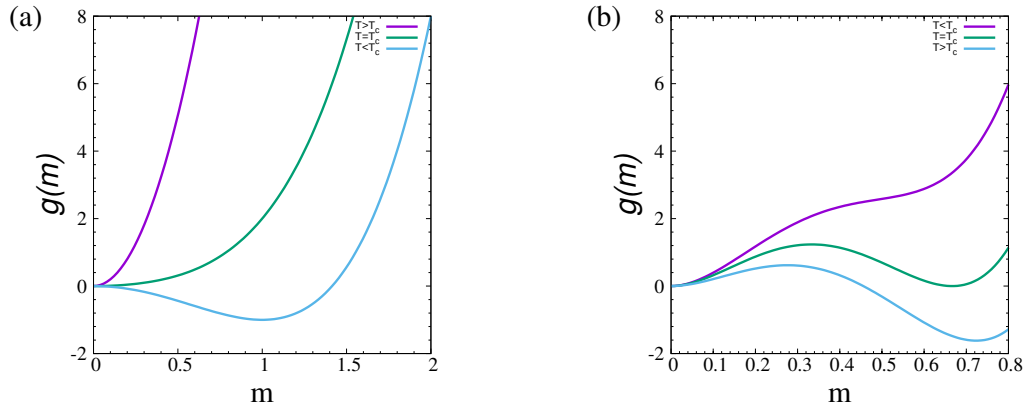

Fig. 2.1: Typical behaviour of the free energy of the Potts model on uncorrelated scale-free networks at zero external field $H = 0$. **(a)**: continuous phase transition; **(b)**: first-order phase transition.

2.4.1 $1 \leq q < 2$

As far as the coefficients K, B and B' at $m^{\lambda-1}$, m^3 and $m^3 \ln m$ are positive in this region of q, it is enough to consider only the three first terms in the free energy expansion:

$$3 < \lambda < 4: \quad g = \frac{A}{2T}(T - T_0)m^2 + \frac{K}{T^{\lambda-2}}m^{\lambda-1} - \frac{D}{T}mH, \tag{2.33}$$

$$\lambda = 4: \quad g = \frac{A}{2T}(T - T_0)m^2 + \frac{B'}{3T^2}m^3 \ln\frac{1}{m} - \frac{D}{T}mH, \tag{2.34}$$

$$\lambda > 4: \quad g = \frac{A}{2T}(T - T_0)m^2 + \frac{B}{3T^2}m^3 - \frac{D}{T}mH. \tag{2.35}$$

The typical m-dependence of functions (2.33)–(2.35) at $H = 0$ is shown in Fig. 2.1**a**. As it is common for the continuous phase transition scenario, the free energy has a single minimum (at $m = 0$) for $T > T_0$. A non-zero value of m that minimizes the free energy appears starting from $T = T_0$. In particular, the transition remains continuous in the percolation limit $q = 1$.

2.4.2 $q = 2$

For $q = 2$, the Potts model corresponds to the Ising model. Indeed, in this case the coefficient at m^3 vanishes and the first terms in the free energy expansion read:

$$3 < \lambda < 5: \quad g = \frac{A}{2T}(T - T_0)m^2 + K\frac{1}{T^{\lambda-2}}m^{\lambda-1} - \frac{D}{T}mH, \tag{2.36}$$

$$\lambda = 5: \quad g = \frac{A}{2T}(T - T_0)m^2 + \frac{C'}{4T^3}m^4 \ln\frac{1}{m} - \frac{D}{T}mH, \tag{2.37}$$

$$\lambda > 5: \quad g = \frac{A}{2T}(T - T_0)m^2 + \frac{C}{4T^3}m^4 - \frac{D}{T}mH. \tag{2.38}$$

It is easy to check that the above coefficients K, C, C' are positive for $q = 2$. Therefore, again the free energy behaviour corresponds to a continuous second-order phase transition, see Fig. 2.1**a**.

2.4.3 $q > 2$

In this region of q, the phase transition scenario depends on the sign of the next-leading contribution to the free energy. Indeed, for positive K the free energy reads:

$$3 < \lambda < \lambda_c(q): \quad g = \frac{A}{2T}(T - T_0)m^2 + K\frac{1}{T^{\lambda-2}}m^{\lambda-1} - \frac{D}{T}mH, \tag{2.39}$$

where K remains positive in the region of λ bounded by the marginal value λ_c defined by the condition

$$c(q, \lambda_c) = 0\,, \tag{2.40}$$

with $c(q, \lambda)$ given by (2.21). The free energy (2.39) is schematically shown in Fig. 2.1**a** for different T. As in the former cases, it corresponds to a continuous phase transition. With an increase of λ ($\lambda_c(q) < \lambda < 4$), the coefficient K becomes negative and one has to include the next term:

$$g = \frac{A}{2T}(T - T_0)m^2 + K\frac{1}{T^{\lambda-2}}m^{\lambda-1} + \frac{B}{3T^2}m^3 - \frac{D}{T}mH, \tag{2.41}$$

$B > 0$ for $\lambda < 4$. Now, because of the negative sign of the coefficient at $m^{\lambda-1}$ the free energy develops a local minimum for lower T (see Fig. 2.1**b**) and the order parameter manifests a discontinuity at the transition point T_c: scenario, typical for a first order phase transition. With further increase of λ, one has to include more terms in the free energy expansion for the sake of thermodynamic stability. However, the sign at the second lowest order term remains negative, which corresponds to the free energy behaviour shown in Fig. 2.1**b**: the phase transition remains first order.

The above considerations can be summarized in the “phase diagram" of the Potts model on uncorrelated scale-free networks, that is shown in Fig. 2.2. There, we show the type of the phase transition for different values of parameters λ and q.

2.4.4 General q, $2 < \lambda \leq 3$

As it was outlined above, for $2 < \lambda \leq 3$ the Potts model remains ordered at any finite temperature. Similar as for the Ising model [63], it is easy to find the high-temperature decay of the order parameter in this region of λ for any value of $q \geq 1$. Since $\langle k^2 \rangle$

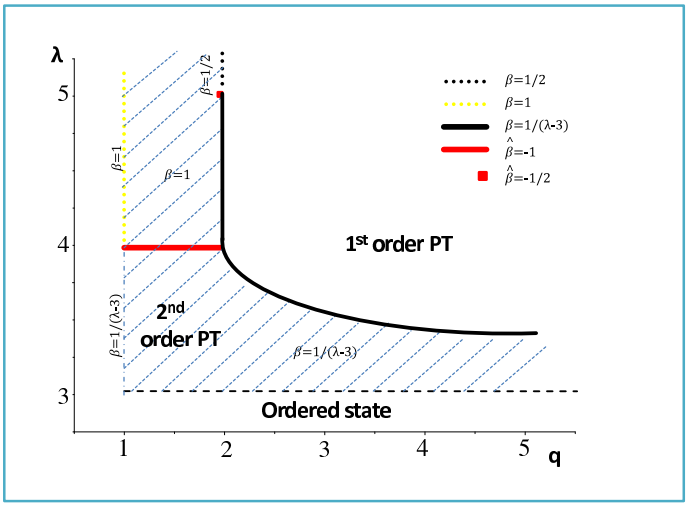

Fig. 2.2: The phase diagram of the Potts model on uncorrelated scale-free network. The black solid line separates the 1st order PT region from the 2nd order PT region (shaded). The critical exponents along the line are λ-dependent. In the 2nd order PT region, the critical exponents are either λ-dependent (below the red solid line) or attain the mean field percolation values (above the red line). For $q = 2$, $\lambda \geq 5$ (shown by the black dotted line), the critical exponents attain the mean field Ising values. Two different families of the logarithmic corrections to scaling appear: at $\lambda = 5$, $q = 2$ (a square) and at $\lambda = 4$, $1 \leq q < 2$ (red solid line). For $\lambda \leq 3$ (the region below the dashed black line) the system remains ordered at any finite temperature. The values for the rest of critical exponents are listed in Tables 2.1, 2.2.

becomes divergent for $2 < \lambda \leq 3$ one does not write this term separately in the expression for the free energy (cf. (2.16)). As a result, the corresponding expressions for the free energy read:

$$g = \frac{A}{2T}m^2 + \frac{K'}{T^{\lambda-2}}m^{\lambda-1} - \frac{D}{T}mH, \qquad 2 < \lambda < 3, \tag{2.42}$$

$$\begin{aligned} g \;=\; & \frac{A}{2T}m^2 + \frac{c_\lambda J^2}{4q^2T}m^2 \ln\frac{1}{m} + \frac{c_\lambda J^2}{T}[\frac{C'(q,3)}{q-1} \\ & + \frac{1}{2q^2}\ln(\frac{Jk_\star}{T})]m^2 - \frac{D}{T}mH\,, \qquad \lambda = 3. \end{aligned} \tag{2.43}$$

Here, the expressions for the coefficients K', $C'(q,3)$ are the same as for K, $C(q,3)$, Eqs. (2.31), (2.26) with the only difference that the function $\varphi(x)$ used for their calculation does not contain the x^2 term. It is easy to check that the free energies (2.42), (2.43) are minimal for any finite temperature at a non-zero value of m that

decays at high T as [87, 93]:

$$2 < \lambda < 3: \quad m \sim \quad T^{-\frac{\lambda-2}{3-\lambda}}, \tag{2.44}$$

$$\lambda = 3: \quad m \sim \quad Te^{-\alpha T}, \quad \alpha > 0\,. \tag{2.45}$$

The above equations (2.44), (2.45) give the temperature behaviour of the mean-field order parameter m. The connection with the magnetization M is found from the self-consistency relation:

$$M = -\Big(\frac{\partial g}{\partial h}\Big)_T. \tag{2.46}$$

One can check that the solution of this equation at large T is of the form $M \sim \frac{m}{T}$. Correspondingly, this leads to the following high temperature decay of M [63]:

$$2 < \lambda < 3: \quad M \sim \quad T^{\frac{1}{\lambda-3}}, \tag{2.47}$$

$$\lambda = 3: \quad M \sim \quad e^{-\alpha T}, \quad \alpha > 0\,. \tag{2.48}$$

For the sake of simplicity, in what follows below we will express the thermodynamic functions in terms of the mean field order parameter m. To get their M dependence, one has to take into account the above considerations.

2.5 Regime of the second order phase transition

2.5.1 Thermodynamic functions, critical exponents, logarithmic corrections to scaling

Let us find the critical exponents, that govern the behaviour of thermodynamic functions in the vicinity of the 2nd order phase transition point $H = 0$, $\tau \equiv |T - T_0|/T_0 = 0$, where T_0 is the critical temperature of the 2nd order phase transition ($T_c^{2nd} = T_0$). To this end, we will be interested in the following exponents, that govern temperature and field dependent behavior of the order parameter m, the isothermal susceptibility $\chi_T = (\frac{\partial m}{\partial H})_T$, the specific heat $c_H = T(\frac{\partial S}{\partial T})_H$, and the magnetocaloric coefficient $m_T = -T(\frac{\partial S}{\partial H})_T$ [5]. In particular at $H = 0$ the order parameter m, isothermal susceptibility χ_T,the specific heat c_H and the magnetocaloric coefficient m_T are governed by

[5]The magnetocaloric coefficient corresponds to amount of heat the system is obtained at isothermal increasing of magnetic field as a sequence of magnetocaloric effect (see [178]).

the following asymptotics near the critical point $\tau = \frac{|T-T_c|}{T_c}$):

$$m = B_-\tau^{\beta}, \qquad \chi_T = \Gamma_{\pm}\tau^{-\gamma}, \qquad c_h = \frac{A_{\pm}}{\alpha}\tau^{-\alpha}, \qquad m_T = B_T^{\pm}\tau^{-\omega}. \tag{2.49}$$

Here indexes $\pm$ correspond to the temperature regions below and above the critical one $T-T_0 \to 0^{\pm}$. In the vicinity of critical point at $T = T_0$ (namely, $\tau = 0$) thermodynamic functions become field-dependent in a following way:

$$m = D_c^{\frac{-1}{\delta}} H^{1/\delta}, \quad \chi = \Gamma_c H^{-\gamma_c}, \quad c_H = \frac{A_c}{\alpha_c} H^{-\alpha_c}, \quad m_T = B_T^c H^{-\omega_c}. \tag{2.50}$$

As in the former subsection, we analyze this behaviour in different regions of q and λ. The results of this analysis are summarized in Table 2.3.

Table 2.3: Leading critical exponents of the Potts model on uncorrelated scale-free network.

q	λ	α	α_c	β	δ	γ	γ_c	ω	ω_c
$1 \le q \le 2$	$3 < \lambda < 4$	$\frac{\lambda-5}{\lambda-3}$	$\frac{\lambda-5}{\lambda-2}$	$\frac{1}{\lambda-3}$	$\lambda - 2$	1	$\frac{\lambda-3}{\lambda-2}$	$\frac{\lambda-4}{\lambda-3}$	$\frac{\lambda-4}{\lambda-2}$
$1 \le q < 2$	$\lambda \ge 4$	-1	$-1/2$	1	2	1	$1/2$	0	0
$q = 2$	$3 < \lambda < 5$	$\frac{\lambda-5}{\lambda-3}$	$\frac{\lambda-5}{\lambda-2}$	$\frac{1}{\lambda-3}$	$\lambda - 2$	1	$\frac{\lambda-3}{\lambda-2}$	$\frac{\lambda-4}{\lambda-3}$	$\frac{\lambda-4}{\lambda-2}$
$q = 2$	$\lambda \ge 5$	0	0	$1/2$	3	1	$2/3$	$1/2$	$1/3$
$q > 2$	$3 < \lambda \le \lambda_c(q)$	$\frac{\lambda-5}{\lambda-3}$	$\frac{\lambda-5}{\lambda-2}$	$\frac{1}{\lambda-3}$	$\lambda - 2$	1	$\frac{\lambda-3}{\lambda-2}$	$\frac{\lambda-4}{\lambda-3}$	$\frac{\lambda-4}{\lambda-2}$

- $1 \le q < 2$

  In this region of q, the free energy is given by the expressions (2.33)–(2.35). For $T > T_0$, g is minimal for $H = 0$ at a zero value of the order parameter $m = 0$. For $T < T_0$, the minimum of the free energy corresponds to the non-zero m. Based on the expressions (2.33)–(2.35) we find in different regions of λ:

$$3 < \lambda < 4: \quad m = T_0^{\frac{\lambda-2}{\lambda-3}} \Big(\frac{A\tau}{K(\lambda-1)}\Big)^{\frac{1}{\lambda-3}}, \tag{2.51}$$

$$\lambda = 4: \quad m = \frac{AT_0^2}{B'}\tau |\ln \tau|^{-1}, \tag{2.52}$$

$$\lambda > 4: \quad m = \frac{AT_0^2}{B}\tau. \tag{2.53}$$

  Using formulas (2.51)–(2.53) at $q = 1$ we reproduce the corresponding results for the percolation on scale-free networks [180]: the usual mean field percolation result for the exponent $\beta = 1$ for $\lambda > 4$ and $\beta = \frac{1}{\lambda-3}$ for $3 < \lambda < 4$. Note

the appearance of the logarithmic correction at the marginal value $\lambda = 4$. The resulting values of the exponent are given in Table 2.3. Subsequently, we obtain the remaining exponents defined in (2.49), (2.50) and display them in the first two rows of Table 2.3 as well.

Similar to the order parameter, (2.52), the temperature and field behaviours of the rest of thermodynamic functions at $\lambda = 4$ in the vicinity of the critical point is characterized by logarithmic corrections. Let us define the corresponding logarithmic-correction-to-scaling exponents by [89]:

$$m \sim \tau^{\beta} |\ln \tau|^{\hat{\beta}}, \qquad \chi_T \sim \tau^{-\gamma} |\ln \tau|^{\hat{\gamma}}, \tag{2.54}$$

$$c_H \sim \tau^{-\alpha} |\ln \tau|^{\hat{\alpha}}, \qquad m_T \sim \tau^{-\omega} |\ln \tau|^{\hat{\omega}}, \tag{2.55}$$

$$m \sim H^{1/\delta} |\ln H|^{\hat{\delta}}, \qquad \chi_T \sim H^{-\gamma_c} |\ln H|^{\hat{\gamma}_c}, \tag{2.56}$$

$$c_H \sim H^{-\alpha_c} |\ln H|^{\hat{\alpha_c}}, \qquad m_T \sim H^{-\omega_c} |\ln H|^{\hat{\omega_c}}. \tag{2.57}$$

The values that we obtain are given in Table 2.4. Note, that all exponents are negative: logarithmic corrections enhance the decay to zero of the decaying quantities and weaken the singularities of the diverging quantities. We discuss this behaviour in more details in Section 2.5.3.

Table 2.4: Logarithmic-corrections exponents for the Potts model on uncorellated scale-free network.

q	λ	$\hat{\alpha}$	$\hat{\alpha_c}$	$\hat{\beta}$	$\hat{\delta}$	$\hat{\gamma}$	$\hat{\gamma_c}$	$\hat{\omega}$	$\hat{\omega_c}$
$1 \le q < 2$	$\lambda = 4$	-2	$-3/2$	-1	$-1/2$	0	$-1/2$	-1	-1
$q = 2$	$\lambda = 5$	-1	-1	$-1/2$	$-1/3$	0	$-1/3$	$-1/2$	$-2/3$

- $q = 2$, the Ising model

  For different λ, the free energy is given by (2.36)–(2.38). Minimizing these expressions one finds for the order parameter at $H = 0$, $T < T_0$:

$$3 < \lambda < 5: \quad m = T_0^{\frac{\lambda-2}{\lambda-3}} \Big(\frac{A\tau}{K(\lambda-1)} \Big)^{\frac{1}{\lambda-3}}, \tag{2.58}$$

$$\lambda = 5: \quad m = \sqrt{\frac{AT_0^3}{C'}} \tau^{1/2} |\ln \tau|^{-1/2}, \tag{2.59}$$

$$\lambda > 5: \quad m = \sqrt{\frac{AT_0^3}{C}} \tau^{1/2}. \tag{2.60}$$

The corresponding critical exponents for the other thermodynamic quantities are given in the third and fourth rows of Table 4.1. Logarithmic corrections to scaling (2.54)–(2.57) appear at $\lambda = 5$, their values are given in the second row of Table 2.4. Critical behaviour of this model on an uncorrelated scale-free network was a subject of intensive analysis, see e.g. the papers [63, 87, 88, 178] and by the result given in Table 2.3 we reproduce the results for the exponents obtained there.

- $q > 2$, $3 < \lambda \leq \lambda_c(q)$

  In this region of q, λ the phase transition remains continuous, see the phase diagram, Fig. 2.2, and the free energy is given by the expression (2.39). Correspondingly, one finds that the spontaneous magnetization behaves as

$$3 < \lambda \leq \lambda_c(q): \; m = T_0^{\frac{\lambda-2}{\lambda-3}} \Big(\frac{A\tau}{K(\lambda-1)} \Big)^{\frac{1}{\lambda-3}}. \tag{2.61}$$

  The values of the rest of the critical exponents are given in the sixth row of Table 4.1. Since the leading terms of the free energy (2.39) at $3 < \lambda \leq \lambda_c(q)$ coincide with that of the Ising model at $3 < \lambda \leq 5$, the behaviour of thermodynamic functions in the vicinity of the second order phase transition is governed by the same set of the critical exponents: the Potts model for $q > 2$, $3 < \lambda \leq \lambda_c(q)$ belongs to the universality class of the Ising model at $3 < \lambda \leq 5$. This result was first obseved in [93] by treating the mean field approximation for the equation of state.

2.5.2 Scaling functions, critical amplitude ratios

The other universal features [6] we will look for in this subsection are scaling functions and critical amplitude ratios for the Potts model on an annealed scale-free network in the vicinity of the critical point. In the previous subsection we introduced the thermodynamic functions in the form of critical amplitudes and critical exponents, see Eqs.(2.49) – (2.50). The critical amplitudes depend on local characteristics of the system, however some universal amplitude ratios do exist [115]. We will be interested

[6] The concept of universality plays a fundamental role in the theory of critical phenomena [181–183]. A lot of systems manifest similar behaviour near the critical point. The universality class does not depend on the local parameters but on global ones: dimensionality, symmetry, nature of interaction etc. If several systems are in the same universality class, they share, besides the values of the critical exponents, identical critical amplitude ratios and scaling functions [115].

in the following ratios:

$$R_\chi^\pm = \Gamma_\pm D_c B_-^{\delta-1}, \quad R_c^\pm = \frac{A_\pm \Gamma_\pm}{\alpha B_-^2}, \tag{2.62}$$

$$R_A = \frac{A_c}{\alpha_c} D_c^{-(1+\alpha_c)} B_-^{-2/\beta}, \quad A_+/A_-, \quad \Gamma_+/\Gamma_-. \tag{2.63}$$

Scaling function can be found experimentally or with the help of numeric simulations. In particular, the scaling hypothesis for the Helmholtz free energy $F(\tau, m)$ states that singular form of this thermodynamic potential is a generalized homogeneous function [184] and can be written as:

$$F(\tau, m) \approx \tau^{2-\alpha} f_\pm(x), \tag{2.64}$$

with the scaling variable $x = m/\tau^\beta$ and scaling function $f_\pm(x)$, signs + and − correspond to $T > T_c$ and $T < T_c$, respectively. The principal content of Eq. (2.64) is that $F(\tau, m)$ as a function of two variables can be mapped onto a single variable scaling function $f_\pm(x)$. It may be shown that all thermodynamic potentials are generalized homogeneous functions, provided one of them possess such property [184].

Based on the expression of the free energy one can represent the thermodynamic functions in terms of appropriate scaling functions too. In particular, magnetic and entropic equations of state read:

$$H(m, \tau) = \tau^{\beta\delta} H'_\pm(x), \tag{2.65}$$

$$S(m, \tau) = \tau^{1-\alpha} \mathcal{S}(x), \tag{2.66}$$

with the scaling functions $H'_\pm(x)$ and $\mathcal{S}(x)$. In turn, the scaling functions for the heat capacity, isothermal susceptibility, and magnetocaloric coefficient are defined via (see e.g. [178]):

$$c_H(m, \tau) = (1 \pm \tau)\tau^{-\alpha} \mathcal{C}_\pm(x), \tag{2.67}$$

$$\chi_T(m, \tau) = \tau^{-\gamma} \chi_\pm(x), \tag{2.68}$$

$$m_T(m, \tau) = (1 \pm \tau)\tau^{\beta-\gamma} \mathcal{M}_\pm(x). \tag{2.69}$$

In the previous section the free energy expressions for the Potts model on a scale-free network in the q-λ plane. Of main interest for us will be the second order phase transition regime at non-integer λ, which corresponds to three different regions: Region I ($q = 2$, $\lambda > 5$), Region II ($1 \leq q < 2$, $\lambda > 4$) and Region III ($3 < \lambda < 5$, $q = 2$;

$3 < \lambda < 4$, $1 \leq q < 2$; $3 < \lambda \leq \lambda_c(q)$, $q > 2$), see Fig. 2.2. The critical exponents in these regions belong to three different universality classes. Region I is governed by the Ising mean field critical exponents; while Region II is governed by the percolation mean field critical exponents and Region III is characterized by a non-trivial λ-dependency of the critical exponents. Values of the critical exponents in all three regions are collected in Table 2.3. Our starting point will be the expression for the Helmholtz free energy obtained in Ref. [18] for different q. For non-integer $\lambda > 3$ the free energy reads:

$$F(\tau, M) = a_1 \tau M^2 + a_2 M^{\lambda-1} + \sum_{i=3}^{[\lambda-1]} a_i M^i + O(M^{[\lambda]}) \,, \tag{2.70}$$

here M is magnetization, a_i are non-universal coefficients, their explicit form is given in [18] and $[\lambda]$ is the integer part of λ. Note that the power law polynomial form (2.70) holds for the Helmholtz potential for non-integer λ only. Logarithmic corrections appear in the case of integer values of λ. As we will discuss below, this will lead to the changes in critical behaviour at $\lambda = 4$ and $\lambda = 5$.

The expression of the free energy of the Potts model on uncorrelated scale-free network (2.70) will be the starting point for the analysis of the critical amplitude ratios and scaling functions. Passing to the dimensionless energy $f(m, \tau)$ and dimensionless magnetization m and leaving leading order contributions for small values of m, we can present (2.70) in three different regions of the phase diagram (Fig. 2.2) in the following form:

$$f(m, \tau) = \pm \frac{\tau}{2} m^2 + \frac{1}{4} m^4, \quad \text{(Region I)}, \tag{2.71}$$

$$f(m, \tau) = \pm \frac{\tau}{2} m^2 + \frac{1}{4} m^3, \quad \text{(Region II)}, \tag{2.72}$$

$$f(m, \tau) = \pm \frac{\tau}{2} m^2 + \frac{1}{4} m^{\lambda-1}, \quad \text{(Region III)}. \tag{2.73}$$

With the expressions of the free energy at hand it is straightforward to write down the equation of state and to derive the thermodynamic functions. The magnetic and entropic equations of state in the dimensionless variables m and τ read:

$$H(m, \tau) = \partial f(m, \tau)/\partial m|_\tau \,, \quad s(m, \tau) = \mp \partial f(m, \tau)/\partial \tau|_m \,. \tag{2.74}$$

Written explicitly in different regions of q and λ the magnetic equation of state attains

Table 2.5: Scaling functions and critical amplitude ratios for the Potts model on an uncorrelated scale-free network.

	Region I	Region II	Region III
$f_\pm(x)$	$\pm\frac{x^2}{2}+\frac{x^4}{4}$	$\pm\frac{x^2}{2}+\frac{x^3}{4}$	$\pm\frac{x^2}{2}+\frac{x^{\lambda-1}}{4}$
$H_\pm(x)$	$x^3 \pm x$	$\frac{3}{4}x^2 \pm x$	$\frac{\lambda-1}{4}x^{\lambda-2} \pm x$
$\mathcal{S}(x)$	$-x^2/2$	$-x^2/2$	$-x^2/2$
$\mathcal{C}_\pm(x)$	$\frac{x^2}{3x^2\pm1}$	$\frac{x^2}{3x/2\pm1}$	$\frac{x^2}{(\lambda-1)(\lambda-2)x^{\lambda-3}/4\pm1}$
$\chi_\pm(x)$	$\frac{1}{3x^2\pm1}$	$\frac{1}{3x/2\pm1}$	$\frac{1}{(\lambda-1)(\lambda-2)x^{\lambda-3}/4\pm1}$
$\mathcal{M}_\pm(x)$	$\frac{x}{3x^2\pm1}$	$\frac{x}{3x/2\pm1}$	$\frac{x}{(\lambda-1)(\lambda-2)x^{\lambda-3}/4\pm1}$
A^+/A^-	0	0	0
Γ^+/Γ^-	2	1	$\lambda-3$
R_χ^+	1	1	1
R_χ^-	$\frac{1}{2}$	1	$\frac{1}{\lambda-3}$
R_c^+	0	0	0
R_c^-	$\frac{1}{4}$	1	$\frac{1}{(\lambda-3)^2}$
R_A	$\frac{1}{3}$	$\frac{1}{2}$	$\frac{1}{\lambda-2}$

the following form:

$$H(m,\tau) = m^3 \pm \tau m, \quad \text{(Region I)}, \tag{2.75}$$

$$H(m,\tau) = \frac{3}{4}m^2 \pm \tau m, \quad \text{(Region II)}, \tag{2.76}$$

$$H(m,\tau) = \frac{\lambda-1}{4}m^{\lambda-2} \pm \tau m, \quad \text{(Region III)}. \tag{2.77}$$

The entropic equation of state is obtained by a temperature derivative at constant magnetization m while the explicit τ-dependency is the same in all regions. Therefore the equation keeps the same form on q–λ plane:

$$s = -m^2/2, \quad \text{(Regions I–III)}. \tag{2.78}$$

Thermodynamic functions χ_T, c_h, and m_T that characterize response on an external action are directly obtained from the above equations of state. We do not present the explicit expressions here, being rather interested in the corresponding critical amplitude ratios. The latter are given in Table 2.5. In the particular case $q = 2$, we recover by these expressions critical amplitude ratios formerly obtained for the Ising model on an uncorrelated scale-free network [88,178], correcting at $3 < \lambda < 5$ the expression for R_A given in [178].

Let us derive now the scaling functions for the free energy and other thermodynamic

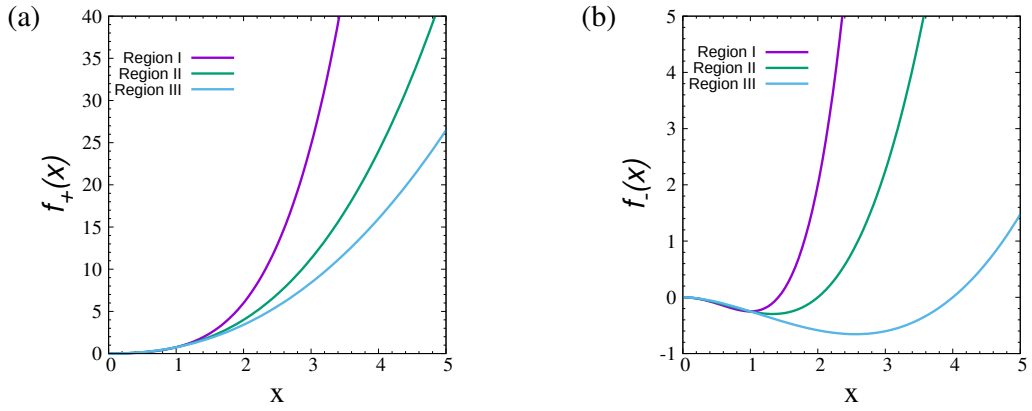

Fig. 2.3: Limiting behaviour of the free energy scaling functions f_+ (**(a)**, $T > T_c$) and f_- (**(b)**, $T < T_c$). The functions remain unchanged for $\lambda > 5$, $q = 2$ and $\lambda > 4$, $1 \leq q < 2$ (Regions I and II, correspondingly). For $q > 2$ the phase transition turns to be of the first order at $\lambda > \lambda_c(q)$. Region III: $q = 4$, $\lambda = \lambda_c(4) \simeq 3.5$.

functions. Using the definition (2.64) and taking into account that the heat capacity and order parameter critical exponents α, β take on different values in different regions of the phase diagram Fig. 2.2 we can recast Helmholtz potential $F(\tau, m)$ in terms of the scaling function $f_\pm(m/\tau^\beta)$. The explicit expressions for the scaling function in all three regions of the phase diagram are given in table 2.5. Typical behaviour of the free energy scaling functions $f_+(x)$ and $f_-(x)$ is shown in Fig. 2.3**a** and 2.3**b**, correspondingly.

At any value of q, the scaling functions share common feature: their curvature gradually increases with an increase of $\lambda > 3$. This happens up to some marginal value $\lambda = \lambda_c$. The marginal value λ_c is q-dependent. For $\lambda > \lambda_c$ and $1 \leq q \leq 2$ the scaling functions remain unchanged: their shape does not change with further increase of λ. The logarithmic corrections to scaling appear at $\lambda = \lambda_c$ and the second order phase transition holds in this case for $\lambda > \lambda_c$ as well [18], see Fig. 2.2. Alternatively, for $\lambda > \lambda_c$ and $q > 2$ the phase transition turns to be of the first order. Curves I of Fig. 2.3 (plotted by solid lines) show the limiting behaviour of the scaling functions at $q = 2$, $\lambda > 5$ (note that $\lambda_c(q = 2) = 5$): the functions remain unchanged for all $\lambda > 5$. Similar behaviour holds for the case $1 \leq q < 2$, the value of λ_c however differs: $\lambda_c(1 \leq q < 2) = 4$. This is shown by curves II in the figure, plotted by dashed lines. Finally, curves III (dotted lines) for $q = 4$ are one of examples of the limiting behaviour of the scaling functions in the region $q > 2$.

Entropy scaling function $\mathcal{S}(x)$ is defined by (2.66). Using expression (2.78) for the entropy and taking into account the values for the critical exponents α and β given in table 2.5 we arrive at the entropy scaling function that remains unchanged in all

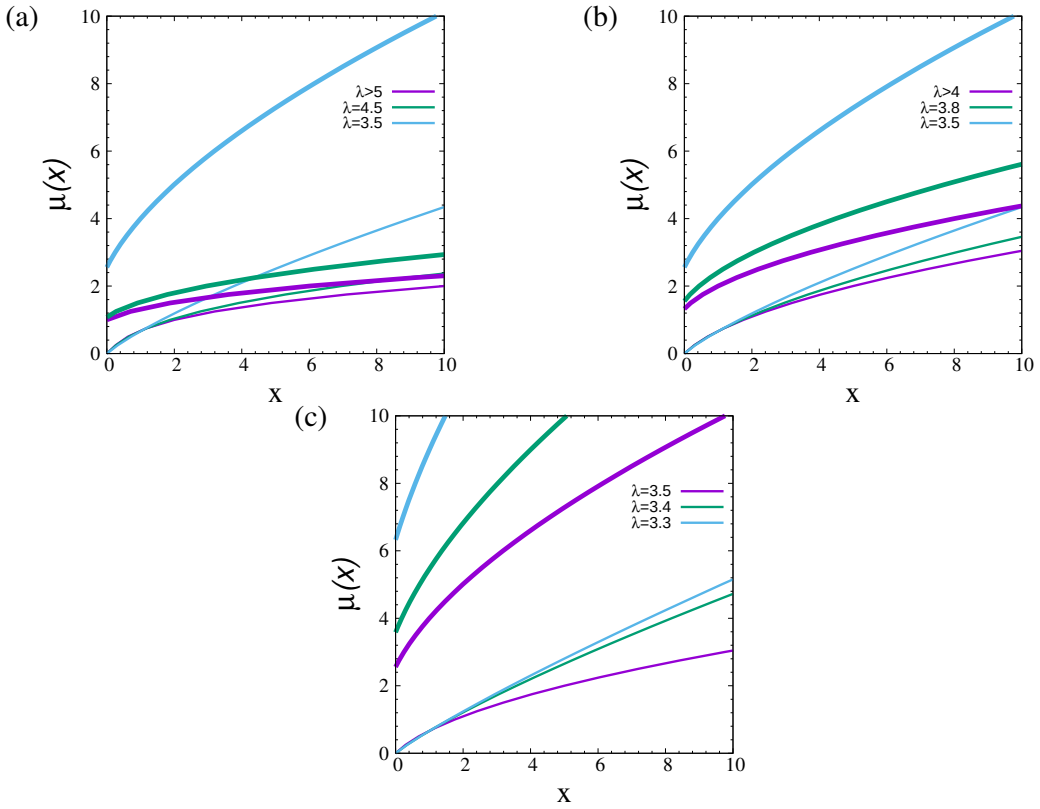

Fig. 2.4: Behaviour of the order parameter scaling functions $\mu_+(x)$ (thin curves) and $\mu_-(x)$ (thick curves) for different values of λ and q. **(a)**: $q = 2$, **(b)**: $1 \leq q < 2$, **(c)**: $q = 4$. Values of λ are shown in the figures.

regions on q–λ plane: $\mathcal{S}(x) = -x^2/2$. In the Widom-Griffiths representation [185, 186] the magnetic equation of state can be written in two equivalent forms:

$$H = m^{\delta} H_{\pm}(\tau/m^{1/\beta}), \qquad H = \tau^{\beta\delta} H'_{\pm}(m/\tau^{\beta}), \tag{2.79}$$

with scaling functions $H_{\pm}(x)$ and $H'_{\pm}(x)$. Alternatively, in Hankey-Stanley representation the magnetization is written as [184]:

$$m = \tau^{\beta} \mu_{\pm}(H/\tau^{\beta\delta}) \tag{2.80}$$

with the scaling function $\mu_{\pm}(x)$.

Starting from the magnetic equation of state given in regions I–III by Eqs. (2.75)–(2.77) it is straightforward to arrive at the scaling functions $H'_{\pm}(x)$. We give the appropriate expressions in table 2.5. Subsequently, one can easily rewrite these expressions to get appropriate $H_{\pm}$-functions. The behaviour of the scaling functions $\mu_{\pm}(x)$

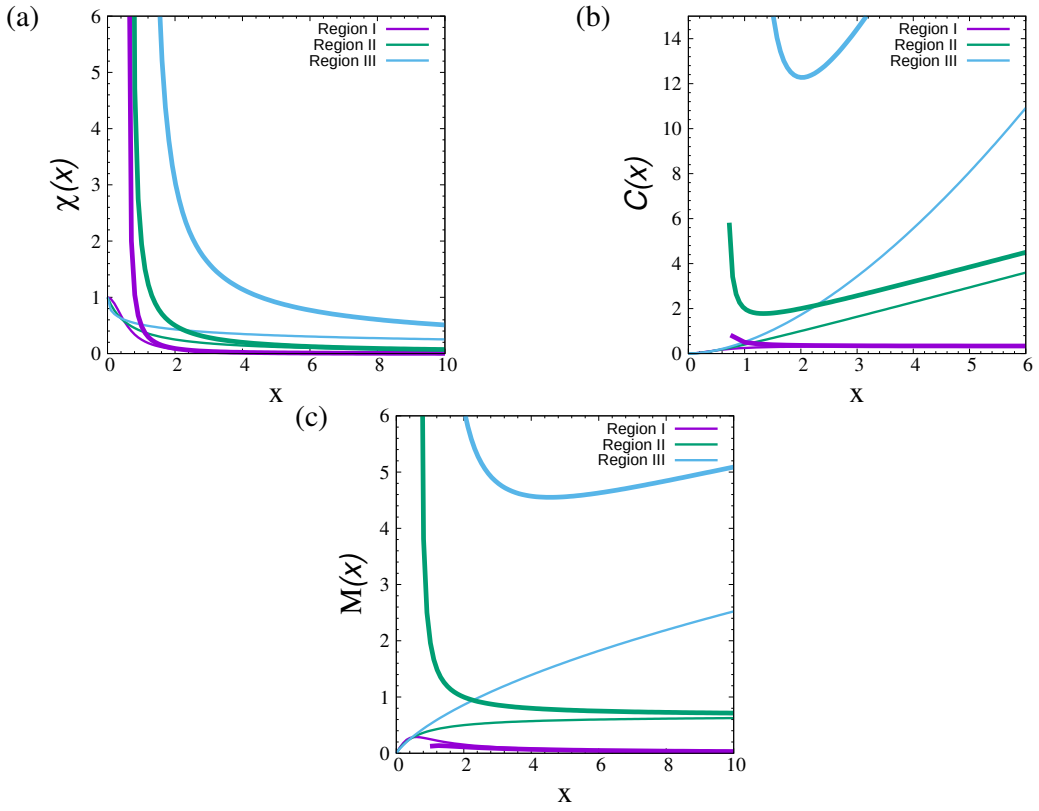

Fig. 2.5: Scaling functions for **(a)** isothermal susceptibility, **(b)** heat capacity, and **(c)** magnetocaloric coefficient. Thin curves, $T > T_c$: $\chi_+(x), \mathcal{C}_+(x), \mathcal{M}_+(x)$. Thick curves, $T < T_c$: $\chi_-(x), \mathcal{C}_-(x), \mathcal{M}_-(x)$. Violet, green and blue curves correspond to the values of q and λ of the free energy scaling functions of Fig. 2.3.

for different values of λ and q is shown in Fig. 2.4. From the explicit form of the equation of state it is easy to evaluate the asymptotic behaviour of the scaling functions. For $q = 2$ and $\lambda > 5$ one gets $\mu_\pm(x) \sim x^{1/3}$, $x \to \infty$. The functions demonstrate a tendency to turn to infinity faster with the decrease of λ: $\mu_\pm(x) \sim x^{1/(\lambda-2)}$, $x \to \infty$ for $3 < \lambda < 5$. A similar feature is observed for the other values of q. At $1 \leq q < 2$, $\lambda > 4$ one gets $\mu_\pm(x) \sim \sqrt{x}$, $x \to \infty$ and $\mu_\pm(x) \sim x^{1/(\lambda-2)}$, $x \to \infty$ for $3 < \lambda < 4$. The last asymptotic behaviour holds also for $q > 2$ and $\lambda \leq \lambda_c(q)$. Note as well that all thin curves of Fig. 2.4 start form the origin: this corresponds to the absence of spontaneous magnetization at $T > T_c$. Correspondingly, the value of the scaling function $\mu_-(x)$ at $x = 0$ gives the spontaneous magnetization critical amplitude B_-, Eq. (2.50). As one can see from the Fig. 2.4, the latter increases with the decrease of λ.

In figures 2.5 we show the behaviour of the scaling functions for the thermodynamic observables that characterize the responses of the system to an external action: the isothermal susceptibility (Fig. 2.5**a**), heat capacity (Fig. 2.5**b**), and magnetocaloric coefficient (Fig. 2.5**c**). The values of q and λ, for which the curves are plotted are

the same as those for the free energy scaling functions of Fig. 2.3: they reflect the limiting behaviour at some marginal value $\lambda_c(q)$. At $1 \leq q \leq 2$ and $\lambda > \lambda_c(q)$ the phase transition remains the second order but the critical exponents do not depend on λ any more, the scaling function do not depend on λ either. However, for $q > 2$, $\lambda > \lambda_c(q)$ the phase transition turns to the first order and the scaling regime does not hold any more. In turn, in the region below λ_c the exponents acquire λ-dependency, so do the scaling functions, as is plotted in the figures.

2.5.3 Notes about percolation on scale-free networks

By the results of previous section we cover also the case $q = 1$, that corresponds to percolation on uncorrelated scale-free networks. The 'magnetic' exponents governing corresponding second order phase transition are given in Tables 4.1, 4.2. Let us discuss them in more detail, in particular relating them to percolation exponents. The following exponents are usually introduced to describe behaviour of different observables near the percolation[7] point p_c [187, 188]: the probability that a given site belongs to the spanning cluster

$$P_\infty \sim (p - p_c)^\beta, \quad p > p_c\,, \tag{2.81}$$

the number of clusters of size s

$$n_s \sim s^{-\tau} e^{-s/s^*}, \tag{2.82}$$

the cluster size at criticality

$$s^* \sim |p - p_c|^{-\sigma}, \tag{2.83}$$

the average size of finite clusters

$$\langle s \rangle \sim |p - p_c|^{-\gamma}. \tag{2.84}$$

The above defined exponents β and γ coincide with the 'magnetic' exponents β and γ of the $q = 1$ Potts model (see Tables 4.1, 4.2). Therefore, the probability that a given site belongs to the spanning cluster and the average size of finite clusters for

[7]For definiteness, let us consider the site percolation and denote by p here and below the site occupation probability.

percolation on uncorrelated scale-free networks are governed by the scaling exponents:

$$\beta = \begin{cases} \frac{1}{\lambda-3}, & 3 < \lambda < 4, \\ 1, & \lambda > 4, \end{cases} \tag{2.85}$$

$$\gamma = 1, \qquad \lambda > 3. \tag{2.86}$$

The exponents τ and σ may be derived with the help of familiar scaling relations [187, 188]:

$$\sigma\beta = \tau - 2, \tag{2.87}$$

$$\gamma = (3 - \tau)/\sigma. \tag{2.88}$$

Substituting the values of β and γ (2.85), (2.86) into (2.87), (2.88) one arrives at the following expressions for the exponents τ and σ:

$$\tau = \begin{cases} \frac{2\lambda-3}{\lambda-2}, & 3 < \lambda < 4, \\ \frac{5}{2}, & \lambda > 4, \end{cases} \tag{2.89}$$

$$\sigma = \begin{cases} \frac{\lambda-3}{\lambda-2}, & 3 < \lambda < 4, \\ 1/2, & \lambda > 4. \end{cases} \tag{2.90}$$

Analysing the high-temperature behaviour of the Potts model magnetization at $2 < \lambda < 3$, one arrives to the scaling exponents $\beta = 1/(3-\lambda)$, $\gamma = -1$ for the corresponding observables for percolation at $p_c = 0$.

Our formulas (2.85), (2.86), (2.89), and (2.90) reproduce the results for the scaling exponents that govern percolation on uncorrelated scale-free networks [180, 189] and also those that were found for the related models of virus spreading [105, 190]. All the above mentioned papers do not discuss explicitly the case $\lambda = 4$ and possible logarithmic corrections that arise there. Moreover, a recent review [191], that also discusses the peculiarities of percolation on uncorrelated scale-free networks does not report about logarithmic corrections (its Eq. (95) is perhaps wrong since it gives no logarithmic corrections for $\lambda = 4$). Our results are listed in the first row of the Table 4.2 where we give a comprehensive list of critical exponents that govern logarithmic corrections to scaling appearing for the Potts model at $q = 1$, $\lambda = 4$, as correctly predicted within the general Landau theory for systems of arbitrary symmetry on uncorrelated scale-free networks [108]. One may compare our values to the corresponding exponents of the d-dimensional lattice percolation at $d = 6$: $\hat{\alpha} = \hat{\beta} = \hat{\gamma} = \hat{\delta} = \hat{\alpha}_c = 2/7$ (see e.g. [89]). In this respect the logarithmic-correction exponents for the lattice percolation at $d = 6$

and for the scale-free network percolation at $\lambda = 4$ belong to different universality classes. It is easy to check, that the exponents quoted in the last row of Table 4.2 obey the scaling relations for the logarithmic-corrections exponents [88, 192, 193]:

$$\hat{\beta}(\delta - 1) = \delta\hat{\delta} - \hat{\gamma}, \qquad \hat{\alpha} = 2\hat{\beta} - \hat{\gamma},$$

$$\hat{\gamma_c} = \hat{\delta}, \qquad \hat{\alpha_c} = \frac{(\gamma + 2)(\hat{\beta} - \hat{\gamma})}{\beta + \gamma} + \hat{\gamma}.$$

2.5.4 The discontinuity of the specific heat

For magnetic systems, it is well known that the isothermal susceptibility χ_T and magnetocaloric coefficient m_T (a mixed derivative of the free energy with respect to magnetic field and temperature) are strongly diverging quantities, whereas the specific heat c_h often does not diverge at T_c. Considered in the mean-field approximation, the first two quantities are singular at $\tau = |T - T_c|/T_c = 0$: $\chi_T \sim \tau^{-\gamma}$, $m_T \sim \tau^{-\omega}$ with $\gamma^{\text{mfa}} = 1$, $\omega^{\text{mfa}} = 1/2$. But the third quantity displays a jump at T_c:

$$\delta c_h = c_h(T \to T_c^-) - c_h(T \to T_c^+), \tag{2.91}$$

with $\delta c_h^{\text{mfa}} = 3/2$ and hence $c_h \sim \tau^{-\alpha}$ with $\alpha^{\text{mfa}} = 0$.

Here, the subject of our analysis is the Ising model on a complex scale-free network. In particular, we will consider the behaviour of the specific heat on an annealed network. This has been widely used to analyze properties of various spin models (see e.g. [62] and references therein). For annealed networks, the links fluctuate on the same time scale as the spin variables [62], therefore the partition function is averaged both with respect to the link distribution as well as the Boltzmann distribution (see section 5 for mode details). The Hamiltonian of the Ising model in the absence of an external magnetic field, reads:

$$\mathcal{H} = -\frac{1}{N\langle k\rangle}\sum_{i>j} k_i k_j S_i S_j. \tag{2.92}$$

Here, $S_i = \pm 1$ is a spin variable, the sum spans all pairs of N nodes and $\langle k\rangle = \sum_{i=1}^{N} k_i/N$.

The prominent feature of (2.92) is that the interaction term attains a separable form. In turn, this allows for an exact representation of the partition function via e.g. Stratonovich-Hubbard transformation, as it is usually done for the Ising model on a complete graph [194], see [21] and references therein. Here we will be interested in the

behaviour of the specific heat in the region $\lambda > 5$, where usual mean-field results for the critical exponents hold. Keeping terms leading in N for the partition function, one can represent it in the form (see [21] or Section 4 for more details)

$$Z_N(T) = \int_{-\infty}^{+\infty} e^{N(\frac{-\langle k\rangle x^2}{2}(T-T_c)-\frac{\langle k^4\rangle x^4}{12})} dx\,, \qquad \lambda > 5, \tag{2.93}$$

where $T_c = \langle k^2\rangle/\langle k\rangle$ and we have omitted a prefactor which is not important for our analysis.

Using the method of steepest descent one finds points of maxima ($x_\star$) of the function under integration at $T > T_c$ ($x_\star = 0$) and $T < T_c$ ($x_\star = \sqrt{-\frac{3\langle k\rangle}{\langle k^4\rangle}(T-T_c)}$). The free energy reads:

$$f(T) \quad = 0, \quad T > T_c\,, \tag{2.94}$$

$$= -\frac{3\langle k\rangle^2}{4\langle k^4\rangle} T(T-T_c)^2, \quad T < T_c. \tag{2.95}$$

Correspondingly, for the specific heat one obtains

$$c_h \quad = 0, \quad T > T_c\,, \tag{2.96}$$

$$= -\frac{9\langle k\rangle^2}{2\langle k^4\rangle} T^2 + \frac{6\langle k\rangle^2}{2\langle k^4\rangle} T T_c, \quad T < T_c. \tag{2.97}$$

The jump of the specific heat at T_c is defined by the ratio

$$\delta c_h = \frac{3\langle k^2\rangle^2}{2\langle k^4\rangle}. \tag{2.98}$$

Substituting the averages calculated with the distribution (1.7) we obtain

$$\delta c_h = \frac{3(\lambda-5)(\lambda-1)}{2(\lambda-3)^2}, \qquad \lambda > 5\,. \tag{2.99}$$

In the limit of large λ this delivers $\delta c_h = 3/2$, which coincides with the corresponding value on a complete graph.

It is well known that Ising model on an annealed scale-free network is characterized by classical mean-field exponents at $\lambda > 5$. As we have shown in this note, the mean-field behaviour does not concern the specific heat jump δc_h at $\lambda > 5$. The jump remains λ-dependent and reaches the mean-field value $\delta c_h = 3/2$ only in the limit $\lambda \to \infty$. The function $\delta c_h(\lambda)$ is shown in Fig. 2.6. Similar effect has been observed for the Ising model

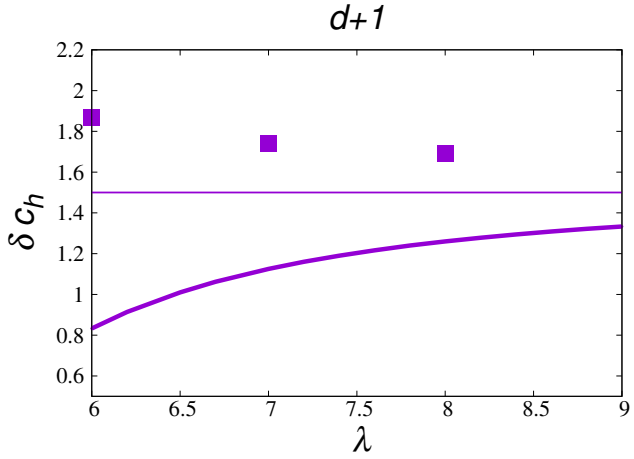

Fig. 2.6: The jump in the specific heat of the Ising model on lattices at $d > 4$ (squares, results of MC simulations [195]) and on an annealed scale-free network for $\lambda > 5$, bold line Eq. (2.99). The thin line shows classical mean-field value $\delta c_h = 3/2$. Although $\delta c_h(\lambda \to \infty) = \delta c_h(d \to \infty) = 3/2$, the functions approach the mean-field limit from below and from above.

on lattices at $d > 4$. We show the results of MC simulations of $d = 5, 6, 7$-dimensional lattices [195] on the figure too. Note, that although $\delta c_h(\lambda \to \infty) = \delta c_h(d \to \infty) = 3/2$, the functions approach the mean-field limit from below and from above. Another essential difference between the behaviour of c_h in the Ising model on scale-free networks and on lattices is observed directly at the upper critical values of λ and of d, respectively. While $\alpha = 0$ in both cases, the overall behaviour of c_h remains singular on lattices at $d = 4$ (logarithmic singularity, $\hat{\alpha} = 1/3$) whereas $\hat{\alpha} = -1$ for networks at $\lambda = 5$ and hence $\delta c_h = 0$. This last case provides an example where the logarithmic correction to scaling leads to smoothing of behaviour of the thermodynamic function at T_c.

2.6 The first order phase transition regime

For $q > 2$, $\lambda > \lambda_c(q)$ the phase transition is of the first order, see the phase diagram on Fig. 2.2. As we have outlined in Sec. 2.4.3, the next-leading order term of the free energy has a negative sign and the free energy behaves as shown in Fig. 2.1**b**. As further analysis shows, the higher the value of λ the more terms one has to take into account in the free energy expansion in order to ensure the correct $g(m)$ asymptotics. Therefore, in the results given below we restrict ourselves by the region $\lambda_c(q) < \lambda < 4$, where the free energy is given by Eq. (2.41). The first order phase transition temperature T_c^{1st} is found from the condition $g(m = 0, T_c^{1st}) = g(m \neq 0, T_c^{1st})$, see the red (middle) curve

in Fig. 2.1**b**:

$$T_c^{1st} = T_0 + \Big(\frac{-B}{3K(\lambda-1)(\lambda-3)}\Big)^{\frac{\lambda-3}{\lambda-4}} \frac{2K(\lambda-1)(\lambda-4)}{A}. \tag{2.100}$$

For the jump of the order parameter Δm at T_c we find:

$$\Delta m = \Big(\frac{-B}{3K(\lambda-1)(\lambda-3)}\Big)^{\frac{1}{\lambda-4}}. \tag{2.101}$$

Another thermodynamics function to characterize the first order phase transition is the latent heat Q. It is defined by:

$$Q = \Delta S \cdot T_c^{1st}, \tag{2.102}$$

where ΔS is the jump of entropy at T_c. With the free energy given by (2.41) we find the entropy as

$$S = -\Big(\frac{\partial g}{\partial T}\Big)_{h,m}. \tag{2.103}$$

Considering the entropy at the transition temperature we can find the latent heat at the first order phase transition for $\lambda_c(q) < \lambda < 4$:

$$Q = \frac{A}{2}(\Delta m)^2. \tag{2.104}$$

2.7 Conclusions

In this section we study the critical behavior of the Potts model on an uncorrelated scale-free network in terms of inhomogeneous mean-field approximation. However, unlike the authors [93], who had analyzed the equation of state, we examined the free energy of the systems. We have firstly obtained a set of scaling functions and critical amplitude ratios for the model in the second order phase transition regime. These values, like critical exponents are quantitative characteristics of the universality class. Although the critical exponent γ for a isothermal susceptibility becomes constant at different λ critical amplitude ratios Γ^+/Γ^- are λ-dependent. For the percolation on a scale-free network (limit $q \to 1$ for the Potts model) the appearance of logarithmic corrections to scaling was observed.

The resent simulations for the Ising model on lattices at $d > 4$ demonstrate that the jump of the heat capacity is d-dependent and tends to the mean-field value $\delta c_H = 3/2$ in the limit $d \to \infty$ [195]. Our analysis for the behavior of heat capacity of Ising model

on a scale-free network demonstrates that the jump of heat capacity δc_H becomes λ-dependent in a region $\lambda > 5$ and $\delta c_H(\lambda \to \infty) = 3/2$.

Chapter 3 | PARTITION FUNCTION ZEROS FOR THE ISING MODEL ON A COMPLETE GRAPH

Contents

In this chapter we present the results obtained using the partition function zeros analysis for the Ising model in the complex temperature (Fisher zeros) and magnetic field (Lee-Yang zeros) plane. We use the method proposed in [196] and generalize it to the case of complex field. Considering the Ising model on a complete graph we obtain the exact representation of the partition in complex plane (section 3.1). Fisher zeros are analyzed in section 3.2 and Lee-Yang zeros are considered in section 3.3. The motion of Fisher zeros in the presence of a real magnetic field will be analyzed in section 3.4. The general conclusions are summarized in section 3.5. The results of this chapter were published in [21, 22].

3.1 Partition function

In this section we consider the infinite-range version of the Ising model which is equivalent to the mean-field version of its lattice counterpart [194,197]. It can be also regarded as an Ising model on a complete graph, where each node of the graph is connected to

every other node making all interspin couplings equal to each other. The Hamiltonian of the model reads

$$-\mathcal{H} = \frac{1}{2N}\sum_{l\neq m} S_l S_m + H\sum_l S_l\,. \tag{3.1}$$

Here, indices l, m label the nodes of the graph so that $(l,m) = 1,\ldots,N$; $S_l = \pm 1$ are the Ising spins; H is an external magnetic field and the sum $\sum_{l\neq m}$ spans all pairs of nodes (not necessarily the nearest neighbours). The coupling between the spins is taken to be inversely proportional to the number of nodes, to make the model meaningful in the thermodynamic limit $N\to\infty$. One can obtain an integral representation for the partition function of the model (3.1) by making use of the equality $(\sum_l S_l)^2 = N + \sum_{l\neq m} S_l S_m$ to write for the N-particle partition function

$$Z_N(T,H) = \mathrm{Tr}\, e^{-\beta\mathcal{H}} = e^{-\frac{\beta}{2}}\prod_{l=1}^{N}\sum_{S_l=\pm 1}\exp\Big(\frac{\beta}{2N}(\sum_l S_l)^2 + \beta H\sum_l S_l\Big)\,, \tag{3.2}$$

and then applying Hubbard-Stratonovich transformation to express the partition function in the form where summation over S_l can be taken exactly:

$$Z_N(T,H) = e^{-\frac{\beta}{2}}\sqrt{\frac{N\beta}{2\pi}}\prod_{l=1}^{N}\sum_{S_l=\pm 1}\int_{-\infty}^{+\infty}\exp\Big(\frac{-Nx^2\beta}{2} + \sum_m S_m\beta(x+H)\Big)dx\,. \tag{3.3}$$

Performing the summation, one arrives at the integral representation for the partition function of the Ising model on the complete graph:

$$Z_N(T,H) = \int_{-\infty}^{+\infty}\exp\Big(\frac{-Nx^2}{2T} + N\ln\cosh[(x+H)/T]\Big)dx\,, \tag{3.4}$$

where we have explicitly written the temperature $T=\beta^{-1}$ dependency taking the Boltzmann constant value $k_B = 1$. In (3.4) and in all other partition function integral representations below, we omit the irrelevant prefactors.

In classical settings, to get thermodynamic functions, the integral (3.4) is taken by the steepest descent method, see, e.g. [194]. In particular, the model undergoes a second order phase transition at $T_c = 1$ which is governed by the standard mean-field values of the critical exponents:

$$\alpha = 0,\quad \beta = 1/2,\quad \delta = 3,\quad \gamma = 1\,. \tag{3.5}$$

For the sake of convenience it is appropriate to rewrite the partition function (3.4) in

the reduced temperature variable $t = (T - T_c)/T_c = T - 1$. Changing the integration variable $\sqrt{N}x/T \to x$ one gets [196]:

$$Z_N(t, H) = \int_{-\infty}^{+\infty} \exp\Big(\frac{-x^2(t+1)}{2} + N \ln\cosh[x/\sqrt{N} + H/(t+1)]\Big) dx\,, \tag{3.6}$$

where the temperature dependent prefactor again has been omitted. Being primarily interested in the properties of the partition function itself, we approximate (3.6) by its expansion at large N and small H. Keeping the leading order contributions in the linear in H term, we expand the exponent function for $N \to \infty$ and get [196]:

$$Z_N^{\exp}(t, H) = \int_{-\infty}^{+\infty} \exp\Big(\frac{-t\,x^2}{2} - \frac{x^4}{12N} + \frac{x\sqrt{N}H}{t+1} + O(1/N^2)\Big) dx. \tag{3.7}$$

In the remainder of this section we analyze the expressions for the exact and approximated partition functions of the Ising model on a complete graph, Eqs. (3.6) and (3.7).

3.2 Fisher zeros

We start from the analysis of the exact integral representation for the partition function at zero external field. First, we obtain the Fisher zeros by solving the system of equations $\mathrm{Re}\, Z(t, H) = 0$ and $\mathrm{Im}\, Z(t, H) = 0$ for the complex variables $t = \mathrm{Re}\, t + i\,\mathrm{Im}\, t$ using function (3.6) at $H = 0$. In Fig. 3.1**a** we show the first five Fisher zeros in the t plane for increasing values of $N = 50$, 200, 2000. They collapse on a master curve and in the vicinity of the critical point, they impact onto the real axis, defining the angle φ.

It is instructive also to observe the motion of the zeros if the temperature is parameterised in a different way. Let us introduce the reduced inverse temperature:

$$\tau = (1/T_c - 1/T)/(1/T_c) = 1 - 1/T\,, \tag{3.8}$$

getting from (3.4) at $H = 0$:

$$Z_N(\tau) = \int_{-\infty}^{+\infty} \exp\Big(\frac{-Nx^2(1-\tau)}{2} + N \ln\cosh[(1-\tau)x]\Big) dx. \tag{3.9}$$

The zeros of the function (3.9) in the complex τ plane are shown in Fig. 3.1**b**. As one can see from the figures, the zeros form a smooth curve and accumulate in the

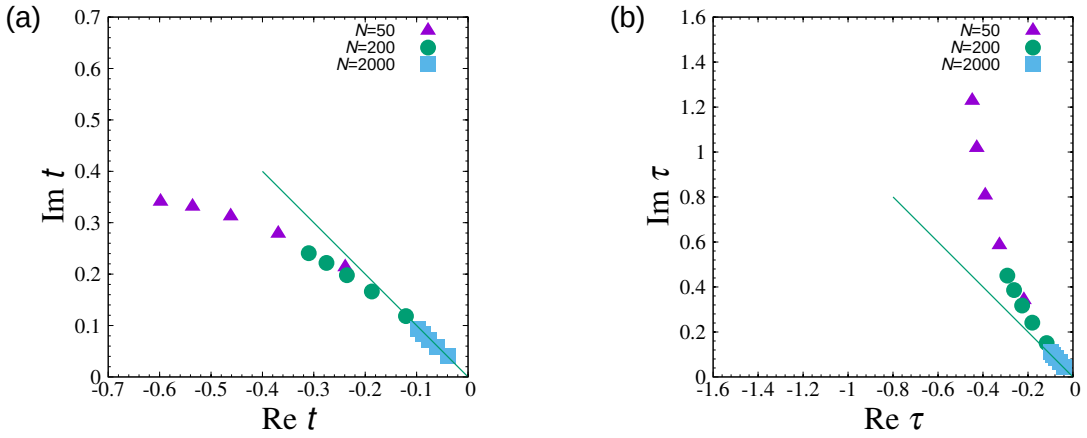

Fig. 3.1: The first five Fisher zeros for the exact partition function (3.6) with different values of N **(a)** in the complex t plane ($t = T - 1$) and **(b)** in the complex τ plane $\tau = 1 - 1/T$. With increasing N, the zeros accumulate at the critical point, pinching the real axis at $t = \tau = 0$. The solid line has an angle $\varphi = \pi/4$ with the real axis.

vicinity of the critical point ($t = \tau = 0$), and with an increase of N they tend to pinch the real positive temperature axis at the critical point. Using known values of the critical exponents and amplitude ratios one can evaluate the value of the angle φ under which the zeros pinch the real axis. Substituting (3.5) into (1.10) and taking that the corresponding heat capacity amplitude ratio $A_+/A_- = 0$ one arrives at

$$\varphi = \pi/4\,. \tag{3.10}$$

This value in shown in the Fig. 3.1 by the solid line. The fact that the lines along which the zeros tend to accumulate with increasing N make the same angle φ both in the t and τ planes illustrates the conformal invariance of this angle – angles are independent of any real analytic parametrization in the complex plane. However, the approach of the angle to its value in the thermodynamic limit $N \to \infty$ is parametrization dependent. Indeed, depending on parametrization, the curves of Fig. 3.1 reach the asymptotics from below (Panel a) or from above (Panel b). This is further outlined in Fig. 3.2, where we show how the values of the angle φ and of the critical temperature change with N. To this end, we calculate the first five Fisher zeros for the system sizes ranging up to $N = 50000$, fit these points by a straight line and find the values of the angle (taking $P = \varphi/\pi$ so that Eq.(3.10) predicts $P = 0.25$) and of the crossing point of this line with the real axis. The larger the system size, the more accurate the fit is (for $N > 100$ the accuracy interval is less than the size of the data symbols in the figure). Starting from $N = 5000$, φ differs from its exact value ($\varphi = \pi/4$) by less than 1% while the critical temperature differs from the exact value at $t = 0$ by less than 1% starting

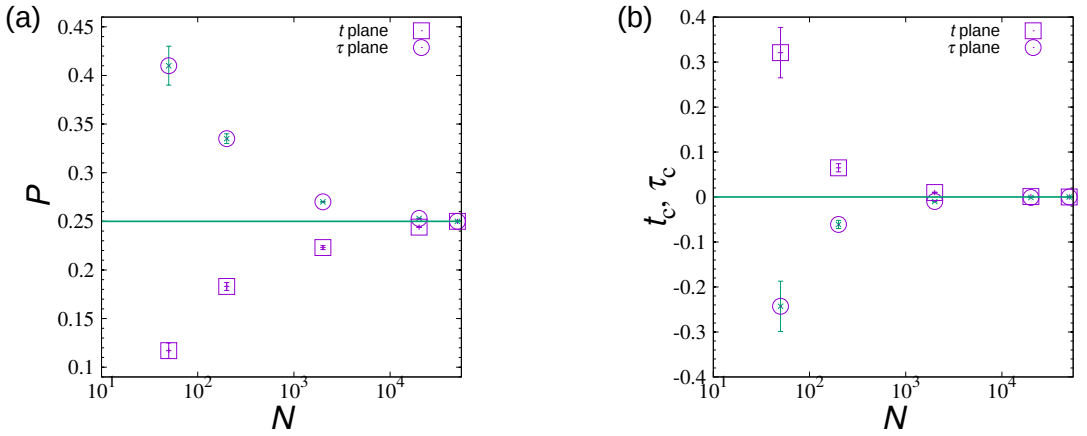

Fig. 3.2: Values of **(a)** the reduced impact angle $P = \varphi/\pi$ and of **(b)** the critical temperature for the exact partition function obtained by fitting of the first five Fisher zeros for different N. Squares: results in the complex t plane; discs: results in the complex τ plane; lines: exact results. The larger the system size, the more accurate is the fit. For $N > 100$ the accuracy interval is less than the size of the data point in the figure.

from $N = 10000$.

Figs. 3.1 and 3.2 quantify the main features of the behaviour of the Fisher zeros for the exact partition function (3.4) in the complex temperature plane. Results for the impact angle φ and for the critical temperature obtained on their basis if compared with the exact results demonstrate two tendencies: (i) they improve with an increase of N and (ii) the agreement is better for smaller values of the index j.

We now turn our attention to the zeros of the approximated partition function (3.7) to check how are these tendencies manifested in this case. For zero magnetic field, keeping only the term leading in $1/N$, the partition function (3.7) reads

$$Z_N^{\exp}(t) = \int_{-\infty}^{+\infty} \exp\Big(-\frac{x^2 t}{2} - \frac{x^4}{12N}\Big) dx\,. \tag{3.11}$$

The first five Fisher zeros for the approximated partition function (3.11) are shown in the complex t plane in Fig. 3.3**a** for different values of N. Similarly as for the exact partition function (cf. Fig. 3.1**a**), with an increase of N, the zeros accumulate in the vicinity of the critical point and tend to pinch the real axis at the critical point. An obvious difference in the behaviour of zeros for the exact and expanded partition functions is that in the last case the angle of zeros accumulation is very robust and almost does not depend on N. The reason becomes apparent when the function under the integral in (3.11) is rewritten as

$$Z(z) = \int_{-\infty}^{+\infty} \exp\Big(-z\,x^2 - x^4\Big) dx\,, \tag{3.12}$$

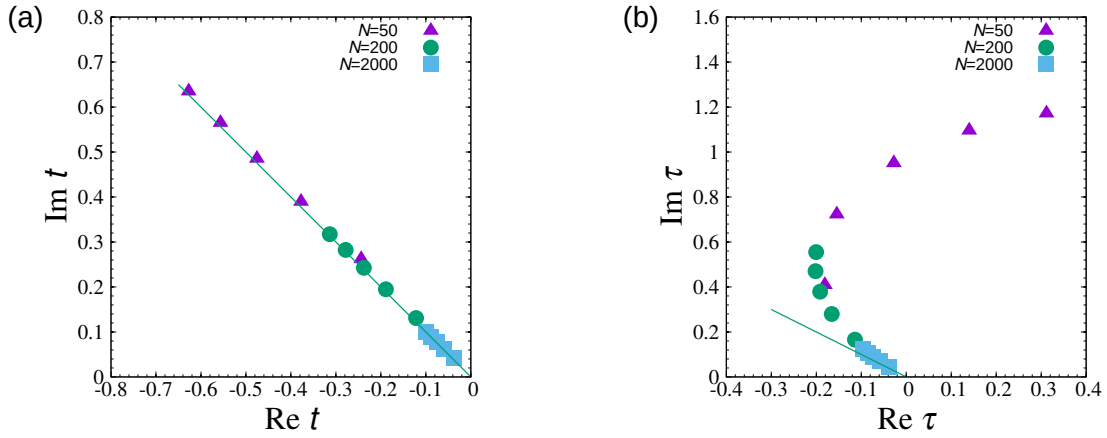

Fig. 3.3: First five Fisher zeros for the approximated partition function for different values of N **(a)** in the complex t plane (Eq. (3.11)) and **(b)** in the complex τ plane (Eq. (3.14)). The solid line has an impact angle $\varphi = \pi/4$.

where the N and temperature dependencies are combined in the single scaling variable z

$$z = \sqrt{3N}t\,. \tag{3.13}$$

Now it is easy to see that the connection between two sets of zeros $t_j(N_1)$ and $t_j(N_2)$ calculated for two different system sizes N_1 and N_2 is given by a simple rescaling: $t_j(N_1) = t_j(N_2)\sqrt{N_1/N_2}$. This, in turn, is manifested by the fact that zeros calculated for different system sizes align along the same curve in Fig. 3.3**a**.

The same expression (3.11), written for different values of N expressed in terms of the variable τ takes the form

$$Z_N^{\exp}(\tau) = \int_{-\infty}^{+\infty} \exp\Big(-\frac{x^2(\tau-\tau^2)}{2} - \frac{x^4(1-\tau)^4}{12N}\Big)dx\,. \tag{3.14}$$

Here, the τ dependence is non-linear and the zeros are non-trivial functions of N. Indeed, the first few are depicted in Fig. 3.3**b** where one finds behaviour rather similar to that demonstrated in Fig. 3.1 for the exact partition function: sets of zeros calculated at different N tend to form the common curved locus. However, evaluating (3.14) near the critical point for small τ and keeping the leading order contributions in the linear term in τ, one arrives at the expression for $Z_N^{\exp}(\tau)$ that coincides with the corresponding expression (3.7) for $Z_N^{\exp}(t)$ in which t is simply substituted by τ. In turn, at zero magnetic field and close to the critical point, functions $Z_N^{\exp}(\tau)$ and $Z_N^{\exp}(t)$ attain the same form given by Eq. (3.11). In particular, in this approximation the $Z_N^{\exp}(\tau)$ function was considered in [196].

Zeros of the partition function (3.12) in the complex z plane are shown in Fig. 3.4.

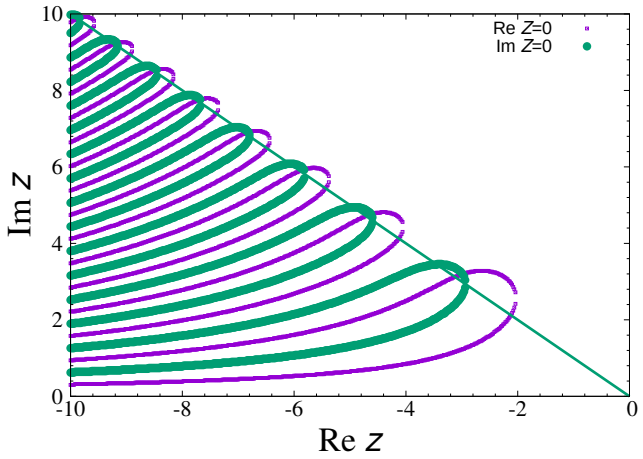

Fig. 3.4: Loci of zeros of the real and imaginary parts of the approximated partition function (3.12) are plotted as thick and thin curves respectively (green and violet dots online). The points where the lines cross give the coordinates of the Fisher zeros. These have to align along the straight solid line in the asymptotic limit.

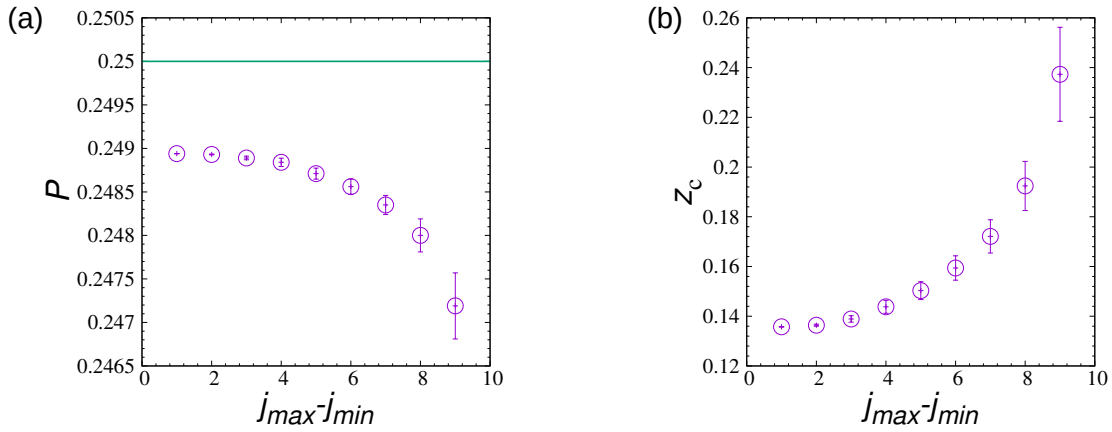

Fig. 3.5: Estimates **(a)** for the reduced impact angle $P = \varphi/\pi$ and **(b)** for the critical temperature z_c for the partition function (3.12) obtained by fitting of Fisher zeros in the interval $j = j_{\min}, \ldots, j_{\max}$ for $j_{\max} = 10$ and different values of $j_{\min}$. The solid line in Panel a represents the exact value $P = 1/4$.

The thick and thin curves (green and violet online) give solutions of the equations $\mathrm{Re}\, Z(z) = 0$ and $\mathrm{Im}\, Z(z) = 0$, respectively. The crossing points of the lines give coordinates of the Fisher zeros. These have to align in the asymptotic limit $N \to \infty$ along the line forming an angle $\varphi = \pi/4$ and starting at the critical point (the straight line in the figure). As it is clearly seen within the scale of the figure, the higher the index of the zero, the closer it is to the line. This tendency is further outlined in Fig. 3.5, which demonstrates the behaviour of the angle φ and of the estimates for critical value z_c if they are obtained by fitting finite numbers of Fisher zeros in the interval $j = j_{\min}, \ldots, j_{\max}$ to a straight line. Fits for high j-values give better results. This tendency differs from the one observed above for the zeros in complex t and τ

planes (see Fig. 3.2) and is explained by the form of the scaling variable (3.13), which incorporates now both the temperature and the system size dependencies.

The coordinates of the first nine Fisher zeros in the z plane as obtained by numerical solution of the system of equations (1.9) are listed in the left column of Table 3.1.

Table 3.1: Fisher zeros of the partition function (3.12). The second column shows our numerical results for the zeros given by $j = 1, \ldots, 9$. In the third column they are compared with the values given by the asymptotic formula (3.16): $\mathrm{Re}\, z_j = -\mathrm{Im}\, z_j = \sqrt{4\pi j}$. When digits in the left and right columns coincide, they are underlined. Starting from $j = 9$ the numerically calculated values coincide with their asymptotic counterparts within the accuracy presented.

j	Numeric	Eq. (3.16)
1	$-2.9852 + i3.2061$	$-2.9823 + i3.2023$
2	$-4.6236 + i4.7707$	$-4.6231 + i4.7700$
3	$-5.8237 + i5.9414$	$-5.8235 + i5.9411$
4	$-6.8167 + i6.9176$	$-6.8167 + i6.9174$
5	$-7.6829 + i7.7725$	$-7.6828 + i7.7724$
6	$-8.4610 + i8.5425$	$-8.4609 + i8.5424$
7	$-9.1734 + i9.2486$	$-9.1733 + i9.2486$
8	$-9.8343 + i9.9046$	$-9.8343 + i9.9045$
9	$-10.4536 + i10.5197$	$-10.4536 + i10.5197$

As one observes from the table, as the zero-index j increases, its real and imaginary part become closer, which corresponds to an approach of φ to the value $\varphi = \pi/4$ (see also Fig. 3.4). The value of z_j for high j can be evaluated asymptotically, writing the partition function (3.12) via the special functions:

$$Z(z) = \frac{\sqrt{z}}{4} \exp\Big(\frac{z^2}{8}\Big) K_{1/4}\Big(\frac{z^2}{8}\Big) = \frac{\sqrt{\pi}}{2^{5/4}} \exp\Big(\frac{z^2}{8}\Big) D_{-1/2}\Big(\frac{z}{2^{1/2}}\Big)\,, \tag{3.15}$$

where $K_{1/4}(x)$ and $D_{-1/2}(x)$ are the Bessel and parabolic cylinder functions [198], respectively. The leading term of the asymptotic expansion reads [196]:

$$z_j \simeq 2(2\pi j)^{1/2} \exp(3\pi i/4)\Big(1 + O(1/j)\Big), \tag{3.16}$$

which in turn leads to the fact that $\mathrm{Re}\, z_j = -\mathrm{Im}\, z_j = \sqrt{4\pi j}$ for high j. This asymptotic value is shown for different j in the right column of Table 3.1. Equation (3.16) has been obtained in Ref. [196] for $|z_j| \gg 1$. Since already for the first zero $|z_1| \simeq 4$, the asymptotic formula gives quite accurate values for the zeros for all j as one may see comparing the left and right columns of the table. Starting from $j = 9$ the numerically calculated values coincide with their asymptotic counterparts within the accuracy

presented.

3.3 Lee-Yang zeros

We now turn to the analysis of the partition function for complex magnetic field H at $T = T_c$. The exact expression for the partition function (3.6) at $t = \tau = 0$ reads:

$$Z_N(H) = \int_{-\infty}^{+\infty} \exp\Big(-\frac{x^2}{2} + N \ln\cosh[x/\sqrt{N} + H]\Big) dx. \tag{3.17}$$

On the other hand, keeping only contributions leading in N^{-1} in the expanded partition function (3.7) one gets:

$$Z_N^{\exp}(H) = \int_{-\infty}^{+\infty} \exp\Big(-\frac{x^4}{12N} + x\sqrt{N}H)\Big) dx\,. \tag{3.18}$$

It has been suggested [124] that at the critical point the partition function zeros scales as a fraction of their total number j/N for large values of the index j . Moreover, many models exhibit a scaling in the variable $(j - C)/N$ in which $C = 1/2$ is an empirical fitting factor [199, 200]. Recently, a more comprehensive form for the scaling of the Lee-Yang zeros in the critical region was suggested [201]. In our case it reads

$$\operatorname{Im} H_j \sim \Big(\frac{j - C}{N}\Big)^{\sigma}, \tag{3.19}$$

where the exponent σ is related to the order parameter and heat capacity critical exponents via

$$\sigma = \frac{\beta\,\delta}{2 - \alpha}\,. \tag{3.20}$$

Substituting the values of the exponents (3.5) into (3.20) one arrives at

$$\sigma = 3/4\,. \tag{3.21}$$

Next we check whether the scaling form (3.19) holds for the Lee-Yang zeros of the exact and approximated partition functions and we seek to estimate the value of the parameter C.

Solving the system of equations $\operatorname{Re} Z(t, H) = 0$ and $\operatorname{Im} Z(t, H) = 0$ at $t = t_c = 0$ for the real and imaginary parts of the exact partition function (3.17) we get coordinates of its zeros in the complex H plane. We find that the Lee-Yang zeros are purely imaginary

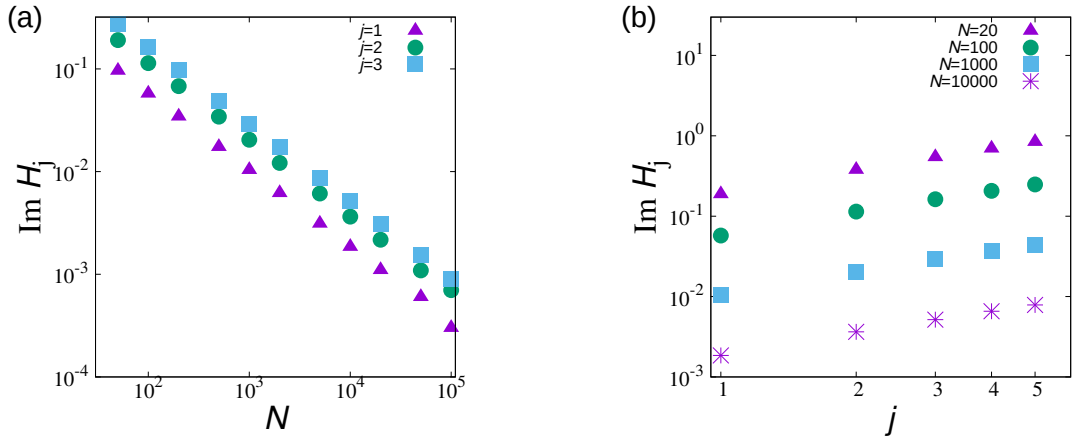

Fig. 3.6: The behaviour of $\mathrm{Im}\, H_j$ for several leading Lee-Yang zeros of the exact partition function (3.17). **(a)** The finite-size $\mathrm{Im}\ H_j(N)$ dependency for first three zeros $j = 1, 2, 3$. The scaling with N, Eq. (3.19), holds even for small N and j with an exponent very close to $\sigma = 3/4$. **(b)** Coordinates of the first five zeros calculated for several values of $N = 20$, 100, 1000, 10000. The scaling exponents remain almost unchanged for different N but they are far from their asymptotic value.

in this case. The fact that they lie on the imaginary axis validates the famous Lee-Yang circle theorem [118, 119]: expressed in terms of the variable e^H all zeros lie on a circle of unit radius. In Fig. 3.6**a** we plot numerical values of the coordinates of the first three Lee-Yang zeros as function of the system size N. There are two remarkable features of the plots of Fig. 3.6**a**: (i) all $H_j(N)$ dependencies are power laws (represented by straight lines in the log-log plots); (ii) these power laws are governed by the same value of the exponent (the lines are parallel) for different j. Therefore, the scaling with N as it is predicted by the equation (3.19) holds even for small N and j. Using linear fits for all eleven data points of the Fig. 3.6**a** we find for each j: $\sigma = 0.749(5)$ $(j = 1)$, $\sigma = 0.744(3)$ $(j = 2)$, $\sigma = 0.750(1)$ $(j = 3)$.

To check how the scaling of the zeros holds with j, we plot in Fig. 3.6**b** coordinates of the first five zeros calculated for several values of $N = 20$, 100, 1000, 10000. The fits to the power law dependency gives the following values of the exponent $\sigma = 0.930(22)$ $(N = 20)$, $\sigma = 0.909(22)$ $(N = 100)$, $\sigma = 0.901(22)$ $(N = 1000)$, $\sigma = 0.900(21)$ $(N = 10000)$: the exponents remain almost unchanged for different N but they are far from their asymptotic value $\sigma = 3/4$, Eq. (3.21). However, introducing a fit parameter C via equation (3.19) changes the picture. We fit the dependence of the first five Lee-Yang zeros on j on a log-log scale by a linear function at different values of the fitting parameter C and evaluate goodness of fits by calculating variance of residuals (reduced χ^2), i.e. the weighted sum-of-squares residuals divided by the number of degrees of freedom, further denoted by Δ. The $\Delta(C)$ curve is shown in Fig. 3.7, the optimal value of the fitting parameter C_{opt} corresponds to minimum of Δ. In our case

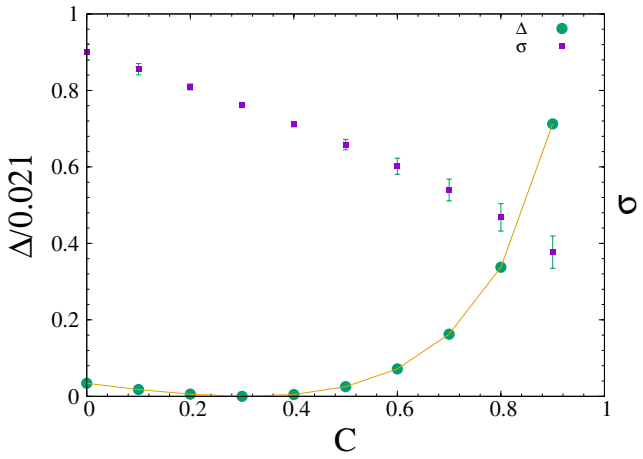

Fig. 3.7: Variance of residuals Δ and exponent σ obtained while fitting coordinates of the first five Lee Yang zeros via Eq. (3.19) as functions of the fitting parameter C. The optimal σ is evaluated at $C_{\rm opt} = 0.31$ where the $\Delta(C)$ curve has minimum. The resulting value $\sigma(C_{\rm opt}) = 0.7563(1)$ is close to the exact result $\sigma = 0.75$.

$C_{\rm opt} = 0.31$. Therefore, the value of the exponent σ is calculated as $\sigma(C_{\rm opt}) = 0.7563(1)$ and is close to the exact result $\sigma = 0.75$.

For the expanded partition function, Eq. (3.18) can be conveniently written in terms of the rescaled variables:

$$Z(h) = \int_{-\infty}^{+\infty} \exp\Big(- x^4 - x\, h\Big) dx, \tag{3.22}$$

where the field and the system size dependence is absorbed into a single variable

$$h = H(12N^3)^{1/4}. \tag{3.23}$$

Fig. 3.8 displays the lines of zeros for the real and imaginary parts of the partition function (3.22) at $T = T_c$ in the complex magnetic field h plane, thin and thick curves (violet and green online) respectively. Again, the coordinates of the Lee-Yang zeros (the crossing points of the lines) are purely imaginary (obeying the Lee-Yang circle theorem). The scaling of h_j with the system size N is given by (3.23) and hence the scaling exponent is equal to its asymptotic value (3.21) for any index j. Note, that since the real part of the Lee-Yang zero coordinate $\mathrm{Re}\, h = 0$, it is straightforward to show from (3.18) that the imaginary coordinate $\mathrm{Im}\, h$ is obtained as a solution of an integral equation:

$$\int_0^{\infty} e^{-x^4} \cos(x \mathrm{Im}\, h)\, dx = 0\,. \tag{3.24}$$

Let us consider now the scaling with j. To this end, in Fig. 3.9**a** we plot numerically

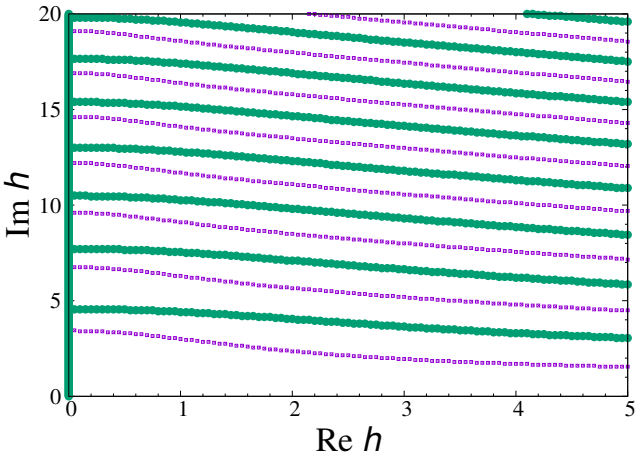

Fig. 3.8: Lines of zeros for the real and imaginary part of the approximated partition function (3.22) at $T = T_c$ in the complex magnetic field plane, thin and thick curves (violet and green online) respectively. The points where the lines of different colour cross give the coordinates of the Lee-Yang zeros. Note that one of the $\mathrm{Im}\, Z(h) = 0$ lines coincides with the vertical axis in the plot.

the coordinates $\mathrm{Im}\, h_j$ of the first sixteen Lee-Yang zeros as functions of $j - C$ for different values of $C = 0,\ 1/4,\ 1/3,\ 1/2$. As expected, for large enough j the linear scaling with j occurs and the data points align along a single line with the tangent $\sigma \simeq 3/4$. However, as for the exact partition function, this dependence is non-linear for smaller values of j and the choice of an appropriate fitting parameter C (see Fig. 3.9**b**) similar as it was done for the exact function, see Fig. 3.7 allows to improve the linearity. As a result, we get the optimal value $C_{\mathrm{opt}} = 0.31$ and $\sigma(C_{\mathrm{opt}}) = 0.7531(2)$.

3.4 Motion of the Fisher zeros in a real external field

In the final part of this section we analyze the motion of the Fisher zeros in the presence of a (real) external field [124]. Since the Lee-Yang zeros of the model under consideration have purely imaginary coordinates, in the vicinity of the critical point the lines of motion of Fisher zeros form an angle ψ that encodes order parameter critical exponents via Eq. (1.20). In our case, for the values of the exponents β and δ given by (3.5) one gets for the angle:

$$\psi = \frac{\pi}{3}\,. \tag{3.25}$$

The expression for the approximated partition function in the vicinity of the critical point is obtained from (3.7) and reads

$$Z_N^{\mathrm{exp}}(t, H) = \int_{-\infty}^{+\infty} \exp\Big(\frac{-t\,x^2}{2} - \frac{x^4}{12N} + x\sqrt{N}H\Big)dx. \tag{3.26}$$

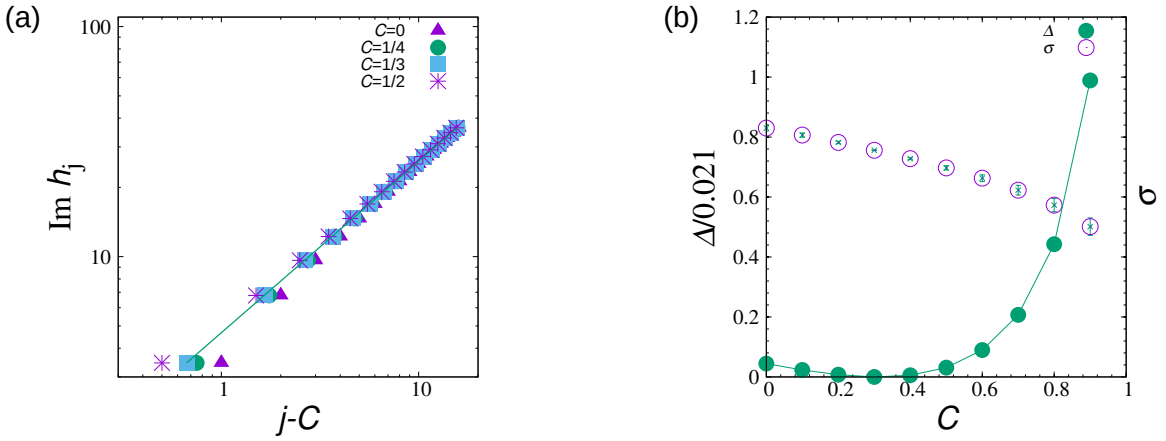

Fig. 3.9: The behaviour of $\mathrm{Im}\, h_j$ for leading Lee-Yang zeros of the approximated partition function (3.22). **(a)** Coordinates $\mathrm{Im}\, h_j$ of numerically calculated first sixteen Lee-Yang zeros as functions of $j - C$ for different values of $C = 0,\ 1/4,\ 1/3,\ 1/2$. The solid line is an eye guide to show linear scaling with an exponent $\sigma = 3/4$. Such scaling is manifested by a merge of the data points with an increase of j. **(b)** Variance of residuals Δ and exponent σ obtained while fitting coordinates of the first sixteen Lee Yang zeros via Eq. (3.19) as functions of the fitting parameter C. The value of the exponent σ calculated at $\sigma(C_{\mathrm{opt}}) = 0.7531(2)$ is close to the exact result $\sigma = 0.75$.

To get (3.26) we have kept, as before, only the leading order contributions in H and t terms. As was pointed above, in this case the approximated expressions for the partition function attain the same form both in t- and τ- representations. Therefore, the analysis of the Fisher zeros presented below concerns both the complex t- and complex τ-planes equally well. The expansion (3.26) can be conveniently rewritten in the rescaled variables z, h, Eqs. (3.13), (3.23):

$$Z^{\exp}(z, h) = \int_0^\infty e^{-zx^2 - x^4 + hx} dx. \tag{3.27}$$

Note that for $h = 0$ or $z = 0$ (3.27) reduces to Eq. (3.12) or (3.22) respectively.

Fig. 3.10**a** shows the coordinates of the first five Fisher zero for different values of the (real) magnetic field in the complex z plane. The coordinates have been calculated for different values of the magnetic field $h_j = j$, $j = 0, 1, \ldots, 20$. For $h_j = 0$ we recover the values of the coordinates shown in Fig. 3.4. One can see the tendency of the zeros to settle along a line forming an angle $\psi = \frac{\pi}{3}$ with the real z axis (shown by a solid line in the figure). However, the asymptotics are preceded by a crossover region for very small values of h. Similar tendency for a first few zeros of a 3D Ising model was observed in Ref. [124] and explained by the finite-size corrections [202]. The closer the zeros to the critical point, the smaller the crossover region.

To further analyze motion of the zeros we apply the finite size scaling (FSS) as outlined below. According to the FSS theory [115, 116], for a d-dimensional system

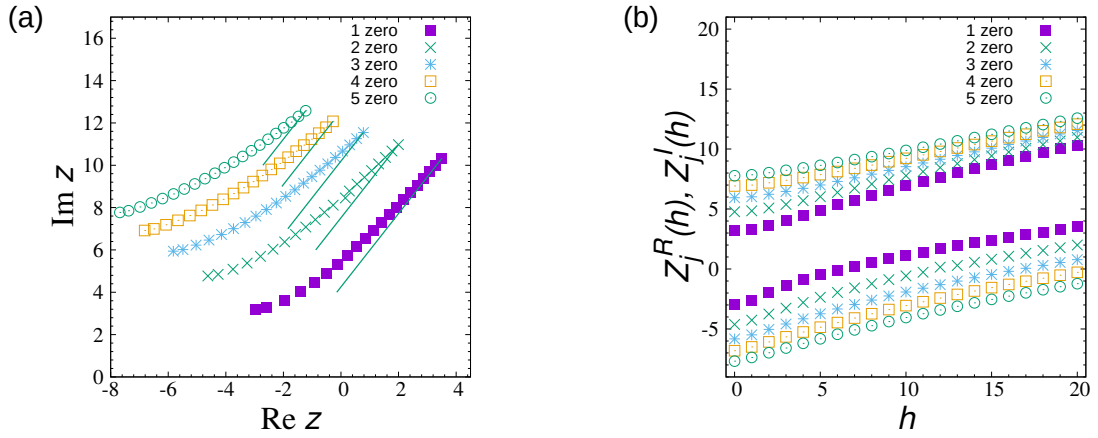

Fig. 3.10: **(a)** Coordinates of the first five Fisher zeros of the partition function (3.27) in the complex z plane for different values of the magnetic field $h_j = j$, $j = 0, 1, \ldots, 20$. The plots have a tendency to settle along lines forming an angle $\psi = \pi/3$ with a real z axis. **(b)** Scaling functions for the first five zeros $\mathcal{Z}_j^{\mathcal{R}}(h)$ (lower plots), $\mathcal{Z}_j^{\mathcal{I}}(h)$ (upper plots) for the real and imaginary part of the first Fisher zero coordinate, Eq. (3.35), as functions of the scaling variable $h = HN^{1+\frac{\beta}{\alpha-2}}$.

in the vicinity of the critical point one expects the following scaling for the real and imaginary parts of the jth zero coordinate in the reduced temperature t plane:

$$\text{Re } t_j(N,H) = b^{-1/\nu}\mathcal{T}_j^{\mathcal{R}}\left(H\, b^{y_H}, N\, b^{-d}\right), \tag{3.28}$$

$$\text{Im } t_j(N,H) = b^{-1/\nu}\mathcal{T}_j^{\mathcal{I}}\left(H\, b^{y_H}, N b^{-d}\right). \tag{3.29}$$

Here, b is the scaling factor, ν and y_H are the correlation length critical exponent and field scaling dimension, $\mathcal{T}_j^{\mathcal{R}}(x, y))$ and $\mathcal{T}_j^{\mathcal{I}}(x, y)$ are scaling functions. Being generalised homogeneous functions of two variables, the scaling functions can be rewritten as functions of a single scaling variable. Choosing the factor $b = N^{-1/d}$ the expressions (3.28), (3.29) attain the following form:

$$\text{Re } t_j(N,H) = N^{-1/d\nu}\mathcal{T}_j^{\mathcal{R}}\left(H\, N^{-y_H/d}, 1\right), \tag{3.30}$$

$$\text{Im } t_j(N,H) = N^{-1/d\nu}\mathcal{T}_j^{\mathcal{I}}\left(H\, N^{-y_H/d}, 1\right). \tag{3.31}$$

making use of the familiar (hyper)scaling relations ($d\nu = 2 - \alpha$, $y_h/d = 1 - \beta/2 - \alpha$) we get the following expressions for the motion of zeros:

$$\text{Re } t_j(N,H) = N^{\frac{1}{\alpha-2}}\,\mathcal{T}_j^{\mathcal{R}}\left(H\, N^{1+\frac{\beta}{\alpha-2}}\right), \tag{3.32}$$

$$\text{Im } t_j(N,H) = N^{\frac{1}{\alpha-2}}\,\mathcal{T}_j^{\mathcal{I}}\left(H\, N^{1+\frac{\beta}{\alpha-2}}\right), \tag{3.33}$$

where we have introduced the single variable functions:

$$\mathcal{T}_j^{\mathcal{R}}(x) \equiv \mathcal{T}_j^{\mathcal{R}}(x,\,1), \qquad \mathcal{T}_j^{\mathcal{I}}(x) \equiv \mathcal{T}_j^{\mathcal{I}}(x,\,1)\,. \tag{3.34}$$

Note that relations (3.32)-(3.33) contain the system size only via the number of particles N (and not via the spatial extent and dimension) and therefore are convenient for systems on graphs, where the notion of Euclidean dimension is not defined. Equations (3.32), (3.33) can be rewritten in the rescaled variables z, h (see Eqs.(3.13) and (3.23)):

$$\begin{aligned} \mathrm{Re}\, z_j &= \mathcal{Z}_j^{\mathcal{R}}(h)\,, \\ \mathrm{Im}\, z_j &= \mathcal{Z}_j^{\mathcal{I}}(h)\,, \end{aligned} \tag{3.35}$$

where

$$\mathcal{Z}_j^{\mathcal{R}}(h) \equiv \sqrt{3}\,\mathcal{T}_j^{\mathcal{R}}(h/\sqrt[4]{12})\,, \qquad \mathcal{Z}_j^{\mathcal{I}}(h) \equiv \sqrt{3}\,\mathcal{T}_j^{\mathcal{I}}(h/\sqrt[4]{12})\,. \tag{3.36}$$

We plot the scaling functions (3.36) in Fig. 3.10**b** for the first five zeros $j = 1, \ldots, 5$. The prominent feature of the plot is that a ratio of the values of the scaling functions at $h = 0$ gives the value of the Fisher pinching angle:

$$\mathcal{T}_j^{\mathcal{I}}(0)/\mathcal{T}_j^{\mathcal{R}}(0) = \mathcal{Z}_j^{\mathcal{I}}(0)/\mathcal{Z}_j^{\mathcal{R}}(0) = \tan\varphi\,. \tag{3.37}$$

Indeed, with the value $\tan\varphi = \tan\pi/4 = -1$, Eq. (3.10), one gets $\mathcal{T}_j^{\mathcal{I}}(0) = -\mathcal{T}_j^{\mathcal{R}}(0)$ or $\mathcal{Z}_j^{\mathcal{I}}(0) = -\mathcal{Z}_j^{\mathcal{R}}(0)$ as is nicely observed in the figure.

3.5 Conclusions

In this section we consider the critical behaviour of the Ising model on a complete graph in terms of Lee-Yang-Fisher partition function zeros analysis. In particular, using the approach of Ref. [196] we have analyzed the behaviour of Lee-Yang zeros as well as tracked the motion of the Fisher zeros in the real external magnetic field. For some other models [124, 202] it has been observed before that this motion is governed by the universal angle ψ, that encodes values of the order parameter critical exponents through (1.20). A fundamental feature of the Ising model on the complete graph, as well as of those models where such behaviour of Fisher zeros in real magnetic field was observed, is that their zeros in complex magnetic field at the critical temperature are governed by the Lee-Yang theorem: plotted in the plane e^{-h} they align along the unit

circle [118, 119]. This confirms that the Lee-Yang circle theorem for the Ising model on a complete graph is satisfied.

Chapter 4 | PARTITION FUNCTION ZEROS FOR THE ISING MODEL ON AN ANNEALED SCALE-FREE NETWORK

Contents

Here we will continue the analysis of the partition function zeros for the Ising model in a complex plane. The subject of our analysis is the Ising model on an annealed scale-free network. It should be noted that this formalism has not been applied to the analysis of a spin model on a scale-free network before our work. In section 4.1 we describe an annealed scale-free network and obtain the exact expressions for the partition function of the Ising model on the network. The partition function zeros in the complex temperature plane are analyzed in section 4.2, and in the complex field plane are investigated in Section 4.3. One of the main results of our study is the notion that the Lee-Yang unit circle theorem does not hold for the Ising model on a scale-free network. This statement is proven in section 4.3. The conclusions are summarized in Section 4.4. The essential results of this chapter were

published in [21, 22].

4.1 Partition function

Now, with knowledge of the behaviour of the partition function zeros on a complete graph at hand, we consider the critical behaviour of the Ising model on complex networks, i.e. on a random graph [3–7]. The Hamiltonian of the model in this case reads

$$-\mathcal{H} = \frac{1}{2}\sum_{l\neq m} J_{lm} S_l S_m + H \sum_l S_l \,. \tag{4.1}$$

Here, the sums are performed over all graph nodes l, m and the adjacency matrix J stores all information about the graph structure: the matrix elements $J_{lm} = 1$ if the nodes are linked and $J_{lm} = 0$ otherwise. In random graphs, different nodes have different number of links (different node degrees K). The node degrees are random variables and inherent features of their distribution $p(K)$ appear to play one of the key roles governing the universal critical behaviour [64]. As a first instance of a complex network we will consider an *annealed* network. This network is defined as an ensemble of all networks consisting of N nodes with a given degree sequence $\{K_1, K_2, \ldots, K_N\}$, maximally random under the constraint that their degree distribution is a given one, $p(K)$ (see e.g. [61]). Such a construction resembles the uncorrelated configurational model of a complex network (see e.g. [63]). However the latter is an example of a quenched network, whereas for the Ising model on an annealed network, the graph configuration is also fluctuating just like Ising spins do. When thermodynamic properties are calculated, the presence of quenched disorder is taken into account by averaging the free energy over different disorder configurations, whereas in the annealed case the partition function is averaged [59]. Therefore, considering the Ising model on an annealed network, we will be interested in the behaviour of the partition function averaged with respect to different network configurations.

For the Hamiltonian (4.1) the corresponding partition function is obtained by:

$$Z_N(T, H) = \mathrm{Tr}_S \, \mathrm{Tr}_J \, e^{-\beta\mathcal{H}} \,. \tag{4.2}$$

As in (3.2), the first trace is taken over the spin system: $\mathrm{Tr}_S \,(\ldots) = \prod_l \sum_{S_l=\pm 1} (\ldots)$, whereas the second one means an averaging with respect to the distribution of the

network links $\mathcal{P}(J)$:

$$\mathrm{Tr}_J\,(\ldots) = \prod_{l\neq m}\sum_{J_{lm}=0,1} \mathcal{P}(J)\,(\ldots).$$

4.1.1 Annealed network approximation

To construct an annealed network of N nodes $l = 1, \ldots, N$, each node l is assigned a label k_l and the probability of a link between nodes l and m is defined as:

$$p_{lm} = \frac{k_l k_m}{N\langle k\rangle}\,, \tag{4.3}$$

where $\langle k\rangle = \frac{1}{N}\sum_l k_l$. The variables k are taken from the distribution $p(k)$ and indicate the expected node degree. Indeed, it is straightforward to show that the expected value of the node degree $\mathbb{E}K_l = \sum_m p_{lm} = k_l$. One can show [61] that averaging (4.2) over the distribution of network links with probability function (4.3) leads to the following expression for the partition function:

$$Z_N(T,H) = \mathrm{Tr}_S\,\exp\left(\frac{1}{2N\langle k\rangle T}\sum_{l\neq m} S_l S_m k_l k_m + \frac{H}{T}\sum_l S_l\right)\,. \tag{4.4}$$

An analogous expression for the partition function is usually obtained also within the mean field approximation for the Ising model on an uncorrelated quenched network [63, 64](configurational model). For the annealed network however the factor in front of the double sum in (4.4) is a certain function of temperature [61]. Since in our study we are interested in the angles of incidence of partition function zeros, which are independent of any real analytic parametrization of the temperature plane, we keep in (4.4) only a linear term of this function.

4.1.2 Exact integral representation

Since for the annealed network the interaction term in (4.1) attains a separable form, one can apply the Stratonovich-Hubbard transformation to (4.4) to take the trace exactly and to get the following expression for the partition function:

$$Z_N(T,H) = \int_{-\infty}^{+\infty}\exp\Big(\frac{-N\langle k\rangle x^2}{2T} + \sum_l \ln\cosh[(xk_l+H)/T]\Big)dx\,. \tag{4.5}$$

As in the previous section, the prefactors are omitted here and below. Now, the sum over l in the exponent (4.5) can be rewritten in terms of the integral over k for a given

distribution function $p(k)$:

$$\sum_l f(k_l) = N \int_{k_{\min}}^{k_{\max}} p(k) f(k) dk \,, \tag{4.6}$$

where $k_{\min}$ and $k_{\max}$ are the minimal and maximal values of the variable k. For further analysis it will be convenient to keep the integral in x in the positive half-plane leading to the representation for the partition function,

$$\begin{aligned} Z_N(T,H) \;=\; & \int_0^{+\infty} e^{\frac{-\langle k\rangle x^2 T}{2}} \Big\{ \exp\Big[N \int_{k_{\min}}^{k_{\max}} dk p(k) \ln\cosh\Big(\frac{xk}{\sqrt{N}} + \frac{H}{T}\Big)\Big] \\ & + \exp\Big[N \int_{k_{\min}}^{k_{\max}} dk p(k) \ln\cosh\Big(-\frac{xk}{\sqrt{N}} + \frac{H}{T}\Big)\Big]\Big\} dx \,. \end{aligned} \tag{4.7}$$

4.1.3 Expanded representation

For the complete graph of N nodes substituting in (4.7) $p(k) = \delta(k - N + 1)$ one recovers (3.6). In this section we are interested in the scale-free networks, when the function $p(k)$ is given by a power law

$$p(k) = c_\lambda \, k^{-\lambda} \,, \tag{4.8}$$

with a normalizing constant c_λ. Note, that scale-free networks with $k_{\min} = 1$ do not possess a spanning cluster for $\lambda > \lambda_c$ ($\lambda_c = 4$ for continuous degree distribution and $\lambda_c \simeq 3.48$ for the discrete one [176]). To avoid this restriction, without loss of generality we choose from now on $k_{\min} = 2$, whereas for the upper integration boundary in (4.6) we take in the thermodynamic limit $\lim_{N\to\infty} k_{\max} \to \infty$.[1] Then, for the scale-free network, Eq. (4.7) can be conveniently rewritten as:

$$Z_N(T,H) = \int_0^{+\infty} e^{\frac{-\langle k\rangle x^2 T}{2}} \Big\{ \exp\Big[I_\lambda^+(x)\Big] + \exp\Big[I_\lambda^-(x)\Big]\Big\} dx \,, \tag{4.9}$$

where

$$I_\lambda^\pm(x) = c_\lambda \Big(\frac{x}{\sqrt{N}}\Big)^{\lambda-1} N \int_{\frac{2x}{\sqrt{N}}}^{\infty} \frac{1}{y^\lambda} \ln\cosh\Big(\pm y + \frac{H}{T}\Big) dy \,. \tag{4.10}$$

Consider the integral in (4.10). For large y the integrand decays as $y^{1-\lambda}$ and the integral is finite at the upper integration boundary for the values $\lambda > 3$ we are interested

[1] The leading in N value of this integral representation does not depend on the way in which $k_{\max}$ tends to infinity. These are the next-leading terms that will depend on the N dependency of the upper cut-off. See Appendix A for more details.

in. However, for small y the integrand behaves as $(\pm y + H/T)^2 y^{-\lambda} + \dots$ and leads to divergent terms when the lower integration boundary is set to zero, i.e. in the thermodynamic limit $N \to \infty$. These divergent terms do not appear in the whole expression since they are canceled by the N-dependent prefactor in (4.10). To single them out and to show this cancelation explicitly, it is instructive to consider the function $I_\lambda^\pm(x)$ (4.10) for different values of λ (see e.g. [18] for a more detailed account). As in the former section, we make asymptotic estimates for small H. Leading terms of the resulting expressions read:

$$I_\lambda^\pm(x) = N\Big[\frac{\langle k^2\rangle}{2}\frac{x^2}{N} - a(\lambda)\Big(\frac{x}{\sqrt{N}}\Big)^{\lambda-1} \pm \frac{\langle k\rangle H x}{T\sqrt{N}}\Big], \quad 3<\lambda<5\,, \tag{4.11}$$

$$I_\lambda^\pm(x) = N\Big[\frac{\langle k^2\rangle}{2}\frac{x^2}{N} - \frac{\langle k^4\rangle}{12}\Big(\frac{x}{\sqrt{N}}\Big)^{4} \pm \frac{\langle k\rangle H x}{T\sqrt{N}}\Big], \quad \lambda>5\,, \tag{4.12}$$

where the numerical values of the coefficients $a(\lambda) = -c_\lambda \int_0^\infty dy\, y^{-\lambda} \times (\ln\cosh y - y^2/2)$, $a(\lambda) > 0$, are listed for different λ in [18] and the moments of the variable k are calculated with the distribution (4.8). The case $\lambda = 5$ is to be considered separately. Integrating out the logarithmic singularity one gets for the first leading terms:

$$I_\lambda^\pm(x) = N\Big[\frac{\langle k^2\rangle}{2}\frac{x^2}{N} - \Big(\frac{x}{\sqrt{N}}\Big)^{4}\frac{\ln N}{24} \pm \frac{\langle k\rangle H x}{T\sqrt{N}}\Big]. \tag{4.13}$$

With the expressions (4.11)–(4.13) for $I_\lambda^\pm(x)$ we are in a position to analyse the partition function (4.9) at different values of λ. As is well established by now, critical behaviour of a system on a scale-free network with the partition function (4.9) depends of the value of the exponent λ in an essential way [3–7, 64]. In particular, the system remains ordered for any finite temperature at $\lambda \le 3$. A second order phase transition at finite temperature occurs for $\lambda > 3$. It is governed by standard mean field exponents (3.5) in the region $\lambda \ge 5$ with logarithmic corrections at $\lambda = 5$, however the exponents attain λ-dependency for $3 < \lambda < 5$ [63]:

$$\alpha = (\lambda-5)/(\lambda-3),\ \ \beta = 1/(\lambda-3),\ \ \delta = \lambda - 2,\ \ \gamma = 1\,. \tag{4.14}$$

The mean-field approximation delivers the classical value for the magnetic susceptibility exponent $\gamma = 1$ for any $\lambda > 3$. The other exponents however become λ dependent at $3 < \lambda < 5$. This is because the Ising model on complex scale-free networks follows a heterogeneous rather than homogeneous mean-field.

Our task will be to describe the phase transition in the Ising model on an annealed

scale-free network in terms of the partition function zeros, similarly as it was done for the complete graph in the previous section. Substituting values of the exponents (4.14) together with the critical amplitude ratio $A_+/A_- = 0$ [88] into relations (1.10), (3.20) we get for the region $3 < \lambda < 5$:

$$\varphi = \frac{\pi(\lambda - 3)}{2(\lambda - 1)}, \tag{4.15}$$

$$\sigma = \frac{\lambda - 2}{\lambda - 1}. \tag{4.16}$$

Let us check if these values can be obtained directly from the analysis of the zeros of the partition function (4.9) in complex T and H planes.

4.2 Fisher zeros

Substituting expressions for $I_\lambda^{\pm}(x)$ (4.11)–(4.13) at $H = 0$ into the partition function (4.9) at different values of λ we get:

$$Z_N(t) = \begin{cases} \int_0^{+\infty} \exp\left[-\frac{\langle k^2\rangle x^2 t}{2} - a(\lambda) N \left(\frac{x}{\sqrt{N}}\right)^{\lambda-1} \right] dx \,, & 3 < \lambda < 5, \\ \int_0^{+\infty} \exp\left[-\frac{\langle k^2\rangle x^2 t}{2} - \frac{x^4}{N}\frac{\ln N}{24} \right] dx \,, & \lambda = 5, \\ \int_0^{+\infty} \exp\left[-\frac{\langle k^2\rangle x^2 t}{2} - \frac{\langle k^4\rangle}{12}\frac{x^4}{N} \right] dx \,, & \lambda > 5, \end{cases} \tag{4.17}$$

with $t = (T - T_c)/T_c$ and the (pseudo)critical temperature $T_c = \langle k^2\rangle/\langle k\rangle$.[2] Similar to the previous section, the partition function can be conveniently represented in terms of a single variable z that combines t and N dependencies, cf. Eq. (3.13). However, now this variable differs in different regions of λ:

$$z = \begin{cases} t\frac{\langle k^2\rangle}{2}[a(\lambda)]^{2/(\lambda-1)} N^{\frac{\lambda-3}{\lambda-1}} \,, & 3 < \lambda < 5, \\ t\langle k^2\rangle\sqrt{6N}/\sqrt{\ln N} \,, & \lambda = 5, \\ t\langle k^2\rangle\sqrt{3N\langle k^4\rangle} \,, & \lambda > 5 \,. \end{cases} \tag{4.18}$$

Written in terms of the variables appearing in (4.18), the partition function (4.17) has a simple form:

$$Z(z) = \begin{cases} \int_0^{+\infty} \exp\Big(-zx^2 - x^{\lambda-1} \Big) dx \,, & 3 < \lambda < 5, \\ \int_0^{+\infty} \exp\Big(-zx^2 - x^4 \Big) dx \,, & \lambda \geq 5. \end{cases} \tag{4.19}$$

[2] For a finite-size system, T_c depends on N via the N-dependency of the moments $\langle k\rangle$, $\langle k^2\rangle$.

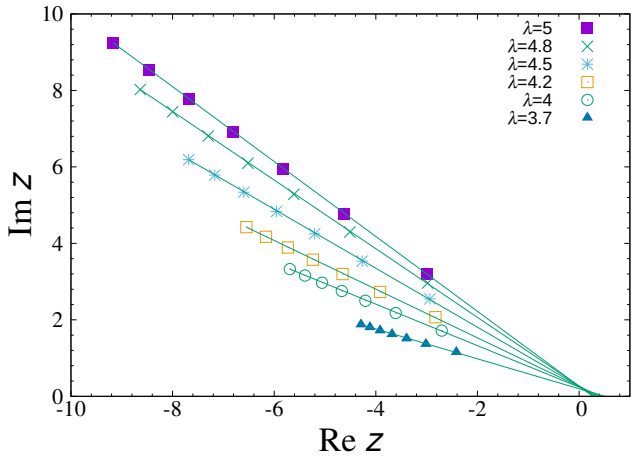

Fig. 4.1: Fisher zeros for the Ising model on an annealed scale-free network at zero magnetic field for different λ. The zeros have a clear tendency to situate along the straight lines crossing the real z axis in the vicinity of the critical point z_c. The angles formed by each of the lines with the real z axis decrease in the region $3 < \lambda < 5$ as predicted by equation (4.15).

Two obvious conclusions follow: (i) since the functional form of $Z(z)$ dependency at $\lambda = 5$ and $\lambda > 5$ is the same, the location of the Fisher zeros in the complex z plane will be the same too. This leads to the conclusion that the impact angle φ that corresponds to the Ising model on an annealed network does not change for $\lambda \geq 5$ and (ii) these expressions coincide with the partition function of the Ising model on the complete graph, Eq. (3.12). Therefore, analysis of the Fisher zeros of the last model, performed in chapter 3 applies equally well to the Fisher zeros of the Ising model on an annealed network. In particular, one concludes, that:

$$\varphi = \pi/4, \qquad \lambda \geq 5\,. \tag{4.20}$$

Let us note as well, that the logarithmic corrections to scaling appear in the marginal case $\lambda = 5$ [87–89, 93, 94]. Such a logarithmic correction appears in $I_\lambda^{\pm}(x)$ at $\lambda = 5$ too. However, it does not contribute to the terms leading in $1/N$, resulting in the conclusion, that the impact angle of Fisher zeros (and, therefore, the leading exponent for the heat capacity) is the same at $\lambda = 5$ and $\lambda > 5$.

Similar to the preceding sections for the Ising model on the complete graph, to proceed with the analysis of the Fisher zeros at $3 < \lambda < 5$, we calculate the numerical values of the coordinates of several first zeros as shown in Fig. 4.1. As is seen from the figure, the zeros have a clear tendency to situate along the straight lines crossing the real z axis in the vicinity of the critical point z_c. Moreover, the angle formed by each of the lines differs for different λ and decreases with λ. To study this dependency in more detail, for each value of λ we fit j Fisher zeros in the interval $j = j_{\min}, \ldots, j_{\max}$

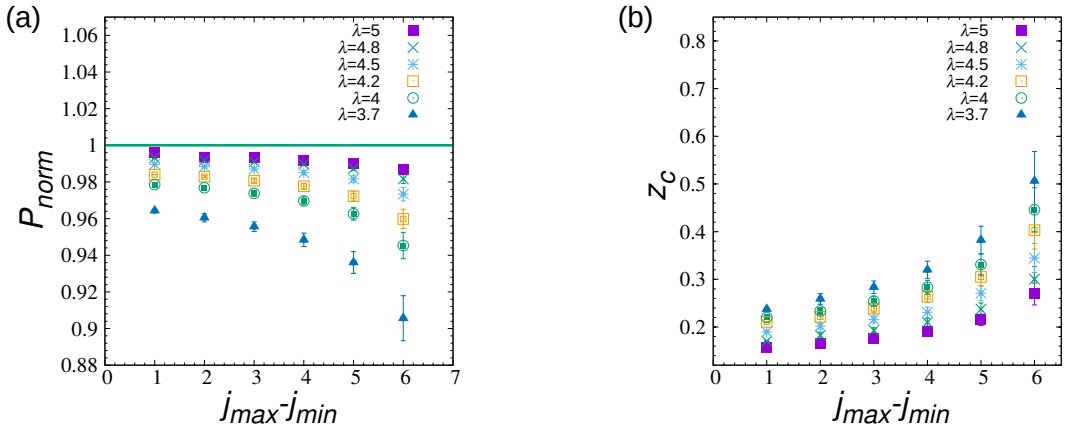

Fig. 4.2: Values **(a)** of the ratio $P_{\rm norm} = \varphi/\frac{\pi(\lambda-3)}{2(\lambda-1)}$ and **(b)** of estimates for the critical temperature z_c for the partition function (4.19) obtained by fitting of j Fisher zeros in the interval $j = j_{\rm min}, \ldots, j_{\rm max}$ for $j_{\rm max} = 7$ and different values of $j_{\rm min}$. A solid line in Panel **(a)** shows an exact value $P_{\rm norm} = 1$.

for $j_{\rm max} = 7$ and give the resulting estimate for φ in Table 4.1. One can see that the values determined numerically approach those predicted by the analytic formula (4.15), the higher the order of the zeros used for the fit, the higher the accuracy. This tendency is quite similar to those observed for the Fisher zeros on a complete graph (cf. Fig. 3.5). To further demonstrate this similarly, we plot in Fig. 4.2**a** the dependency of the ratio of the numerically calculated angle φ to its value predicted by formula (4.15): $P_{\rm norm} = \varphi/\frac{\pi(\lambda-3)}{2(\lambda-1)}$. This ratio tends to $P_{\rm norm} = 1$ with the increase of the order of the zeros used for the fit. One can notice a similar tendency for the behaviour of the critical temperature z_c, see Fig. 4.2**b**. Again one observes similarity with the behaviour of z_c for the Ising model on a complete graph, cf. Fig. 3.5b.

Table 4.1: Numerically calculated values of the angle φ for different λ. The angle is calculated by linear fitting of Fisher zeros with the indices $j = j_{\rm min}, ..., 7$. The confidence interval, when not written explicitly, is less than the last significant digit. The last row gives φ predicted by the analytic formula (4.15).

$j_{\rm min}$	$\lambda \geq 5$	$\lambda = 4.8$	$\lambda = 4.5$	$\lambda = 4.2$	$\lambda = 4$	$\lambda = 3.7$
1	$0.246(5)\pi$	$0.233(1)\pi$	$0.209(1)\pi$	$0.180(1)\pi$	$0.158(1)\pi$	$0.117(2)\pi$
2	0.248π	0.234π	0.210π	0.182π	$0.160(1)\pi$	$0.121(1)\pi$
3	0.248π	0.234π	0.211π	0.183π	0.162π	0.123π
4	0.248π	0.235π	0.212π	0.184π	0.162π	0.124π
5	0.248π	0.235π	0.212π	0.184π	0.163π	0.125π
6	0.249π	0.235π	0.212π	0.185π	0.163π	0.125π
exact	0.250π	0.237π	0.214π	0.188π	0.167π	0.130π

Another inherent feature of the locations of the Fisher zeros is that the distance

between two successive zeros decreases with increasing index (see Fig. 4.1 for the annealed scale-free network as well as Fig. 3.4 for the complete graph). Indeed, taken that the finite size scaling of the j-th zero t_j in the complex t plane for large j is given by [124]:

$$t_j \sim \left(\frac{j}{N}\right)^{\frac{1}{2-\alpha}} \tag{4.21}$$

one arrives at the conclusion that $\Delta t_j \equiv t_j - t_{j-1} \sim j^{\kappa}$, with $\kappa = (\alpha - 1)/(2 - \alpha)$. The last exponent is negative for the values of α we are interested in: $\kappa = -1/2$, $\lambda \geq 5$ and $\kappa = -2/(\lambda - 1)$, $3 < \lambda < 5$. Rewriting (4.21) in terms of z_j (4.18) gives:

$$z_j \sim j^{\frac{1}{2-\alpha}}. \tag{4.22}$$

To check how does the scaling of the Fisher zeros hold with j, we calculate the value of the exponent in (4.22) fitting the function $\ln|z_j| = a + b \ln j$ for the Fisher zeros with indices $j = j_{\min}, ..., 7$ at different λ. The results are compared with the exact value in Table 4.2. One can see the right tendency of approach of the numerically calculated numbers to their exact counterparts with an increase of j.

Table 4.2: Linear fitting of the function $\ln|z_j| = a + b \ln j$ for the Fisher zeros with indices $j = j_{\min}, ..., 7$ at different λ. The table shows results for the angle coefficient b. The confidence interval, when not written explicitly, is less than the last significant digit. The last row gives the value $b = 1/(2 - \alpha)$ as predicted by an analytic formula (4.22).

$j_{\min}$	$\lambda > 5$	$\lambda = 4.8$	$\lambda = 4.5$	$\lambda = 4.2$	$\lambda = 4$	$\lambda = 3.7$
1	0.558(8)	0.528(7)	0.477(6)	0.417(5)	0.370(5)	0.286(3)
2	0.537(4)	0.509(3)	0.460(3)	0.402(3)	0.357(2)	0.277(2)
3	0.529(2)	0.501(2)	0.453(2)	0.396(2)	0.352(1)	0.274(1)
4	0.525(1)	0.497(1)	0.450(1)	0.393(1)	0.349(1)	0.271(1)
5	0.522(1)	0.494(1)	0.447(1)	0.391(1)	0.348(1)	0.270(1)
6	0.520	0.492	0.445	0.390	0.346	0.269
exact	0.500	0.474	0.429	0.375	0.333	0.259

In order to check scaling of the Fisher zeros t_j with N, there is no need to calculate explicitly their coordinates at different values of N. Indeed, the $t_j(N)$ dependency follows from the $z(t, N)$ functional form, as given by (4.18). Expressing t from there one gets that the power law scaling $t_j \sim N^{1/(\alpha-2)}$ holds for $3 < \lambda < 5$ and $\lambda > 5$ whereas it is enhanced by a logarithmic correction at $\lambda = 5$: $t_j \sim N^{-1/2}(\ln N)^{1/2}$.

4.3 Lee-Yang zeros for the partition function

Substituting expressions for $I_\lambda^{\pm}(x)$ (4.11)–(4.13) at $T = T_c = \langle k^2\rangle/\langle k\rangle$ into the partition function (4.9) at different values of λ and keeping the leading contributions in $1/N$ we get:

$$Z(h) = \begin{cases} \int_0^{+\infty} \exp\Big(-x^{\lambda-1}\Big)\cosh(hx)dx\,, & 3<\lambda<5, \\ \int_0^{+\infty} \exp\Big(-x^{4}\Big)\cosh(hx)dx\,, & \lambda \geq 5\,. \end{cases} \tag{4.23}$$

Here, the H- and N-dependencies of the partition function are adsorbed in a single variable h. Its explicit form differs for different regions of λ:

$$h = \begin{cases} H\frac{\langle k\rangle^2}{\langle k^2\rangle} a(\lambda)^{1/(1-\lambda)} N^{\frac{\lambda-2}{\lambda-1}}\,, & 3<\lambda<5, \\ H\frac{\langle k\rangle^2}{\langle k^2\rangle}\Big(\frac{24}{\ln N}\Big)^{1/4} N^{3/4}\,, & \lambda = 5, \\ H\frac{\langle k\rangle^2}{\langle k^2\rangle}\Big(\frac{12}{\langle k^4\rangle}\Big)^{1/4} N^{3/4}\,, & \lambda > 5\,. \end{cases} \tag{4.24}$$

4.3.1 Violation of the Lee-Yang theorem

Similar to the discussion for the $t_j(N)$ scaling at the end of the previous subsection, here, the scaling of $h_j(N)$ directly follows from the $h(H,N)$ dependency given by (4.24). Comparing (4.24) with the definition (3.19) one gets:

$$\sigma = \begin{cases} \frac{\lambda-2}{\lambda-1}\,, & 3<\lambda<5, \\ 3/4\,, & \lambda>5\,. \end{cases} \tag{4.25}$$

The logarithmic correction appears at $\lambda = 5$: $H_j \sim N^{-3/4}\Big(\ln N\Big)^{1/4}$.

In Fig. 4.3 we plot lines of zeros for the real and imaginary parts of the partition function (4.23) at $T = T_c$ and different values of λ in the complex magnetic field $h = \mathrm{Re}\,h + i\,\mathrm{Im}\,h$ plane. The points where the lines of different colour cross give the coordinates of the Lee-Yang zeros. Note that whereas the coordinate of the first Lee-Yang zero (that closest to the origin) is purely imaginary for any value of $3 < \lambda < 5$ (and it is its presence that allows to make conclusions about the scaling with N governed by the exponent (4.25)), it is not the case for the zeros of higher order: the number of zeros with $\mathrm{Re}\,h_j = 0$ decreases with j. In this respect the behaviour of Lee-Yang zeros for the Ising model on an annealed scale-free network differs crucially from the behaviour on the complete graph (see the previous section). Whereas in the complete

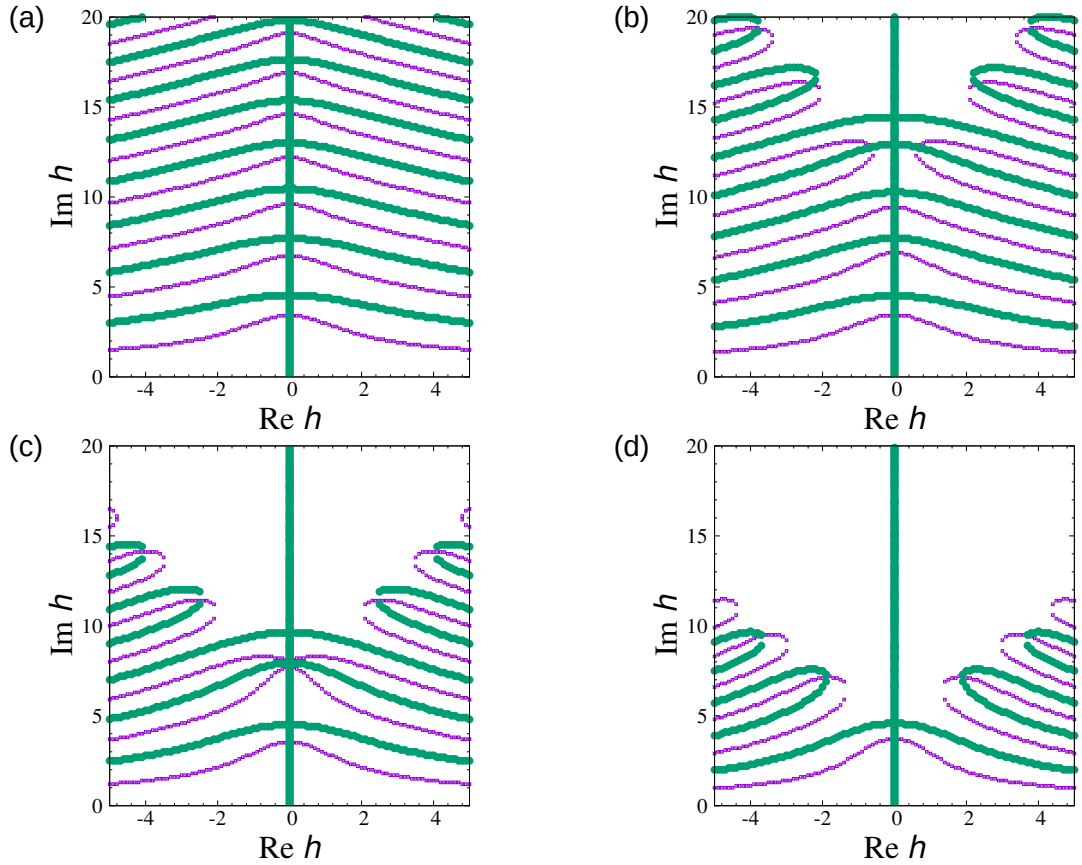

Fig. 4.3: Lines of zeros for the real and imaginary part of the partition function (4.23) at $T = T_c$ and different values of λ in the complex magnetic field plane, thin and thick curves (violet and green dots online) respectively: **(a)** $\lambda \geq 5$; **(b)** $\lambda = 4.5$; **(c)** $\lambda = 4$; **(d)** $\lambda = 3.5$. The points where the lines of different colours cross give the coordinates of the Lee-Yang zeros. Note that one of the $\mathrm{Im}\, Z = 0$ lines coincides with the vertical axis in the plot.

graph the zeros were entirely imaginary and obeyed the Lee-Yang circle theorem, this theorem is violated in the case of the annealed scale-free network.

As seen in Fig. 4.3, the imaginary part of $Z(h)$ vanishes when h itself is imaginary. This is because the partition function is an even function of h. The intersections of the different types of contour on the plot give the locations of the Lee-Yang zeros. When $\lambda \geq 5$ all zeros are on the imaginary axis. But for $\lambda = 4.5$ only first three zeros are imaginary and zeros of higher order (h_j for $j > 3$) have non-vanishing real parts. Similar behaviour is found for all values of λ between 3 and 5; there is a number, $\mathcal{N}$, finite in size, such that h_j is purely imaginary for $j \leq \mathcal{N}$ but has non-vanishing real part for $j > \mathcal{N}$. The number $\mathcal{N}$ decreases with decreasing λ.

The values of Lee-Yang zeros determined numerically are listed in Table 4.3 for different values of $3 < \lambda < \lambda_{\mathrm{uc}} = 5$, and for $\lambda \geq 5$. When $\lambda = 4$, $\mathcal{N} = 3$ while for $\lambda = 3.5$, $\mathcal{N} = 1$. In this respect the behaviour of the zeros differs for $\lambda \geq 5$ (where it is

the same as for the partition function of the Ising model on a complete graph) and for $3 < \lambda < 5$. In next subsection we confirm this observation showing that the asymptotic behaviour of the integral (4.23) for non-integer $3 < \lambda < 5$ qualitatively differs from that at $\lambda \geq 5$.

Table 4.3: Coordinates of the few first Lee-Yang zeros h_j for the Ising model on an annealed scale-free network for different λ. In the region $3 < \lambda < 5$ the number of purely imaginary zeros decreases with a decrease of λ. However, the coordinate of the first Lee-Yang zero remains purely imaginary for any value of λ.

$j\backslash\lambda$	$\lambda > 5$	$\lambda = 4.5$	$\lambda = 4$	$\lambda = 3.5$
$j = 1$	$i3.453$	$i3.495$	$i3.569$	$i3.762$
$j = 2$	$i6.784$	$i6.933$	$i7.823$	$1.875 + i7.212$
$j = 3$	$i9.636$	$i9.474$	$i8.149$	$3.659 + i9.496$
$j = 4$	$i12.229$	$0.589 + i12.848$	$2.418 + i11.466$	$5.138 + i11.351$
$j = 5$	$i14.650$	$2.297 + i16.346$	$4.014 + i14.174$	$6.435 + i12.983$
$j = 6$	$i16.945$	$3.761 + i19.405$	$5.446 + i16.574$	$7.608 + i14.470$
$j = 7$	$i19.140$	$5.130 + i22.229$	$6.767 + i18.776$	$8.690 + i15.850$
$j = 8$	$i21.254$	$6.427 + i24.886$	$8.005 + i20.835$	$9.702 + i17.146$
$j = 9$	$i23.301$	$7.667 + i27.414$	$9.176 + i22.783$	$10.656 + i18.375$
$j = 10$	$i25.289$	$8.859 + i29.838$	$10.293 + i24.642$	$11.563 + i19.548$

The picture in Fig. 4.4 demonstrates that the circle theorem does not hold for the Ising model on an annealed scale-free network in the complex e^h-plane: while for $\lambda \geq 5$ all zeros lie on the unit circle, it does not hold at $\lambda = 4.5$. In a later case only a few low index zeros lie on the unit circle, the rest being scattered in the complex plane.

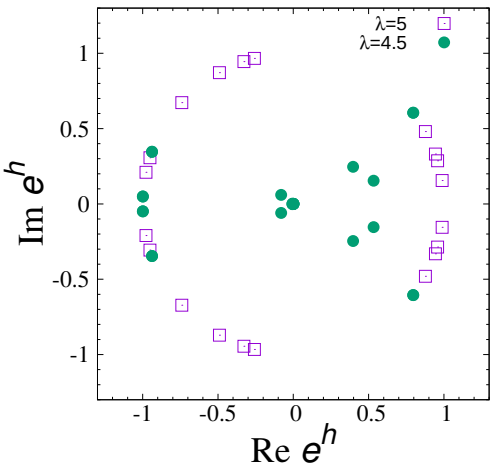

Fig. 4.4: Lee-Yang zeros in the complex e^h-plane at $\lambda \geq 5$ and the circles to $\lambda = 4.5$, squares and circles correspondingly. The plot depicts only those zeros that fit into the region shown.

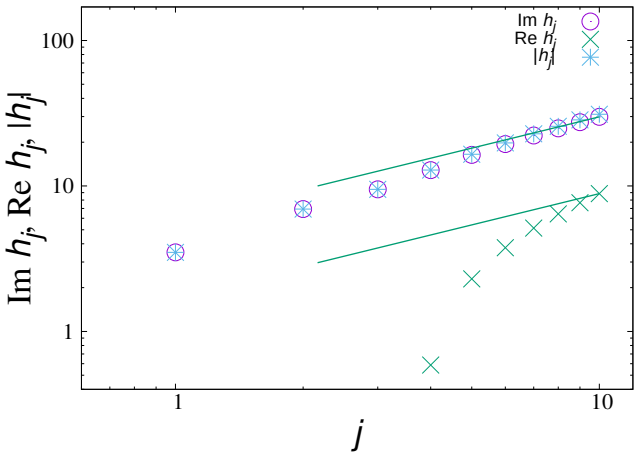

Fig. 4.5: Coordinates of the first ten Lee-Yang zeros h_j of the Ising model on an annealed scale-free network at $\lambda = 4.5$. Different curves correspond to $\mathrm{Im}\, h_j$, $\mathrm{Re}\, h_j$, $|h_j|$ as shown in the legend. One can see that the curves for $\mathrm{Im}\, h_j$ and $|h_j|$ are very close to each other (since the value of $\mathrm{Re}\, h_j$ is relatively small). The lines correspond to the expected value $\sigma(\lambda = 4.5) \simeq 0.714$, from (4.25).

Consequently, the Ising model on an annealed scale-free network at $3 < \lambda < 5$ belongs to the group of models where the Lee-Yang theorem is violated, whereas the model on the complete graph obeys the theorem. The difference in behaviour of the Lee-Yang zeros of the Ising model on a complete graph and on an annealed scale-free network manifests itself also when one checks the scaling of the zero coordinates with j. The coordinate of the zeros being complex, the scaling in principle can be observed with respect to the real or imaginary part of the coordinates or their combination. Typical results of our calculations are demonstrated in Fig. 4.5, where we plot coordinates of $\mathrm{Im}\, h_j$, $\mathrm{Re}\, h_j$ and $|h_j|$ for the first ten Lee-Yang zeros of the Ising model on an annealed scale-free network at fixed value of $\lambda = 4.5$. The solid lines correspond to the expected value $\sigma(\lambda = 4.5) \simeq 0.714$, cf. (4.25). One can see that the curves for $\mathrm{Im}\, h_j$ and $|h_j|$ are very close to each other, since the value of $\mathrm{Re}\, h_j$ is relatively small. Similar behaviour is observed for the other values of λ. In particular, for high j the $\mathrm{Im}\, h_j$ and $|h_j|$ functions are governed by the power law asymptotics with an exponent given by (4.25).

In turn, for small j the power law behaviour may be regained by introducing a more general form of scaling that involves the parameter C as it was done for the complete graph, see equation (3.19). We check whether the scaling form (3.19) holds for the Lee-Yang zeros for the Ising model on an annealed scale-free network. Details of our calculations are collected in the Appendix C. We fit the dependence of Lee-Yang zeros on j in the log-log scale by a linear function at different values of the fitting parameter C and λ. We calculate variance of residuals and find the $\sigma(C_{opt})$. Here, in Fig. 4.7**a, c** we have the exponent σ as the function of λ. The solid line shows the exact values,

Eq. (4.16), the squares are results of fitting by Eq.(3.19) at optimal value of the fitting parameter C_{opt}. In Fig. 4.6**c, d** we plot the fitting parameter C_{opt} as the function of λ. In case of the fitting over the purely imaginary Lee-Yang zeros we can observe, that the value of C_{opt} decreases with λ and $\sigma(C_{opt})$ increase with λ approaching its exact value for large λ, when the number of purely imaginary zeros becomes large (see Fig. 4.6**a, b**). Such fitting cannot be used for the case $\lambda < 4$, while only 1 purely imaginary zero exists. So, we investigate the linear fitting over j for the imaginary part h_j of the first 10 zeros (see Fig. 4.6**c, d**). For the small $\lambda < 4$, σ and C_{opt} increase with λ, while for $\lambda > 4$ we observe non monotonously tendency for σ and C_{opt} with λ.

The power law behaviour is less pronounced for small j. Secondly, the power law behaviour of the function is less defined for small values of j. Namely, such way of approximation is not universal and introducing a more general form of scaling that involves the parameter C as it was done for the complete graph, see equation (3.19), does not help to improve the picture (see Appendix III). On the other hand, by linear approximation for a given number of zeros and different fitting parameters that is possible to choose an optimal value closed to exact one (see Appendix IV). The above analysis shows that expected scaling for Lee-Yang zeros on an annealed scale-free network over j in the region $3 < \lambda < 5$ does not hold.

Let us next consider the motion of the Fisher zeros in the real magnetic field. To this end, similar as it was done in the former section for the Ising model on the complete graph, we present the partition function of the Ising model on an annealed scale-free network as a function of rescaled variables z and h. Substituting expansions (4.11)–(4.13) for the functions $I^{\pm}_{\lambda}(x)$ into the partition function (4.9) one arrives at the following representations:

$$Z(t,h) = \begin{cases} \int_0^{+\infty} \exp\Big(- tx^2 - x^{\lambda-1}\Big) \cosh(hx) dx\,, & 3 < \lambda < 5, \\ \int_0^{+\infty} \exp\Big(- tx^2 - x^4\Big) \cosh(hx) dx\,, & \lambda \geq 5\,, \end{cases} \tag{4.26}$$

where t and h are defined by the Eqs. (4.18) and (4.24) respectively.

Fig. 4.7**a** shows the results obtained for the motion of the Fisher zeros in the real magnetic field calculated at different λ for functions (4.26). The squares correspond to $\lambda \geq 5$ and the expected value of the angle of motion from (4.27) is $\psi = \pi/3$. Therefore, in this region of λ our numerical results are in a good agreement with the analytical prediction as we get $\psi \simeq 59°$. However, this is not the case for the smaller values of $3 < \lambda < 5$. Indeed, naively substituting critical exponents values into the equation

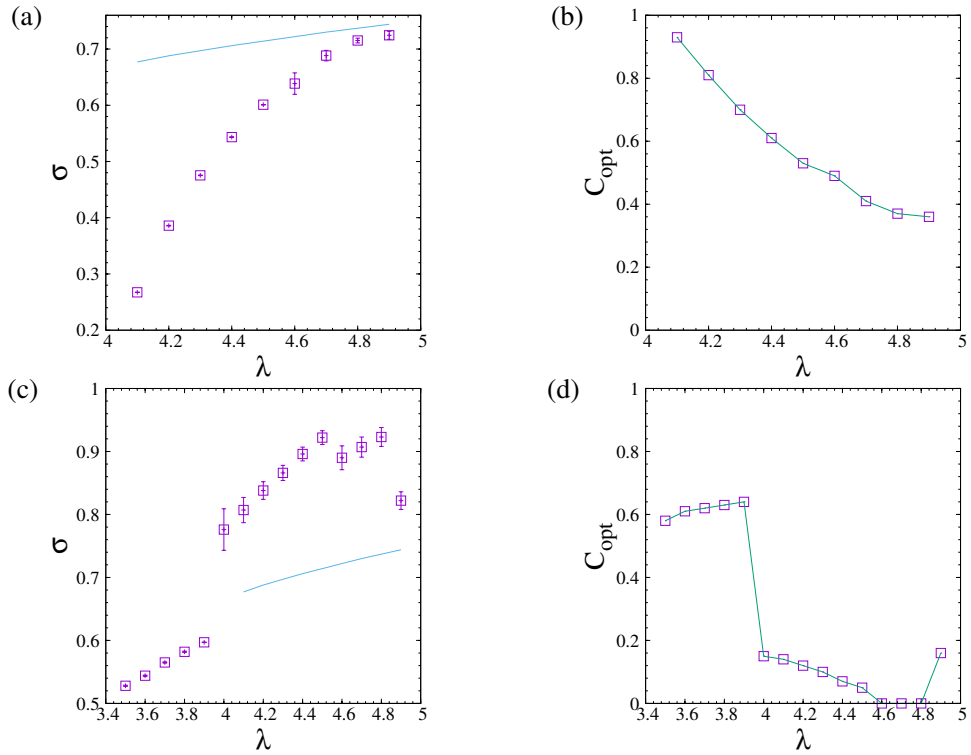

Fig. 4.6: **(a)**, **(c)**: The exponent σ for the Ising model on an annealed scale-free network as function of λ calculated by fitting over the $\mathcal{N}$ Lee-Yang zeros and the imaginary part of the first 10 Lee-Yang zeros zeros at different λ, respectively. Solid line: the line of exact values of σ, Eq. (4.25). Rectangles: numerically calculated best fitting results via equation (3.19). **(b)**, **(d)**: Optimal value of the fitting parameter C_{opt} as function of λ calculated by fitting over the $\mathcal{N}$ Lee-Yang zeros and the imaginary part of the first Lee-Yang zeros zeros at different λ, respectively.

(1.20) for the angle ψ one gets

$$\psi = \frac{\pi(\lambda - 3)}{2(\lambda - 2)}\,. \tag{4.27}$$

In particular, from (4.27) one expects that the angle of motion will decrease with λ. The three curves from the Fig.4.7**a**, calculated for $\lambda = 4.8$, 4.5 and 4 demonstrate the opposite behaviour: the angle increases with decreasing λ with a tendency to reach asymptotics at $\psi = \pi/2$. As we have shown above, for the model under consideration the zeros at the critical point do not obey the Lee-Yang theorem: there is only a small number of zeros with purely imaginary coordinates for $3 < \lambda < 5$. Therefore the equation (4.27) that was obtained under an assumption that this theorem holds is not applicable. The angle ψ (1.20) describing the motion of Fisher zeros in real magnetic field does not seem to be related by a simple scaling relation to the critical exponents.

Similar to what was done for the Ising model on a complete graph, one can define scaling functions for the real and imaginary parts of the jth zero z_j. Using the definition (3.36) of the scaling functions from the subsection 3.4 for $\mathcal{Z}_j^{\mathcal{R}}(h)$, $\mathcal{Z}_j^{\mathcal{I}}(h)$ in different

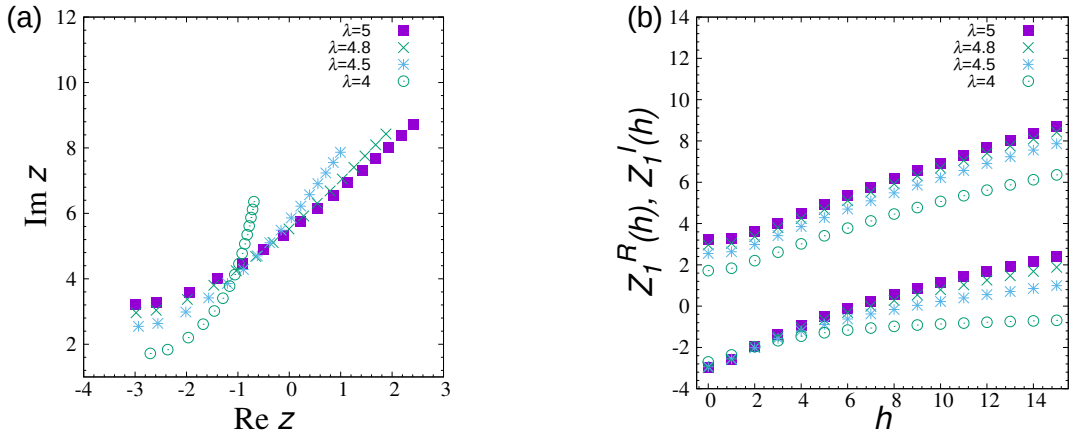

Fig. 4.7: **(a)** Motion of the first Fisher zeros of the partition function (4.26) in the complex z plane for different values of the real magnetic field $h = s$, $s = 0, 1, \ldots, 15$ and λ. **(b)** Scaling functions $\mathcal{Z}_1^{\mathcal{R}}(h)$ (lower plots), $\mathcal{Z}_1^{\mathcal{I}}(h)$ (upper plots) (4.28) for the real and imaginary part of the first Fisher zero coordinate z_1, as functions of the scaling variable h at different values of λ.

regions of λ we define the scaling functions for the Ising model on an annealed scale-free network as

$$\mathcal{Z}_j^{\mathcal{R},\mathcal{I}}(h) \equiv \begin{cases} \frac{\langle k^2\rangle}{2}[a(\lambda)]^{2/(\lambda-1)}\,\mathcal{T}_j^{\mathcal{R},\mathcal{I}}\left(h\frac{\langle k^2\rangle}{\langle k\rangle^2}a(\lambda)^{1/(\lambda-1)}\right)\,, & 3<\lambda<5, \\ \langle k^2\rangle\sqrt{6}/\sqrt{\ln N}\,\mathcal{T}_j^{\mathcal{R},\mathcal{I}}\left(h\frac{\langle k^2\rangle}{\langle k\rangle^2}(\frac{\ln N}{24})^{1/4}\right)\,, & \lambda=5, \\ \langle k^2\rangle\sqrt{3\langle k^4\rangle}\,\mathcal{T}_j^{\mathcal{R},\mathcal{I}}\left(h\frac{\langle k^2\rangle}{\langle k\rangle^2}(\frac{\langle k^4\rangle}{12})^{1/4}\right), & \lambda>5\,, \end{cases} \tag{4.28}$$

and expressions for h at different λ are given by (4.24). The scaling functions for the first Fisher zero z_1 at different values of λ are plotted in Fig. 4.7**b**. From Eq. (3.37) we expect that the ratio $\mathcal{Z}_1^{\mathcal{I}}(0)/\mathcal{Z}_1^{\mathcal{R}}(0)$ gives the Fisher pinching angle φ, which in the case of the scale-free network is λ-dependent (see subsection 3.4). From Fig. 4.7**b** we calculate $\mathcal{Z}_i^{\mathcal{I}}(0)/\mathcal{Z}_i^{\mathcal{R}}(0) = 0.921;\ 0.798;\ 0.577$ or $\varphi \simeq 0,249\pi;\ 0.228\pi;\ 0.18\pi$ for $\lambda = 4,8;\ 4.5;\ 4$ respectively. These values agree with those predicted by equation (4.15) and given in Table 4.1. Note that the agreement increases with an increase of the zero number j.

4.3.2 The asymptotic behaviour of Lee-Yang zeros

We determine an asymptotic estimate for the behaviour of the partition function $Z(h)$ (4.23) at $\mathrm{Re}\,h = 0$ in the limit of large $\mathrm{Im}\,h$ at $\lambda \leq 5$. To this end, let us consider an integral

$$Z(ir) = \int_0^\infty e^{-x^{\lambda-1}}\,\cos(rx)dx\,, \tag{4.29}$$

that depends on the real variable r. At $r = \mathrm{Im}\, h$ (4.29) gives an imaginary part of the partition function (4.23). Asymptotic behaviour of $Z(ir)$ follows from the Erdelyi lemma (see e.g. [203]) as explained below.

The Erdelyi lemma gives an asymptotic behaviour of the integral:

$$F(y) = \int_0^A x^{b-1} f(x) e^{iyx^a} dx. \tag{4.30}$$

According to the lemma, if $a \geq 1$, $b > 0$ and the function $f(x)$ becomes zero together with all its derivatives at the upper integration limit: $f(A) = f'(x)|_{x=A} = ... = f^{(n)}(x)|_{x=A} = 0$, the following asymptotic estimate for the integral (4.30) is valid:

$$F(y) \sim \sum_{k=0}^{\infty} a_k y^{-\frac{k+b}{a}}, \qquad y \to \infty, \tag{4.31}$$

where the coefficients a_k are given by

$$a_k = \frac{f^k(0)}{k!a} \Gamma\Big(\frac{k+b}{a}\Big) \exp\Big(\frac{i\pi(k+b)}{2a}\Big). \tag{4.32}$$

Changing variables in (4.29) one can represent $J_\lambda(y)$ in the form similar to (4.31):

$$Z(ir) = \frac{5}{\lambda - 1} \mathrm{Re} \int_0^\infty x^{\frac{5}{\lambda-1}-1} e^{-x^5} e^{irx^{5/(\lambda-1)}} dx. \tag{4.33}$$

Note that the upper integration limit is this case is $a = \infty$. It is easy to see that the conditions of the lemma are satisfied and an asymptotic expansion for the function (4.29) follows:

$$Z(ir) \sim \sum_{k=0}^{\infty} b_k r^{-\frac{k(\lambda-1)}{5}-1}, \qquad r \to \infty, \tag{4.34}$$

where the coefficients b_k are defined as

$$b_k = \frac{(\lambda-1) f^k(0)}{5k!} \Gamma\Big(\frac{k(\lambda-1)}{5} + 1\Big) \cos\Big(\frac{\pi(k(\lambda-1)+5)}{10}\Big). \tag{4.35}$$

Note, that coefficients $b_k = 0$ for the marginal values $\lambda = 3$ and $\lambda = 5$: the decay differs from the power law. To evaluate it, we proceed as follows.

- $\lambda = 3$

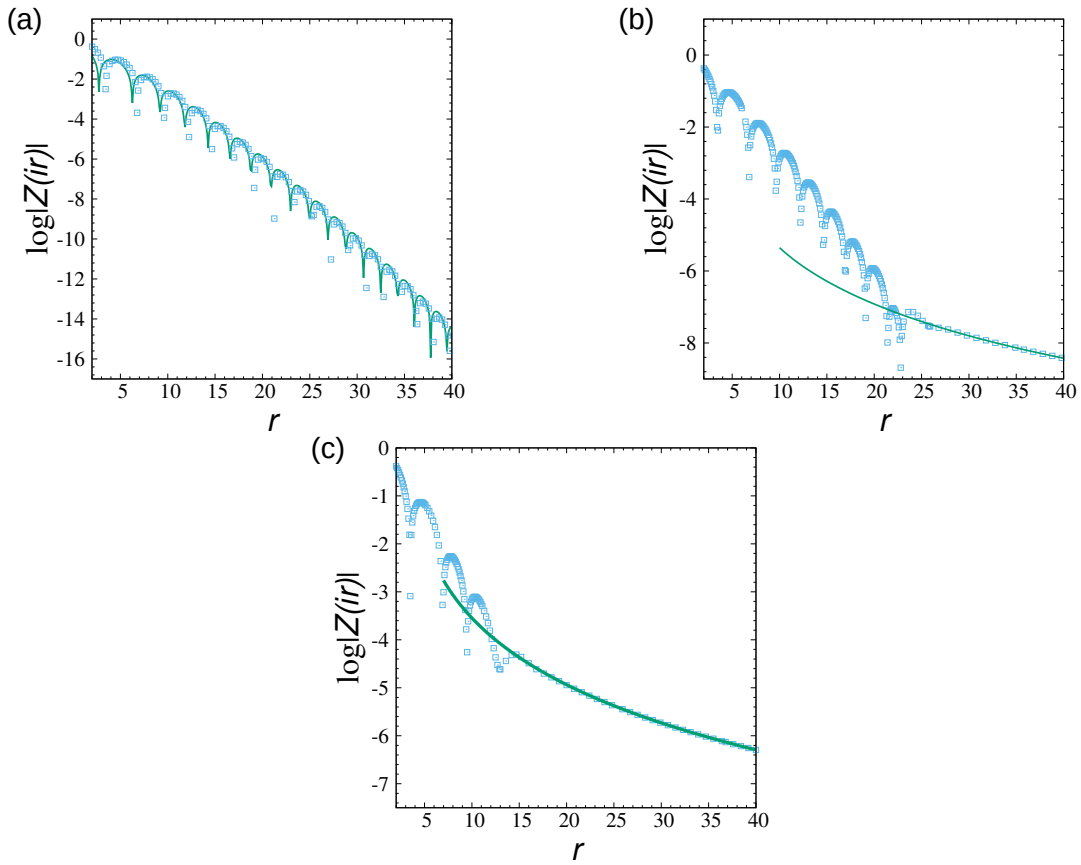

Fig. 4.8: Function $\log|Z(ir)|$ for: **(a)** $\lambda \geq 5$, **(b)** $\lambda = 4.99$, and **(c)** $\lambda = 4.5$. Solid lines: results of asymptotic expansions. Squares: numerically calculated values. For $\lambda \geq 5$ the function keeps oscillating in the asymptotics (meaning that the number of zeros is unbounded), it is not the case for $\lambda < 5$.

For $\lambda = 3$ the integral (4.29) is taken exactly leading to

$$Z(ir) = \sqrt{\pi/2}\exp\Big(-r^2/4\Big)\,. \tag{4.36}$$

Therefore, in the limit of large r the integral decays exponentially. Moreover, $Z(ir) > 0$ for any $0 < r < \infty$ which signals about an absence of partition function zeros on the complex h plane at $\lambda = 3$. In turn, this brings about an absence of the phase transition in this case.

- $\lambda = 5$

In this case integral (4.29) can be rewritten as:

$$Z(ir) = \int_0^{+\infty} e^{-x^4}\,\cos(rx)dx = \frac{1}{2}\mathrm{Re}\int_{-\infty}^{+\infty} e^{-x^4}\,e^{ixr}dx\,. \tag{4.37}$$

Its asymptotics can be evaluated by a steepest descent method, calculating the

function under the integral in the point of extremum at $x = (ir/4)^{1/3}$ and leading to:

$$Z(ir) \sim \frac{1}{2} \exp\Big(-\frac{3}{2}(r/4)^{4/3}\Big) \cos\Big(\frac{3\sqrt{3}}{2}(r/4)^{4/3}\Big)\,, \qquad r \to \infty\,. \tag{4.38}$$

The integral $Z(ir)$ has an infinite number of zeros due to the presence of an oscillating function in the r.h.s., as we further demonstrate below.

In Fig. 4.8 we compare behaviour of the numerically calculated function $\log|Z(ir)|$ with its asymptotic expansion using Eqs. (4.34) and (4.38) for different λ. One can see that behaviour of the function for $\lambda < 5$ is qualitatively different from that at $\lambda \geq 5$: whereas in the last case the function keeps oscillating in the asymptotics (meaning that the number of zeros is unbounded), it is not the case for $3 < \lambda < 5$. Here, after finite number of oscillations the function approaches its asymptotics from above. Therefore, the number of zeros is limited. As one can see from the Figs. 4.8**a**, **b**, **c**, the number of oscillations decreases with the decrease of λ.

4.4 Conclusions

In this chapter we investigate the complex partition function zeros of the Ising model on an annealed scale-free network with a node degree distribution decay exponent λ. During the study several new and rather unexpected features were observed.

It was known that critical exponents, scaling functions and critical amplitudes ratios for the Ising model on scale-free network depend on the value of global parameter λ. Analyzing the partition function zeros we find that the pinching angle φ as well as the Lee-Yang edge exponent σ are λ-dependent too. In the region $\lambda > 5$ we recover the values obtained previously for the Ising model on the complete graph and in case $3 < \lambda < 5$ ones are given by equations (4.15), (4.16).

Secondly, the logarithmic corrections to leading scaling behaviour that arise for the spin models on scale-free networks [88, 89, 93, 94] at $\lambda = 5$ are observed for the exponents that govern condensation of Lee-Yang and Fisher zeros with the increase of the system size. Corresponding gaps in H- and t planes decrease with N at $\lambda = 5$ as

$$H_j \sim N^{-3/4}\Big(\ln N\Big)^{1/4}, \qquad t_j \sim N^{-1/2}(\ln N)^{1/2}\,. \tag{4.39}$$

Note, that the powers of the logarithms comply with the corresponding scaling relations [89].

The striking feature of the Ising model on an annealed scale-free network is that its partition function zeros calculated at T_c in complex magnetic field does not obey the Lee-Yang theorem in a region $3 < \lambda < 5$. At $\lambda \geq 5$ all zeros are purely imaginary while at $\lambda < 5$ with the decrease of λ the zeros acquire both real and imaginary parts. This is a surprising result, because it means that the role of decay exponent λ (for networks) and dimensionality d (for lattices) is not equivalent on the Lee-Yang zeros level. Note that experimental identification of the Lee-Yang zeros [17] has so far only been made for purely imaginary zeros [152], but there are other models, for which the Lee-Yang theorem does not hold [136–147]. The results identified herein show that while these are accessible for lattices and complex networks for sufficiently large λ, not all network zeros are accessible in this manner for $\lambda < 5$. A challenge for experiment is to find another way to access them.

Unlike the above examples, the problem that we have considered in this chapter concerns ferromagnetic Ising model, and the Lee-Yang theorem was proven [204] to hold for any Ising-like model with ferromagnetic interaction, see also [205, 206]. In this respect the Hamiltonian analyzed here (4.1) looks as if it will lead to the Lee-Yang property of the partition function. Averaging twice the partition function over spins and all possible network configurations we find a place which leads to the violation of the Lee-Yang unit circle theorem in the region $3 < \lambda < 5$: indeed, if one takes a sum (or an integral) of functions each of which possesses the Lee-Yang property, the sum might not possess such property at all. That is exactly what is observed for the annealed network.

CONCLUSIONS

In this thesis we investigate the critical behaviour of the spin models on scale-free networks and on a complete graph. The critical behaviour of spin models on scale-free networks with a power law node degree distribution decay depends on the value of the decay exponent λ (2.2). The critical exponents, amplitude ratios and scaling functions appear to be λ-dependent. Thereby the concept of universality for spin model on scale-free networks is modified: λ plays the role of a global parameter which defines the universality class. Together with traditional mean-field method for a complex networks we used the method of partition function zeros analysis in the complex plane. We firstly apply this method to spin models on scale-free networks. The results obtained show perspectives and open a new way for further investigation of phase transitions on complex networks. We shortly summarized the main original results obtained in the previous three chapters below.

1. For the q-state Potts model on an uncorrelated scale-free network in the presence of quenched disorder using the mean field approach the expressions for a free energy was obtained. The phase diagram of the model (Fig. 2.2) indicates that the ordering and order of phase transition are dependent on the number of Potts states q, as well as on the decay exponent λ in appropriate way. For the second order phase transition regime firstly a scaling functions and critical amplitude ratios had been obtained.

2. For percolation (Potts model in the limit $q \to 1$) on scale-free networks we demonstrate the appearance of logarithmic corrections to scaling. The logarithmic corrections obtained have a negative sign. This weakens the singularities of observables near the percolation point.

3. We found that the jump of the heat capacity δc_H for the Ising model on a scale-free network is λ-dependent even at $\lambda > 5$, while all critical exponents are λ-independent and correspond on the values predicted by mean field theory. For that case the value of the heat capacity jump tends to the predicted mean field one in the limit $\delta c_H(\lambda \to \infty) = 3/2$.

4. We complete the analysis for the Ising model on a complete graph using the Lee-Yang-Fisher formalism for the partition function zeros. Using the method proposed for zeros in complex temperature plane (Fisher zeros) we found: the appropriate integral representations for the partition function in complex magnetic field plane (Lee-Yang zeros); values of conformal invariant angles and scaling exponent for Lee-Yang zeros.

5. First we apply the method of partition function zeros analysis for an investigation of spin models behaviour on scale-free networks. The conformal invariant characteristics of zeros location appear to be λ-dependent for the Ising model on a scale-free network. In particular, the Fisher zeroes condensation angle φ and scaling exponent σ in the region $\lambda \geq 5$ correspond to ones on a complete graph, and in case $3 < \lambda < 5$ are defined by formulas (4.15), (4.16).

6. For the Ising model on a scale-free network the logarithmic corrections to the zeros coordinates as a function of system size N appear at $\lambda = 5$ (see Eq. (4.39)) with exponents satisfied the scaling relations to those logarithmic corrections.

7. The Lee-Yang circle theorem for the Ising model on an annealed scale-free network is violated in a region $3 < \lambda < 5$. If at $\lambda \geq 5$ whole zeros are purely imaginary, it is not the case for $3 < \lambda < 5$: if the decay exponent λ decrease then the number of purely imaginary zeros decrease and zeros with imaginary and real parts appears which contradict the theorem conditions.

Bibliography

[1] L. Eulero, *Commentarii academiae scientiarum Petropolitanae* **8**, 128, (1741). *"Solutio problematis ad geometriam situs pertinentis"*.

[2] J. A. Bondy, U. S. R. Murty, *Graph theory and applications*, The Macmillan Press Ltd (1976).

[3] R. Albert, A.-L. Barabási, *Rev. Mod. Phys.* **74**, 47 (2002). *"Statistical mechanics of complex networks"*.

[4] S. N. Dorogovtsev, J. F. F. Mendes, *Evolution of Networks: From Biological Networks to the Internet and WWW*, Oxford University Press (2003).

[5] Yu. Holovatch, C. von Ferber, O. Olemskoi, T. Holovatch, O. Mryglod, I. Olemskoi, V. Palchykov, *J. Phys. Stud.* **10**, 247 (2006). *"Complex networks"* (in ukrainian).

[6] A. Barrat, M. Barthelemy, A. Vespignani, *Dynamical Processes on Complex Networks*, Cambridge University Press (2008).

[7] M. Newman, *Networks: An Introduction*, Oxford University Press (2010).

[8] I. P. Erdös, A. Rényi, *Publ. Math. (Debrecen)* **6**, 290 (1959). *"On random graphs"*.

[9] D. J. Watts, S. H. Strogatz, *Nature (London)* **393**, 440 (1998). *"Collective dynamics of small-world networks"*.

[10] D. J. Watts, *Small Worlds*, Princeton University Press (1999).

[11] R. Cohen, K. Erez, D. ben-Avraham, and S. Havlin, *Phys. Rev. Lett.* **85**, 4626 (2000). *"Resilience of the Internet to random breakdowns"*.

[12] B. Berche, C. von Ferber, T. Holovatch, Yu. Holovatch, *Eur. Phys. J. B* **71**, 125 (2009). *"Resilience of public transport networks against attacks"*.

[13] A.-L. Barabási, A. Reka, *Science* **286**, 509 (1999). *"Emergence of Scaling in Random Networks"*.

[14] A.-L. Barabási, R. Albert, H. Jeong, *Physica A* **281**, 69 (2000). *"Scale-free characteristics of random networks: the topology of the world wide web "*.

[15] S. Galam, *Sociophysics: A Physicist's Modeling of Psycho-political Phenomena (Understanding Complex Systems)*, Springer (2012).

[16] B. Tadić, K. Malarz, K. Kułakowski, *Phys. Rev. Lett.* **94**, 137204 (2005). *"Magnetization Reversal in Spin Patterns with Complex Geometry"*.

[17] X. Peng, H. Zhou, B.-B. Wei, J. Cui, J. Du, R. B. Liu, *Phys. Rev. Lett.* **114**, 010601 (2015). *"Experimental Observation of Lee-Yang Zeros"*.

[18] M. Krasnytska, B. Berche, Yu. Holovatch, *Condens. Matter Phys.* **16**, 23602 (2013). *"Phase transitions in the Potts model on complex networks"*.

[19] M. Krasnytska, *Condens. Matter Phys.* **17**, 23602 (2014). *"Scaling functions and amplitude ratios for the Potts model on an uncorrelated scale-free network "*.

[20] M. Krasnytska, B. Berche, Yu. Holovatch, R. Kenna, *Condens. Matter Phys.* **18**, 44601 (2015). *"On the discontinuity of the specific heat of the Ising model on a scale-free network"*.

[21] M. Krasnytska, B. Berche, Yu. Holovatch, R. Kenna, *Eur. Phys. Lett.* **111**, 60009 (2015). *"Violation of Lee-Yang circle theorem for Ising phase transitions on complex networks"*.

[22] M. Krasnytska, B. Berche, Yu. Holovatch, R. Kenna, *J. Phys. A: Math. Theor.* **49**, 135001 (2016). *"Partition function zeros for the Ising model on complete graphs and on annealed scale-free networks"*.

[23] M. Krasnytska, B. Berche, Yu. Holovatch, *Scaling functions and critical amplitude ratios for the Potts model on scale-free networks*. In: "Proceedings of VI International Conference: Physics of Disordered Systems", Lviv: ICMP NASU, 2013.

[24] M. Krasnytska, B. Berche and Yu. Holovatch, *Critical behaviour of the Potts model on complex networks*. In: "Book of abstracts. Christmass discussions 2013", Lviv, 2013.

[25] M. Krasnytska, B. Berche and Yu. Holovatch, *Phase transitions for the Potts model on a complex networks.* In: "Book of abstracts. 13-th Ukrainian School of young scientists in Statistical Physics and Condensed Matter theory", Lviv: ICMP, 2013.

[26] M. Krasnytska, B. Berche and Yu. Holovatch, *Scaling functions and amplitude ratios for the Potts model on uncorrelated scale-free network.* In: "Book of abstracts. 5-th Young Scientists Conference: Problems of Theoretical Physics", Kyiv, 2013.

[27] M. Krasnytska, B. Berche, Yu. Holovatch, R. Kenna, *Lee-Yang-Fisher zeros for the Ising model on complex networks.* In: "Book of abstracts. MECO-39 Conference", Coventry, 2014.

[28] M. Krasnytska, B. Berche, Yu. Holovatch, R. Kenna, *Lee-Yang-Fisher zeros for the Ising model on complex networks.* In: "Book of abstracts. CompPhys-2014", Leipzig, 2014.

[29] M. Krasnytska, B. Berche, Yu. Holovatch, R.Kenna, *Violation of the Lee-Yang circle theorem for the Ising model on complex network.* In: "Book of abstracts. Christmass discussions 2015", Lviv, 2015.

[30] M. Krasnytska, *Zeros for the partition function of the Ising model on scale free networks.* In: "Book of abstracts. 15-th Ukrainian School of young scientists in Statistical Physics and Condensed Matter theory", Lviv: ICMP NASU, 2015.

[31] M. Krasnytska, B. Berche, Yu. Holovatch, R. Kenna, *Violation of Lee-Yang circle theorem for Ising phase transitions on complex networks.* In: "Book of abstracts. MECO-41 Conference", Vienna, 2016.

[32] M. Krasnytska, B. Berche, Yu. Holovatch, R. Kenna, *On the discontinuity of the specific heat of the Ising model on a scale-free network.* In: "Book of abstracts. MECO-41 Conference", Vienna, 2016.

[33] R. Diestel, *Graph Theory*, Springer-Verlag, Graduate Texts in Mathematics, Vol. **173** (2005).

[34] S. Bornholdt, H. Schuster, *Handbook of Graphs and Networks*, Wiley-VCH (2003).

[35] M. Faloutsos, P. Faloutsos, C. Faloutsos, *Computer Communications Rev.* **29**, 251 (1999). *"On power-law relationships of the internet topology".*

[36] R. Albert, H. Jeong, A.-L. Barabási, *Nature (London)* **401**, 130 (1999). *"Diameter of the world wide web ".*

[37] H. Jeong, B. Tombor, R. Albert, Z. N. Oltvai, A.-L. Barabási, *Nature (London)* **407**, 651 (2000). *"The large-scale organization of metabolic networks".*

[38] F. Liljeros, C. R. Edling, L. A. N. Amaral, H. E. Stanley, Y. Aberg, *Nature* **411**, 907 (2001). *"The Web of Human Sexual Contacts".*

[39] R. Kumar, P. Raghavan, S. Rajalopagan, A. Tomkins, *Extracting large-scale knowledge bases from the web.* In: "Proceedings of 9th ACM Symposium on Principles of Database Systems", Philadephia, 1999.

[40] J. M. Kleinberg, R. Kumar, P. Raghavan, S. Rajagopalan, A. Tomkins. In: "Proceedings of the Int. Conf. on Combinatorics and Computing, Lect. Notes in Comput. Sci." Berlin: Springer-Verlag, 1999.

[41] L. A. Adamic, B. A. Huberman, *Science* **287**, 2115 (2000). *"Power-law distribution of the world wide web".*

[42] M. E. J. Newman, *Proc. Natl. Acad. Sci. USA.* **98**, 404 (2001). *"The structure of scientific collaboration networks".*

[43] E. J. Newman, *SIAM Review* **45**, 167 (2003). *"The structure and function of complex networks".*

[44] A. L. Barabási, H. Jeong, Z. Neda, E. Ravasz, A. Schubert, T. Vicsek, *Physica A* **311**, 590 (2002). *"Statistical mechanics and its applications".*

[45] M. E. J. Newman, *Proc. Natl. Acad. Sci. USA* **101**, 5200 (2004). *"Coauthorship networks and patterns of scientific collaboration".*

[46] L. A. N. Amaral, A. Scala, M. Barthelemy, H. E. Stanley, *Proc. Natl. Acad. Sci. USA* **97**, 11149 (2000). *"Classes of small-world networks".*

[47] R. Guimera, L. A. N. Amaral, *Eur. Phys. J. B* **38**, 381 (2004). *"Modeling the world-wide airport network ".*

[48] R. Guimera, S. Mossa, A. Turtschi, L. A. N. Amaral, *Proc. Nat. Acad. Sci. USA* **102**, 7794 (2005). *"The worldwide air transportation network: Anomalous centrality, community structure, and cities' global roles".*

[49] A. Barrat, M. Barthelemy, R. Pastor-Satorras, A. Vespignani, *Proc. Natl. Acad. Sci. USA* **101**, 3747 (2004). *"The architecture of complex weighted networks"*.

[50] W. Li, X. Cai, *Phys. Rev. E* **69**, 046106 (2004). *"Statistical analysis of airport network of China"*.

[51] M. Guida, F. Maria, *Chaos Solitons & Fractals* **31**, 527 (2007). *"Topology of the Italian airport network: A scale-free small-world network with a fractal structure?"*.

[52] P. Sen, S. Dasgupta, A. Chatterjee, P. A. Sreeram, G. Mukherjee, S. S. Manna, *Phys. Rev. E* **67**, 036106 (2003). *"Small-world properties of the Indian railway network "*.

[53] V. Latora, M. Marchiori, *Phys. Rev. Lett.* **87**, 198701 (2001). *"Efficient Behavior of Small-World Networks "*.

[54] V. Latora, M. Marchiori, *Physica A* **314**, 109 (2002). *"Is the Boston subway a small-world network?"*.

[55] K. A. Seaton, L. M. Hackett, *Physica A* **339**, 635 (2004). *"Stations, trains and small-world networks "*.

[56] C. von Ferber, Yu. Holovatch, V. Palchykov, *Condens. Matter Phys.* **8**, 225 (2005). *"Scaling in public transport networks"*.

[57] J. Sienkiewicz, J. A. Holyst, *Phys. Rev. E* **72**, 046127 (2005). *"Log-periodic oscillations due to discrete effects in complex networks"*.

[58] X. Xu, J. Hu, F. Liu, L. Liu, *Physica A* **374**, 441 (2007). *"Scaling and correlations in three bus-transport networks of China"*.

[59] R. Brout, *Phys. Rev.* **115**, 824 (1959). *"Statistical mechanical theory of a random ferromagnetic system"*.

[60] E. A. Bender, E. R. Canfield, *Journ. Comb. Theory A* **24**, 296 (1978). *"The asymptotic number of labelled graphs with given degree sequences"*.

[61] S. H. Lee, M. Ha, H. Jeong, J. D. Noh, H. Park, *Phys. Rev. E* **80**, 051127 (2009). *"Critical Behavior of the Ising Model in Annealed Scale-free Networks"*.

[62] G. Bianconi, *Phys. Rev. E* **85**, 061113 (2012). *"Superconductor-insulator transition in annealed complex networks"*.

[63] S. N. Dorogovtsev, A. V. Goltsev, J. F. F. Mendes, *Phys. Rev. E* **66**, 016104 (2002). *"Ising model on networks with an arbitrary distribution of connections"*.

[64] S. N. Dorogovtsev, A. V. Goltsev, J. F. F. Mendes, *Rev. Mod. Phys.* **80**, 1275 (2008). *"Critical phenomena in complex networks"*.

[65] A. Aleksiejuk, J. A. Ho lyst, D. Staufer, *Physica A* **310**, 260 (2002). *"Ferromagnetic phase transition in Barabasi-Albert networks"*.

[66] G. Bianconi, *Phys. Lett. A* **303**, 166 (2002). *"Mean field solution of the Ising model on a Barabasi–Albert network"*.

[67] F. Y. Wu, *Rev. Mod. Phys.* **54**, 235 (1982). *"The Potts model"*.

[68] E. Müller-Hartmann , J. Zittartz, *Phys. Rev. Lett.* **33**, 893 (1974). *"New type of phase transition "*.

[69] E. Müller-Hartmann, J. Zittartz, *Z. Physik.* **22**, 59 (1975). *"Phase transitions of continuous order: Ising model on a Cayley tree"*.

[70] Y. K. Wang, F. U. Wu, *J. Phys. A* **9**, 593 (1976). *"Multi-component spin model on a Cayley tree"*.

[71] L. Turban, *Phys. Lett. A* **78**, 404 (1980). *"S-state Potts model on a Cayley tree"*.

[72] N. Ganikhodjaev, F. Mukhamedov, J. F. F. Mendes, *J. Stat. Mech.: Theor. and Exper.*, 08012 (2006). *"On the three state Potts model with competing interactions on the Bethe lattice"*.

[73] N. Ganikhodjaev, F. Mukhamedov, C. H. Pah, *Phys. Lett A* **373**, 33 (2008). *"Phase diagram of the three states Potts model with next nearest neighbour interactions on the Bethe lattice"*.

[74] R. J. Baxter, *Exactly solved models in statistical physics*, Academic Press (1982).

[75] R. Folk, Yu. Holovatch, T. Yavors'kii, *Uspiekhi Fizichieskikh Nauk* **173**, 175 (2003). *"Critical exponents of a three-dimensional weakly diluted quenched Ising model"*.

[76] V. Dotsenko, *Introduction to the replica theory of disordered statistical systems*, Cambridge university press (2001).

[77] A. Barrat, M. Weigt, *Eur. Phys. J. B* **13**, 547 (2000). *"On the properties of small-world network models"*.

[78] B. J. Kim, H. Hong, P. Holme, G. S. Jeon, P. Minnhagen, M. Y. Choi, *Phys. Rev. E* **64**, 056135 (2001). *"XY model in small-world networks"*.

[79] C. P. Herrero, *Phys. Rev. E* **65**, 066110 (2002). *"Ising model in small-world networks"*.

[80] M. B. Hastings, *Phys. Rev. Lett.* **91**, 098701 (2003). *"Mean-Field and Anomalous Behavior on a Small-World Network "*.

[81] C. P. Herrero, *Phys. Rev. E* **77**, 041102 (2008). *"Antiferromagnetic Ising model in small-world networks"*.

[82] M. E. J. Newman, *Phys. Rev. E* **66**, 016128 (2002). *"Spread of epidemic disease on networks"*.

[83] C. Song, S. Havlin, H. A. Makse, *Nature (London)* **433**, 392 (2005). *"Topological self-similarity. Box-covering renormalization in complex networks "*.

[84] A. T. Adai, S.V. Date, S. Wieland, E. M. Marcotte, *J. Mol. Biol.* **340**, 179 (2004). *"LGL: creating a map of protein function with an algorithm for visualizing very large biological networks"*.

[85] L. K. Gallos, C. Song, H. A. Makse, *Phys. Rev. Lett.* **100**, 248701 (2008). *"Scaling of degree correlations and its influence on diffusion in scale-free networks"*.

[86] G. Bianconi, *Eur. Phys Lett.* **111**, 56001 (2015). *"Interdisciplinary and physics challenges of network theory"*.

[87] M. Leone, A. Vázquez, A. Vespignani, R. Zecchina, *Eur. Phys. Journ. B* **28**, 191 (2002). *"Ferromagnetic ordering in graphs with arbitrary degree distribution"*.

[88] V. Palchykov, C. von Ferber, R. Folk, Yu. Holovatch, R. Kenna, *Phys. Rev. E* **82**, 011145 (2010). *"Critical phenomena on scale-free networks: Logarithmic corrections and scaling functions"*.

[89] See e.g. R. Kenna, *"Universal Scaling Relations for Logarithmic-Correction Exponents"*. In: *Order, Disorder and Criticality Advanced Problems of Phase Transition Theory. vol. 3.* Yu. Holovatch (editor), World Scientific (2012).

[90] J. M. Kosterlitz, *J. Phys. C: Solid State Physics* **7**, 6 (1974). *"The critical properties of the two-dimensional xy model"*.

[91] M. Hinczewski,A. N. Berker, *Phys. Rev. E* **73**, 066126 (2006). *"Inverted Berezinskii-Kosterlitz-Thouless singularity and high-temperature algebraic order in an Ising model on a scale-free hierarchical-lattice small-world network"*.

[92] N. A. M. Araújo, R. F. S. Andrade, H. J. Herrmann, *Phys. Rev. E* **82**, 046109 (2010). em "q-state Potts model on the Apollonian network".

[93] F. Iglói, L. Turban, *Phys. Rev. E* **66**, 036140 (2002). *"First- and second-order phase transitions in scale-free networks"*.

[94] S. Dorogovtsev, A. V. Goltsev, J. F. F. Mendes, *Eur. Phys. Journ. B* **38**, 177 (2004). *"Potts model on complex networks"*.

[95] G. C. M. A. Ehrhardt, M. Marsili, *J. Stat. Mech.: Theor. and Exper.* 02006 (2005). *"Potts model on random trees "*.

[96] C. Shen, H. Chen, Z. Hou, H. Xin, *Phys. Rev. E* **83**, 066109 (2011). *"Coarse-grained Monte Carlo simulations of the phase transition of the Potts model on weighted networks"*.

[97] D. Stauffer, A. Aharony, *Introduction to percolation theory*, Taylor & Francis (1991).

[98] B. Bollobás, *Cambridge University Press Cambridge Studies in Advanced Mathematics* No. 73, 130 (2001). *"The evolution of random graphs—the giant component"*.

[99] D. S. Callaway, M. E. J. Newman, S. H. Strogatz, D. J. Watts, *Phys. Rev. Lett.* **85**, 5468 (2000). *"Network robustness and fragility: Percolation on random graphs"*.

[100] M. Molloy and B. Reed, *Random Structures and Algorithms* **6**, 161 (1995). *"Critical Point for Random Graphs with a Given Degree Sequence"*.

[101] R. Albert, H. Jeong, A. -L. Barabási, *Nature (London)* **406**, 378 (2000). *"Error and attack tolerance of complex networks".*

[102] Y. Tu, *Nature (London)* **406**, 353-354 (2000). *"How robust is the Internet?".*

[103] R. V. Sole, J. M. Montoya, *Proc. R. Soc. Lond. B* **268**, 2039 (2001). *"Complexity and fragility in ecological networks".*

[104] H. Jeong, S. P. Mason, A.-L. Barabási, Z. N. Oltvai, *Nature (London)* **411**, 41 (2001). *"Lethality and centrality in protein networks".*

[105] R. Pastor-Satorras, A. Vespignani, *Phys. Rev. Lett.* **86**, 3200 (2001). *"Epidemic Spreading in Scale-Free Networks".*

[106] Y. Moreno, R. Pastor-Satorras, A. Vespignani, *Eur. Phys. Journ. B* **26**, 521 (2002). *"Epidemic outbreaks in complex heterogeneous networks".*

[107] A.-L. Barabási, R. Albert, H. Jeong, *Physica A* **272**, 173 (1999). *"Mean-field theory for scale-free random networks ".*

[108] A. V. Goltsev, S. N. Dorogovtsev, J. F. F. Mendes, *Phys. Rev. E* **67**, 026123 (2003). *"Critical phenomena in networks ".*

[109] S. V. Buldyrev, R. Parshani, G. Paul, H. E. Stanley, S. Havlin, *Nature* **464**, 1025 (2010). *"Catastrophic cascade of failures in interdependent networks".*

[110] R. Parshani, S. V. Buldyrev, S. Havlin, *Phys. Rev. Lett.* **105**, 048701 (2010). *"Long-Term Memory: A Natural Mechanism for the Clustering of Extreme Events and Anomalous Residual Times in Climate Records".*

[111] G. Bianconi, S. N.Dorogovtsev, J. F. F. Mendes, *Phys. Rev. E* **91**, 012804 (2015). *"Mutually connected component of network of networks with replica nodes".*

[112] K. Suchecki, J. A. Holyst, *Phys. Rev. E* **74**, 011122 (2006). *"Ising model on two connected Barabasi-Albert networks".*

[113] K. Suchecki, J. A. Holyst, *Phys. Rev. E* **80**, 031110 (2009). *"Bistable-monostable transition in the Ising model on two connected complex networks".*

[114] K. Suchecki, J. A. Holyst, *Order Ising model on Connected complex networks.* In: *Order, Disorder and Criticality: Advanced Problems of Phase Transition Theory*, vol. 3). Ed. Yu. Holovatch, World Scientific (2013).

[115] V. Privman, P. C. Hohenberg, A. Aharony, *Phase Transitions and Critical Phenomena,* vol. 14. Ed. C. Domb and J. L. Lebowitz, Academic Press (1991).

[116] J. L. Cardy, *Finite-Size Scaling. Current Physics - Sources and Comments*, vol. 12. Ed. J. L. Cardy, Elsevier Science Publishers (1988).

[117] H. Hong, M. Ha, H. Park, *Phys. Rev. Lett.* **98**, 258701 (2007). *"Finite-size scaling in complex networks".*

[118] C. N. Yang, T. D. Lee, *Phys. Rev.* **87**, 404 (1952). *"Statistical Theory of Equations of State and Phase Transitions. I. Theory of Condensation".*

[119] T. D. Lee, C. N. Yang, *Phys. Rev.* **87**, 410 (1952). *"Statistical Theory of Equations of State and Phase Transitions. II. Lattice Gas and Ising Model".*

[120] M. E. Fisher, *The nature of critical points: Lecture Notes in Theoretical Physics*, Vol. 7c, University of Colorado Press (1965).

[121] F. Y. Wu, *Int. J. Mod. Phys. B* **22**, 1899 (2008). *"Professor C. N. Yang and Statistical Mechanics ".*

[122] I. Bena, M. Droz, A. Lipowski, *Int. J. Mod. Phys. B* **19**, 4269 (2005). *"Statistical Mechanics of Equilibrium and Nonequilibrium Phase Transitions: The Yang-Lee Formalism ".*

[123] R. B. Pearson, *Phys. Rev. B* **26**, 6285 (1982). *"Partition function of the Ising model on the periodic* $4 \times 4 \times 4$ *lattice".*

[124] C. Itzykson, R. B. Pearson, J. B. Zuber, *Nucl. Phys. B* **220**, [FS8], 415 (1983). *"Diistribution of Zeros in Ising and Gauge Models".*

[125] C. Itzykson, J. M. Luck, *Prog. Phys.* **11**, 45 (1985). *"Zeros of the partition function for statistical models on regular and hierarhical lattices".*

[126] R. Abe, *Prog. Theor. Phys.* **37**, 1070 (1967). *"Logarithmic Singularity of Specific Heat near the Transition Point in the Ising Model".*

[127] W. Janke, D. A. Johnston, R. Kenna, *Nucl. Phys. B* **736**, 319 (2006). *"Properties of higher-order phase transitions".*

[128] P. J. Kortman, R. B. Griffiths, *Phys. Rev. Lett.* **27**, 1439 (1971). *"Density of Zeros on the Lee-Yang Circle for Two Ising Ferromagnets".*

[129] Z. Glumac, K. Uzelac, *Phys. Rev. E* **66**, 022140 (2013). *"Yang-Lee zeros and the critical behavior of the infinite-range two- and three-state Potts models"*.

[130] F. Dunlop, C. M. Newman, *Commun. Math. Phys.* **44**, 223 (1975). *"Multicomponent field theories and classical rotators"*.

[131] B. Simon, R. B. Griffiths, *Commun. Math. Phys.* **33**, 145 (1973). *"The $(\phi^2)_2$ field theory as a classical Ising model"*.

[132] X. Z. Wang, *Physica A* **380**, 163 (2007). *"Yang–Lee circle theorem for an ideal pseudospin-1/2 Bose gas in an arbitrary external potential and in an external magnetic field"*.

[133] R. A. Blythe, M. R. Evans, *Phys. Rev. Lett.* **89**, 080601 (2002). *"Lee-Yang Zeros and Phase Transitions in Nonequilibrium Steady States"*.

[134] O. J. O'Loan, M. R. Evans, M. E. Cates, *Phys. Rev. E* **58**, 1404 (1998). *"Jamming transition in a homogeneous one-dimensional system: The bus route model"*.

[135] T. Chou, D. Lohse, *Phys. Rev. Lett.* **82**, 3552 (1999). *"Entropy-Driven Pumping in Zeolites and Biological Channels"*.

[136] S. Y. Kim, *Phys. Rev. Lett.* **93**, 130604 (2004). *"Yang-Lee Zeros of the Antiferromagnetic Ising Model"*.

[137] S. Y. Kim, *Nucl. Phys. B* **705**, 504 (2005). *"Density of Lee-Yang zeros and Yang-Lee edge singularity in the antiferromagnetic Ising model"*.

[138] M .Suzuki, *J. Math. Phys.* **14**, 1088 (1973). *"Rigorous results for Ising ferromagnets of general spin with degeneracy or symmetric potentials"*.

[139] K. Yamada, H. Nakano, M. Yamashita, *Prog. Theor. Phys.* **65**, 1603 (1981). *"Distribution of zeros of the partition function in the first and second order phase transitions: extension of the Lee-Yang theorem"*.

[140] J. L. Monroe, *J. Stat. Phys.* **65**, 445 (1991). *"Restrictions on the phase diagrams for a large class of multisite interaction spin systems"*.

[141] K. K. Chin, D. P. Landau, *Phys. Rev. B* **36**, 275 (1987). *"Monte Carlo study of a triangular Ising lattice-gas model with two-body and three-body interactions"*.

[142] T. S. Nilsen, *Physica* **37**, 47 (1967). *"Yang-Lee distribution of zeros for a van der Waals gas"*.

[143] P. C. Hemmer P C, H. E. Hiis, *Phys. Rev.* **133**, A1010 (1964). *"Yang-Lee Distribution of Zeros for a van der Waals Gas"*.

[144] K. C. Lee, *Phys. Rev. Lett.* **73**, 2801 (1994). *"Generalized Circle Theorem on Zeros of Partition Function at Asymmetric First-Order Transitions"*.

[145] M. Biskup, C. Borgs, J. T. Chayes, L.J. Kleinwaks, R. Kotecký, *Phys. Rev. Lett.* **84**, 4794 (2000). *"General Theory of Lee-Yang Zeros in Models with First-Order Phase Transitions"*.

[146] X. Z. Wang, J. S. Kim, *Phys. Rev. E* **58**, 4174 (1998). *"Yang-Lee edge singularity of a one-dimensional Ising ferromagnet with arbitrary spin"*.

[147] P. Tong, X. Liu, *Phys. Rev. Lett.* **97**, 017201 (2006). *"Lee-Yang Zeros of Periodic and Quasiperiodic Anisotropic XY Chains in a Transverse Field"*.

[148] M. L. Glasser, V. Privman, L. S. Schulman, *Phys. Rev. B* **35**, 1841 (1987). *"Complex-temperature-plane zeros: Scaling theory and multicritical mean-field models"*.

[149] H. E. Stanley, *Rev. Mod. Phys.* **71**, 358 (1999). *"Scaling, universality, and renormalization: Three pillars of modern critical phenomena"*.

[150] Ch. Binek, *Phys. Rev. Lett.* **81**, 5644 (1998). *"Density of Zeros on the Lee-Yang Circle Obtained from Magnetization Data of a Two-Dimensional Ising Ferromagnet"*.

[151] V. M. Tkachuk, *Fundamental problems of quantum mechanics (in ukrainian)*, LNU (2011).

[152] B. B. Wei, R. B. Liu, *Phys. Rev. Lett.* **109**, 185701 (2012). *"Lee-Yang Zeros and Critical Times in Decoherence of a Probe Spin Coupled to a Bath"*.

[153] B. B. Wei, S. W. Chen, H. C. Po, R. B. Liu, *Sci. Reports.* **4**, 5202 (2014). *"Phase transitions in the complex plane of physical parameters"*.

[154] B. Berche, C. Chatelain, *Phase Transitions in Two-Dimensional Random Potts Models.* In: *Order, Disorder and Criticality Advanced Problems of Phase Transition Theory.* Ed. Yu. Holovatch, World Scientific (2004).

[155] C. Chatelain, B. Berche, W. Janke, P.-E. Berche, *Nucl. Phys. B* **719**, 275 (2005). *"Monte Carlo study of phase transitions in the bond-diluted 3D 4-state Potts model"*.

[156] P. W. Kasteleyn, C. M. Fortuin, *J. Phys. Soc. Jpn. (Suppl.)* **26**, 11 (1969). *"Phase transitions in lattice systems with random local properties"*.

[157] M. R. Giri, M. J. Stephen, G. S. Grest, *Phys. Rev. B* **16**, 4971 (1977). *"Spin models and cluster distributions for bond and site percolation models"*.

[158] M. J. Stephen, *Phys. Lett. A* **56**, 149 (1976). *"Percolation problems and the Potts model"*.

[159] S. N. Majumdar, D. Dhar, *Physica A* **185**, 129 (1992). *"Equivalence between the Abelian sandpile model and the $q > 0$ limit of the Potts model"*.

[160] A. Aharony, *J. Phys. C: Solid State Phys.* **11**, L457 (1978). *"Low-temperature phase diagram and critical properties of a dilute spin glass"*.

[161] A. Aharony, P. Pfeuty, *J. Phys. C: Solid State Phys.* **12**, L128-5 (1979). *"Dilute spin glasses at zero temperature and the 1/2-state Potts model"*.

[162] T. C. Lubensky, J. Isaacson, *Phys. Rev. Lett.* **41**, No. 12 (1978). *"Field theory for the statistics of branched polymers, gelation, and vulcanization"*.

[163] D. Mukamel, M. E. Fisher, E. Domany, *Phys. Rev. Lett.* **37**, 565 (1976). *"Magnetization of Cubic Ferromagnets and the Three-Component Potts Model"*.

[164] S. Alexander, *Phys. Lett. A* **54**, 353 (1975). *"Lattice gas transition of He on Grafoil. A continuous transition with cubic terms"*.

[165] M. Bretz, *Phys. Rev. Lett.* **38**, 9 (1977). *"Helium Films on Highly Uniform Graphite—Finite-Size Effects, Critical Parameters, and the Three-State Potts Model"*.

[166] E. Domany, M. Schick, J. S. Walker, *Phys. Rev. Lett.* **38**, 1148 (1977). *"Classification of Order-Disorder Transitions in Common Adsorbed Systems: Realization of the Four-State Potts Model"*.

[167] S. Turner, J. A. Sherratt, *J. theor. Biol.* **216**, 85 (2002). *"Intercellular adhesion and cancer invasion: a discrete simulation using the extended Potts model"*.

[168] L. Laanait, A. Messager, S.Miracle-Sole, S. Shlosman, *Commun. Math. Phys.* **140**, 81 (1991). *"Interfaces in the Potts model I: Pirogov-Sinai theory of the Fortuin-Kasteleyn representation"*.

[169] K. Suchecki, J. A. Hołyst, *Phys. Rev. E* **80**, 031110 (2009). *"Bistable-monostable transition in the Ising model on two connected complex networks"*.

[170] K. Suchecki, J. A. Hołyst, *Ising Model on Connected Complex Networks*. In: *Order, Disorder and Criticality Advanced Problems of Phase Transition Theory, vol. 3*. Ed. Yu. Holovatch, World Scientific (2012).

[171] L. A. Pastur, A. L Figotin, *Theor. Math. Phys.* **35**, 403 (1978). *"Theory of disordered spin systems"*.

[172] J. J.Hopfield, *Proc. Nat. Acad. Sci. USA* **79**, 2554 (1982). *"Neural networks and physical systems with emergent collective computational abilities"*.

[173] V. Gayrard, *Journ. Stat. Phys.* **68**, 977 (1992). *"Thermodynamic limit of theq-state Potts-Hopfield model with infinitely many patterns"*.

[174] A. Bovier, V. Gayrard, P. Picco, *Probab. Theory Relat. Fields* **101**, 511 (1995). *"Large deviation principles for the Hopfield and the Kac-Hopfield model"*.

[175] For a recent application of the Hopfield model in natural language processing see: S. F. Fernández Sabido, *Applications exploratoires des modèles de spins au Traitement Automatique de la Langue*. PhD Thesis, University Henri Poincaré, Nancy I, Nancy, France (2009).

[176] W. Aiello, F. Park , L. Lu. In: "Proceedings of the thirty-second annual ACM symposium on Theory of computing", ACM New York, 2000.

[177] See e.g. p. 253 in: C. M. Bender, A. O. Steven, *Advanced mathematical methods for scientists and engineers*, McGraw-Hill (1978).

[178] C. von Ferber, R. Folk, Yu. Holovatch, R. Kenna, V. Palchykov, *Phys. Rev. E* **83**, 061114 (2011). *"Entropic equation of state and scaling functions near the critical point in uncorrelated scale-free networks"*.

[179] A. V. Goltsev, S. Dorogovtsev, J. F. F. Mendes, *Phys. Rev. E* **67**, 026123 (2003). *"Critical phenomena in networks"*.

[180] R. Cohen, D. ben-Avraham, S. Havlin, *Phys. Rev. E* **66**, 036113 (2002). *"Percolation critical exponents in scale-free networks"*.

[181] M. E. Fisher, *Rep. Prog. Phys.* **30**, 615 (1967). *"The theory of equilibrium critical phenomena"*.

[182] L. P. Kadanof, W. Gitze, D. Hamblen, R. Hecht, E. A. S. Levis, V. V. Palciauskas, M. Rayl, J. Swift, D. Aspnes, J. Kane, *Rev. Mod. Phys.* **39**, 395 (1967). *"Static Phenomena Near Critical Points: Theory and Experiment"*.

[183] C. Domb, *The critical point*, Taylor & Francis (1996).

[184] A. Hankey, H.E. Stanley, *Phys. Rev. B* **6**, 3515 (1972). *"Systematic application of generalized homogeneous functions to static scaling, dynamic scaling, and universality"*.

[185] R. B. Griffiths, *Phys. Rev.* **180**, 176 (1967). *"Thermodynamic functions for fluids and ferromagnets near the critical point"*.

[186] B. Widom, *J. Chem. Phys.* **43**, 3898 (1965). *"Equation of state in the neighborhood of the critical point"*.

[187] J. W. Essam, *Rep. Prog. Phys.* **43**, 833 (1980). *"Percolation theory"*.

[188] D. Stauffer, A. Aharony, *Introduction to percolation theory*, Taylor & Francis (1991).

[189] R. Cohen, K. Erez, D. ben-Avraham, S. Havlin, *Phys. Rev. Lett.* **86**, 3882 (2001). *"Breakdown of the internet under intentional attack"*.

[190] Y. Moreno, R. Pastor-Satorras, A. Vespignani, *Eur. Phys. J. B* **26**, 521 (2001). *"Epidemic outbreaks in complex heterogeneous networks"*.

[191] T. Hasegawa, *Interdisc. Inform. Sci.* **17**, 175 (2011). *"An Introduction to Complex Networks"*.

[192] R. Kenna, D. A. Johnston, W. Janke, *Phys. Rev. Lett.* **96**, 115701 (2006). *"Scaling Relations for Logarithmic Corrections"*.

[193] R. Kenna, D. A. Johnston, W. Janke, *Phys. Rev. Lett.* **97**, 115702 (2006). *"Self-Consistent Scaling Theory for Logarithmic-Correction Exponents"*.

[194] H. E. Stanley, *Introduction to Phase Transitions and Critical Phenomena*, Oxford University Press (1971).

[195] P. H. Lundow, K. Markström, *Nucl. Phys. B* **895**, 305 (2015). *"The discontinuity of the specific heat for the 5D Ising model"*.

[196] M. L. Glasser. V. Privman, L. S. Schulman, *J. Stat. Phys.* **45**, 451 (1986). *"Complex Temperature Plane Zeros in the Mean-Field Approximation"*.

[197] M. Kac, In: *Mathematical Mechanisms of Phase Transitions Statistical Physics: Phase Transitions and Superfluidity*. Ed. M. Chretien et al., Gordon and Breach (1968).

[198] I. S. Gradshteyn, I. M. Ryzhik, *Table of Integrals, Series, and Products (Eighth edition)*. Ed. D. Zwillinger, V. Moll, Academic Press, 2014.

[199] W. Janke, R. Kenna, *J. Stat. Phys.* **102**, 1211 (2001). *"The Strength of First and Second Order Phase Transitions from Partition Function Zeroes"*.

[200] R. A. Baños, J. M. Gil-Narvion, J. Monforte-Garcia, J. J. Ruiz- Lorenzo, D. Yllanes, *J. Stat. Mech.: Theory Exp.*, 02031 (2013). *"Numerical study of the overlap Lee-Yang singularities in the three-dimensional Edwards-Anderson model"*.

[201] A. Gordillo-Guerrero, R. Kenna. J. J. Ruiz-Lorenzo, *Phys. Rev. E* **88**, 062117 (2013). *"Scaling behavior of the Heisenberg model in three dimensions"*.

[202] J. B. Zuber, *Non-perturbative Field Theory and QCD*. In:*Trieste, Proceedings* SACLAY-SPH-T-83-004 CEA-CONF-6639, Trieste (1982).

[203] M. V. Fedoryuk, Asymptotic Methods in Analysis (*Analysis I Encyclopaedia of Mathematical Sciences*,vol 13). Ed. R. V. Gamkrelidze, Springer Berlin Heidelberg (1989).

[204] E. H. Lieb, A. D. Sokal, *Commun. Math. Phys.* **80**, 153 (1981). *"A general Lee-Yang theorem for one-component and multicomponent ferromagnets"*.

[205] Yu. Kozitsky, *J. Stat. Phys.* **87**, 3/4 (1997). *"Hierarchical ferromagnetic vector spin model possessing the Lee-Yang property. Thermodynamic limit at the critical point and above"*.

[206] Yu. Kozitsky, *Appl. Math. and Comput.* **141**, 103 (2003). *"Laguerre entire functions and the Lee–Yang property"*.

Bibliography

[207] W. Aiello, F. Chung, L. Lu, *Experimental Math.* **10**, 53 (2001). *"A random graph model for power law graphs"*.

[208] M. Boguna, R. Pastor-Satorras, A. Vespignani, *Eur. Phys. J. B* **38**, 205 (2004). *"Cut-offs and finite size effects in scale-free networks"*.

APPENDICES

Appendix 1. Notes on the natural cut-off

In this Appendix we discuss in more detail the choice of the upper cut-off in Eq. (4.7). A network of finite size (finite number of nodes N) cannot contain a node of infinite degree k by definition. For a scale-free network, the maximal node degree $k_{\max}$ for finite N (the so-called natural cut-off) can be defined in different ways. In Ref. [207] it was proposed to define a cut-off $k_{\max}$ as the value of the degree for which one expects to observe one vertex at most:

$$Np(k_{\max}) \sim 1. \tag{A.1}$$

From here one gets an N dependency of the cut-off:

$$k_{\max} \sim N^{1/\lambda}. \tag{A.2}$$

The drawback of (A.2) is that for continuous k this definition contains the probability of a single point (which is zero). Another definition of cut-off was given in [63]. There, the cut-off is interpreted as the value of the degree k above which one expects to find at most one vertex:

$$N \int_{k_{\max}}^{\infty} p(k)dk \sim 1, \tag{A.3}$$

leading to

$$k_{\max} \sim N^{1/(\lambda-1)}. \tag{A.4}$$

In Ref. [208] the extreme value theory was used to define the natural cut-off. In this case the exact value for $k_{\max}$ slightly differs, however it remains N dependent. Below we will show that the form of $k_{\max}(N)$ dependence does not change the asymptotic estimate for the partition function (4.9) in the leading order in N.

For simplicity, let us consider the partition function (4.5) for zero magnetic field

$H = 0$ (the derivation for non-zero H is quite similar):

$$Z_N(T) = \int_{-\infty}^{+\infty} \exp\Big(\frac{-N\langle k\rangle x^2 T}{2} + \sum_l \ln\cosh(xk_l)\Big)dx\,. \tag{A.5}$$

Using (4.6) we rewrite the sum over network nodes $\sum_l$ in the exponent in terms of the integral over k for a given distribution function $p(k)$, keeping the lower and upper cut-off:

$$Z_N(T) = \int_{-\infty}^{+\infty} \exp\Big\{N\Big[\frac{-\langle k^2\rangle x^2\, t}{2} \tag{A.6}$$

$$+ \int_{k_{\min}}^{k_{\max}} p(k)[\ln\cosh(xk) - \frac{1}{2}(xk)^2]dk\Big]\Big\}dx\,,$$

with $t = (T - T_c)/T_c$ and $T_c = \langle k^2\rangle/\langle k\rangle$. To evaluate (A.6) we make use of the fact that at large N the main contribution comes from small x. In turn, this means that we need to evaluate the integral over k in (A.6) at small x and for large N. To keep the network connected for all $3 < \lambda < 5$ we have chosen the lower cut-off value to be $k_{\min} = 2$. The crucial point is that the value of this integral does not depend on the way in which $k_{\max}$ tends to infinity (e.g. $k_{\max} \sim N^{\frac{1}{\lambda-1}}$). It is because $k_{\min}$ and $k_{\max}$ are the only terms in (A.6) that depend on N. Moreover, this dependence may be taken in the form of the natural cut-off (A.4) or in any other form that satisfies $\lim_{N\to\infty} k_{\max} \to \infty$. Therefore, one gets:

$$\lim_{x\to 0}\lim_{N\to\infty} \int_{k_{\min}}^{k_{\max}} p(k)[\ln\cosh(xk) - \frac{1}{2}(xk)^2]dk \tag{A.7}$$

$$= \lim_{x\to 0} \int_2^{\infty} p(k)[\ln\cosh(xk) - \frac{1}{2}(xk)^2]dk\,.$$

The integral in the right-hand side of (A.7) has been already evaluated (see e.g. [93] or [18]). It is

$$\lim_{x\to 0} \int_2^{\infty} p(k)[\ln\cosh(xk) - \frac{1}{2}(xk)^2]dk = a_\lambda x^{\lambda-1} + O(x^\lambda), \tag{A.8}$$

with known values of the coefficients a_λ [18, 93]. Substituting (A.8) into (A.6) we arrive at:

$$Z_N(\tau) \sim \int_0^{\infty} \exp\Big\{-N\Big(\frac{\langle k^2\rangle x^2\tau}{2} + a(\lambda)x^{\lambda-1}\Big)\Big\}dx\,, \qquad 3 < \lambda < 5\,. \tag{A.9}$$

Now the integral (A.9) can be taken by a steepest descent. The result we have obtained is consistent with the Landau theory for the Ising model on scale-free networks [108] as well as with the mean field analysis [87, 93, 94]. In this way, all three approaches (Landau, mean field, and the current one - based on the integral representation) lead to the same thermodynamics.

Appendix 2. Partition function zeros for 2- and 3-particle Ising model on a complete graph

For the better understanding of the procedure of partition function zeros search we will consider two simple cases, namely 2- and 3-particle Ising model on a complete graph. For simplicity let us consider the model without external field $H = 0$ and find partition function zeros in the complex temperature plane.

2-particle Ising model Hamiltonian reads:

$$-\mathcal{H} = \sum_{i \neq j} S_i S_j, \qquad i, j = 1, 2. \tag{A.10}$$

Averaging the partition function over the spin configurations we get:

$$Z = 2(e^{\beta} + e^{-\beta}). \tag{A.11}$$

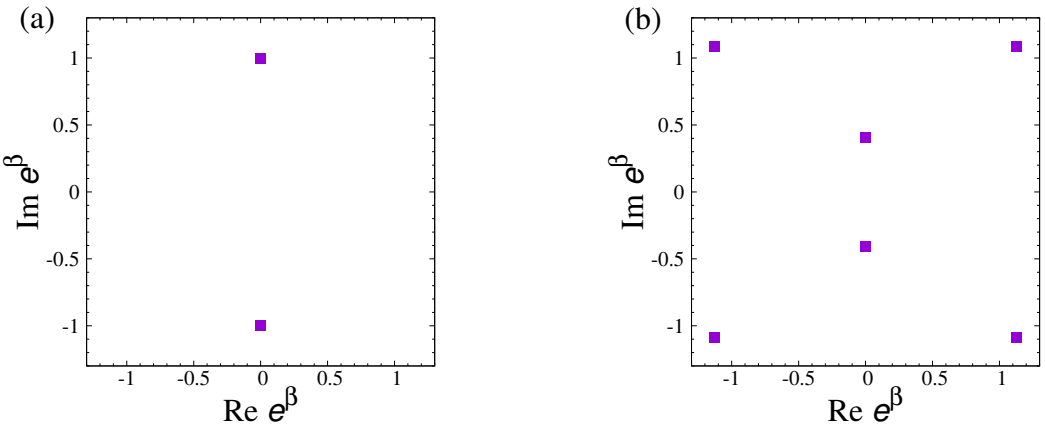

Fig. 1: Fisher zeros for **(a)** 2-particle and **(b)** 3-particle Ising model on a complete graph in complex e^{β}-plane.

Turn to another temperature representation, because the angles of partition function zeros location are conformal invariant. Designate variable $x = e^{\beta}$, where $\beta = 1/(Tk_B)$ is a complex temperature. Since the variable x is complex we find the solutions of the equation $Z = 0$ in a complex $x = x_r + ix_i$ plane, when for the real and imaginary parts is valid: $x_r = \mathrm{Re}\, \mathrm{e}^{\beta}$ i $x_r = \mathrm{Im}\, \mathrm{e}^{\beta}$. Equating the partition function (A.11) to zero and changing the variables we look on the solutions in complex plane for the polynomial:

$$x^2 + 1 = 0. \tag{A.12}$$

That is easy to note, that for the second order polynomial in complex temperature plane only two complex solutions for the partition function zeros exist: $x_{1,2} = \pm i$. In the complex x =-plane the solutions correspond to two points on imaginary axis (see Fig. 1**a**).

Let us find Fisher zeros for 3-particle Ising model on a complete graph at $H = 0$ then. The Hamiltonian of the system can be written as follows:

$$-\mathcal{H} = \sum_{i \neq j} S_i S_j, \qquad i, j = 1, 2, 3. \tag{A.13}$$

Averaging the partition function over spin configurations and equating it to zero, we get the following polynomial in x-representation:

$$x^6 + 6x^2 + 1 = 0. \tag{A.14}$$

We can find six possible analytical roots for the polynomial (A.14): $x_{1,2} = \pm 0.407i$ or $x_{3,4} = 1.127 \pm i1.089$, $x_{5,6} = -1.127 \pm i1.089$. The first two solutions are purely imaginary, while $x_{3,4,5,6}$ contain both, real and imaginary, parts of Fisher zero coordinates (see Fig. 1**b**).

Similar analysis for the Fisher zeros search we can proceed for large systems size, however the order of polynomial increases with the system size, which makes the analysis more and more complicated. In the thesis an integral representation for the partition function is analyzed and analytical complex zeros are fond.

Appendix 3. Numerically calculated values of the exponent σ for the Ising model on an annealed scale-free network (1st case)

In this Appendix we describe details of the fitting procedure that is used to define the values of the exponent σ for the model on an annealed scale-free network with the node degree exponent λ. For the rescalled imaginary part of Lee-Yang zeros Eq. (3.19) reads:

$$\mathrm{Im}h_j \sim (j - C)^{\sigma} . \tag{A.15}$$

Our goal is to check how the power law (A.15) holds for scale j at different values of C and λ. In Fig. 2 we plot the first 7 Lee-Yang zeros at $\lambda = 4.9$ for $C = 0; 0.5; 0, 7$ and fit them in the ln-ln scale by linear function. Repeating such fits at different C for fixed λ we evaluate goodness of the fits by using variance of residuals Δ. Dependencies $\Delta(C)$ and $\sigma(C)$ at λ are given in Fig. 3. At optimal value $C_{\mathrm{opt}} = 0.36$ the value of the exponent $\sigma(C_{\mathrm{opt}}) = 0.724(7)$, while the exact result is $\sigma = 0.744$.

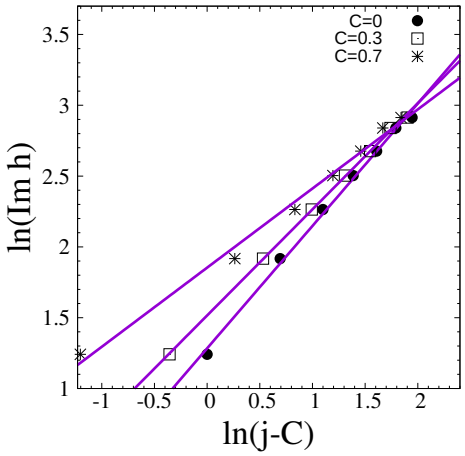

Fig. 2: Linear fitting of the coordinate of the first 7 Lee-Yang zeros at $\lambda = 4.9$ for $C = 0; 0.5; 0, 7$ (discs, rectangles and stars, correspondingly).

In Tab. 1, Tab. 2 we give the numerically calculated values of the purely imaginary Lee-Yang zeros for $\lambda = 4.1 \div 4.9$ and the imaginary part of the first 10 Lee-Yang zeros at $\lambda = 3.5 \div 4.9$. Using the fitting procedure, described above, we find the variance of residuals Δ, anomalous dimension σ and optimal value of the fitting parameter C_{opt} for the Ising model on an annealed scale-free network by fitting over the $\mathcal{N}$ Lee-Yang zeros and the imaginary part of the first 10 Lee-Yang zeros zeros at different λ (see Tables 3 and 4, respectively).

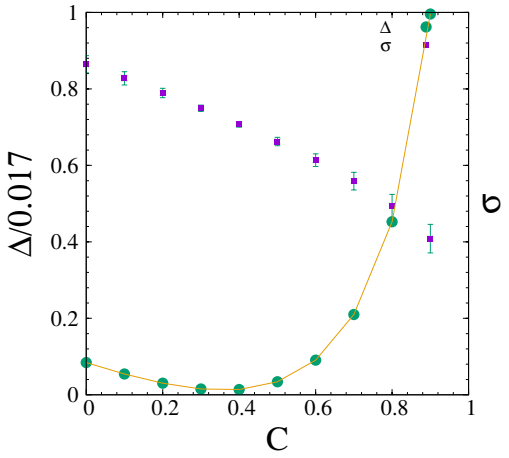

Fig. 3: Variance of residuals Δ and exponent σ at $\lambda = 4.9$ obtained while fitting coordinates of the first 7 Lee Yang zeros via Eq. (3.19) as functions of the fitting parameter C. The the value of the exponent σ calculated at $\sigma(C_{\rm opt}) = 0.724(7)$ tends to be close to the exact result $\sigma = 0.744$.

Table 1: Numerically calculated values of the purely imaginary ($\mathcal{N}$) Lee-Yang zeros for the Ising model on an annealed scale-free network with the node degree decay power λ (λ differs from 4.1 to 4.9 by 0.1).

λ	Imh_1	Imh_2	Imh_3	Imh_4	Imh_5	Imh_6	Imh_7
4.1	3.549	7.354	8.778	–	–	–	–
4.2	3.533	7.178	9.072	–	–	–	–
4.3	3.518	7.068	9.262	–	–	–	–
4.4	3.506	6.991	9.388	–	–	–	–
4.5	3.495	6.933	9.474	–	–	–	–
4.6	3.485	6.889	9.531	12.491	13.577	–	–
4.7	3.476	6.855	9.571	12.301	14.065	–	–
4.8	3.468	6.827	9.599	12.239	14.352	–	–
4.9	3.460	6.804	9.620	12.223	14.533	17.111	18.420

Table 2: Numerically calculated values of the imaginary part of the first 10 Lee-Yang zeros for the Ising model on an annealed scale-free network with the node degree decay power λ (λ differs from 3.5 to 4.9 by 0.1)

λ	Imh_1	Imh_2	Imh_3	Imh_4	Imh_5	Imh_6	Imh_7	Imh_8	Imh_9	Imh_{10}
3.5	3.762	7.212	9.496	11.351	12.983	14.470	15.850	17.146	18.375	19.548
3.6	3.702	7.417	9.940	11.976	13.770	15.406	16.927	18.358	19.716	21.014
3.7	3.657	7.597	10.357	12.570	14.522	16.305	17.964	19.528	21.014	22.437
3.8	3.621	7.752	10.750	13.134	15.240	17.165	18.961	20.655	22.268	23.813
3.9	3.593	7.881	11.119	13.668	15.923	17.989	19.918	21.740	23.478	25.143
4	3.569	7.823	8.149	11.466	14.174	16.574	18.776	20.835	22.783	24.642
4.1	3.549	7.354	8.778	11.791	14.654	17.194	19.528	21.714	23.785	25.762
4.2	3.533	7.178	9.072	12.094	15.108	17.785	20.248	22.556	24.746	26.840
4.3	3.518	7.068	9.262	12.374	15.540	18.349	20.936	23.364	25.670	27.877
4.4	3.506	6.991	9.388	12.626	15.952	18.887	21.595	24.140	26.558	28.875
4.5	3.495	6.933	9.474	12.848	16.346	19.405	22.229	24.886	27.414	29.838
4.6	3.485	6.889	9.531	12.491	13.577	16.726	19.904	22.841	25.607	28.240
4.7	3.476	6.855	9.571	12.301	14.065	17.092	20.393	23.438	26.308	29.044
4.8	3.468	6.827	9.599	12.239	14.352	17.442	20.883	24.032	27.003	29.838
4.9	3.460	6.804	9.620	12.223	14.533	17.111	18.420	21.412	24.662	27.728

Table 3: Variance of residuals Δ, anomalous dimension σ and optimal value of the fitting parameter C_{opt} for the Ising model on an annealed scale-free network with the node degree decay power λ (λ differs from 4.1 to 4.9 by 0.1) calculated by fitting over the $\mathcal{N}$ Lee-Yang zeros. Number of the purely imaginary Lee-Yang zeros ($\mathcal{N}$) are given on second column. The exact value of exponent σ_{exact} are given in the last column.

λ	$\mathcal{N}$	C_{opt}	σ	σ_{exact}
4.1	3	0.93	0.267	0.677
4.2	3	0.81	0.386	0.688
4.3	3	0.70	0.475	0.697
4.4	3	0.61	0.543	0.706
4.5	3	0.53	0.601	0.714
4.6	5	0.49	0.639(19)	0.722
4.7	5	0.41	0.688(9)	0.730
4.8	5	0.37	0.715(4)	0.737
4.9	7	0.36	0.724(7)	0.744

Table 4: Variance of residuals Δ, anomalous dimension σ and optimal value of the fitting parameter C_{opt} for the Ising model on an annealed scale-free network with the node degree decay power λ (λ differs from 3.5 to 4.9 by 0.1) calculated by fitting over the imaginary part of the first 10 Lee-Yang zeros. The exact value of exponent σ_{exact} are given in the last column. $\mathcal{N}$ corresponds to the number of purely imaginary Lee-Yang zeros.

λ	$\mathcal{N}$	C_{opt}	σ	σ_{exact}
3.5	1	0.58	0.528(1)	0.6
3.6	1	0.61	0.544(1)	0.615
3.7	1	0.62	0.565(1)	0.630
3.8	1	0.63	0.582(1)	0.643
3.9	1	0.64	0.597	0.655
4	3	0.15	0.776(33)	0.667
4.1	3	0.14	0.807(20)	0.677
4.2	3	0.12	0.838(14)	0.688
4.3	3	0.10	0.866(12)	0.697
4.4	3	0.07	0.896(11)	0.706
4.5	3	0.05	0.922(11)	0.714
4.6	5	0	0.890(19)	0.722
4.7	5	0	0.907(16)	0.730
4.8	5	0	0.923(15)	0.737
4.9	7	0.16	0.822(14)	0.744

Appendix 4. Numerically calculated values of the exponent σ for the Ising model on an annealed scale-free network (2nd case)

Let us consider the behaviour of an imaginary Lee-Yang zero coordinate $\mathrm{Im}\, h_j$ at small j for a different values of λ. In Fig. 4**a**–**c** we plot the coordinates of an imaginary part of the first ten Lee-Yang zeros $\mathrm{Im}\, h_j$ at $\lambda = 4.5$, $\lambda = 4$ and $\lambda = 3.5$, as a function of $j - C$ for different $C = 0$, $1/4$, $1/3$, $1/2$, 0.6, 0.9, correspondingly. The solid lines correspond to the expected scaling with predicted by (4.25) exponents $\sigma(\lambda = 4.5) \simeq 0.714$, $\sigma(\lambda = 4) \simeq 0.667$, $\sigma(\lambda = 3.5) \simeq 0.6$. It is obvious that the optimal value C for the curves $\mathrm{Im}\, h_j$ does not exist. Currently, this value becomes to be λ-dependent, as well as the exponent σ. Moreover to choose the optimal value C for a fixed λ we should to define the region of j when the best adjustment with a straight line exists. In a table 5 we present the numerically obtained values for the exponent σ. In the Fig. 5 we compare the exact value of the exponent σ (4.25) with a numerically obtained σ using the linear approximation of the imaginary part of the first ten Lee-Yang zero coordinates with the zeros order j.

In a Table 5 the numerically calculated values of the exponent σ for the Ising model on an annealed scale-free network with the node degree decay power $\lambda = 4.5$, $\lambda = 4$, and $\lambda = 3.5$ are shown. The exponent σ are calculated by linear fitting of the imaginary parts $\mathrm{Im}\, h_j$ of j Lee-Yang zeros. The last row gives σ^{exact} predicted by an analytic formula (4.15). The optimal value of the exponent C can be chosen from comparison of numerically obtained value of σ and the analytical one.

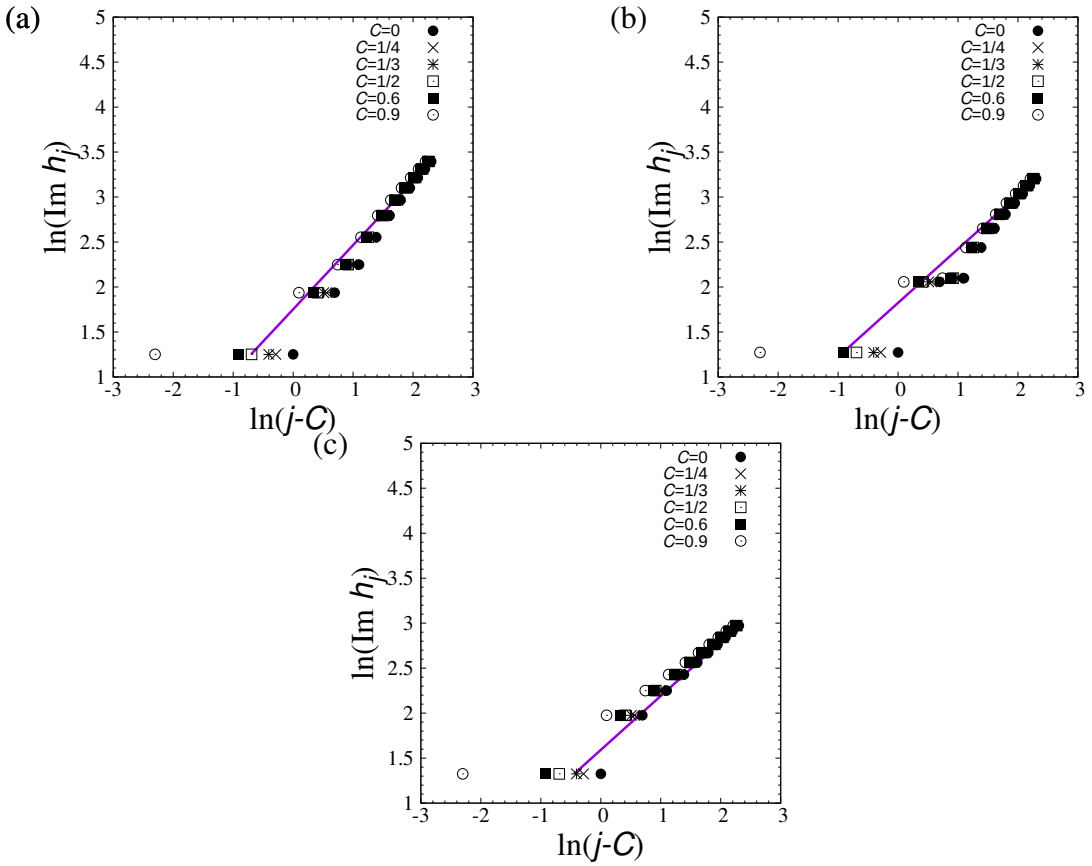

Fig. 4: Imaginary part of the first ten Lee-Yang zero coordinates $\mathrm{Im}\, h_j$ for the Ising model on an annealed scale-free network at **(a)** $\lambda = 4.5$, , **(b)** $\lambda = 4$ and **(c)** $\lambda = 3.5$, as a function of $j - C$ at different $C = 0,\ 1/4,\ 1/3,\ 1/2,\ 0.6,\ 0.9$. For the better demonstration of the expected scaling with different exponents $\sigma(\lambda = 4.5) \simeq 0.714$, $\sigma(\lambda = 4) \simeq 0.667$, $\sigma(\lambda = 3.5) \simeq 0.6$ the solid curves are plotted.

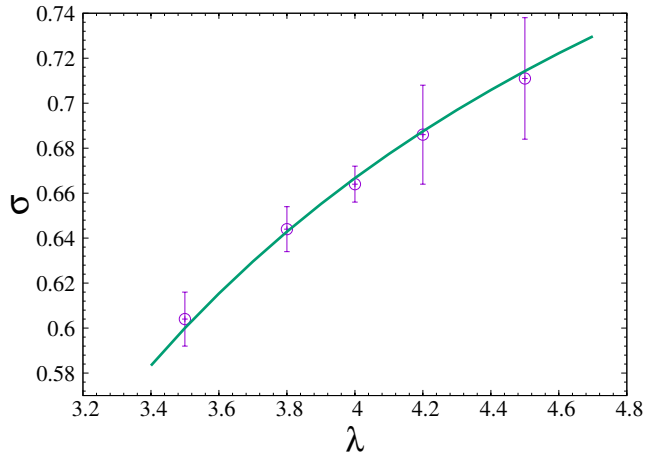

Fig. 5: Anomalous dimension σ for the Ising model on an annealed scale-free network as function of λ. Black curve: the line of exact values of σ, Eq. (4.25). Discs (red online): numerically calculated best fitting results via equation (3.19). The parameter C changes with λ: $C = 0.58$, $C = 0.53$, $C = 0.50$, $C = 0.47$ and $C = 0.33$ for $\lambda = 4.5$, $\lambda = 4.2$, $\lambda = 4$, $\lambda = 3.8$, and $\lambda = 3.5$, respectively.

Table 5: Numerically calculated values of the exponent σ for the Ising model on an annealed scale-free network with the node degree decay power $\lambda = 4.5$, $\lambda = 4$, and $\lambda = 3.5$. The values of σ are calculated by linear fitting of the imaginary parts $\mathrm{Im}\, h_j$ of j Lee-Yang zeros with the indices $j = j_{\min}...10$ by equation (3.19) for several values of C. The last row gives σ^{exact} predicted by an analytic formula (4.15).

C	$j_{\min}$	$\lambda = 4.5$	$\lambda = 4$	$\lambda = 3.5$
0	1	0.939(11)	0.840(61)	0.690(26)
0	2	0.932(17)	0.738(19)	0.614(7)
0	3	0.950(23)	0.691(6)	0.598(3)
0	4	0.911(23)	0.679(3)	0.593(1)
0	5	0.866(13)	0.673(2)	0.590(1)
0	6	0.842(9)	0.669(1)	0.589
0	7	0.825(7)	0.667(1)	0.588
0	8	0.813(5)	0.665(1)	0.587
0	9	0.804	0.664	0.587
1/4	1	0.850(12)	0.764(24)	0.627(16)
1/4	2	0.876(17)	0.695(14)	0.577(29)
1/4	3	0.906(19)	0.658(3)	0.570
1/4	4	0.874(19)	0.651(1)	0.569
1/4	5	0.835(11)	0.649(1)	0.569
1/4	6	0.814(8)	0.647	0.570
1/4	7	0.801(6)	0.646	0.570
1/4	8	0.791(4)	0.646	0.571
1/4	9	0.783	0.646	0.571
1/3	1	0.818(16)	0.736(19)	0.604(12)
1/3	2	0.857(17)	0.680(13)	0.565(2)
1/3	3	0.891(17)	0.647(2)	0.560(1)
1/3	4	0.862(18)	0.642(1)	0.561(1)
1/3	5	0.825(10)	0.640	0.562(1)
1/3	6	0.805(7)	0.640	0.563(1)
	σ^{exact}	0.714	0.667	0.6

Table 5: (Continued.) Numerically calculated values of the exponent σ for the Ising model on an annealed scale-free network with the node degree decay power $\lambda = 4.5$, $\lambda = 4$, and $\lambda = 3.5$. The values of σ are calculated by linear fitting of the imaginary parts $\mathrm{Im}\, h_j$ of j Lee-Yang zeros with the indices $j = j_{\min}...10$ by equation (3.19) for several values of C. The last row gives σ^{exact} predicted by an analytic formula (4.15).

C	$j_{\min}$	$\lambda = 4.5$	$\lambda = 4$	$\lambda = 3.5$
1/3	7	0.792(5)	0.640	0.564(1)
1/3	8	0.783(4)	0.640	0.565(1)
1/3	9	0.776	0.640	0.566
1/2	1	0.748(23)	0.676(9)	0.554(4)
1/2	2	0.818(18)	0.649(9)	0.539(1)
1/2	3	0.860(14)	0.625(1)	0.541(2)
1/2	4	0.837(16)	0.624	0.544(2)
1/2	5	0.804(9)	0.624	0.548(1)
1/2	6	0.787(6)	0.625	0.550(1)
1/2	7	0.776(4)	0.626(1)	0.552(1)
1/2	8	0.768(3)	0.628(1)	0.554(1)
1/2	9	0.762	0.629	0.556
0.6	1	0.701(28)	0.635(4)	0.521(2)
0.6	2	0.794(19)	0.630(7)	0.524(3)
0.6	3	0.842(13)	0.611(1)	0.529(3)
0.6	4	0.823(15)	0.612(1)	0.535(2)
0.6	5	0.791(8)	0.615(1)	0.539(2)
0.6	6	0.776(5)	0.617(1)	0.543(2)
0.6	7	0.766(4)	0.618(1)	0.545(1)
0.6	8	0.759(3)	0.620(1)	0.548(1)
0.6	9	0.753	0.622	0.550
	σ^{exact}	0.714	0.667	0.6

TRANSITIONS DE PHASE DANS LES RÉSEAUX COMPLEXES

Cette thèse est consacrée à l'étude du comportement critique de modèles de spins sur réseau invariant d'échelle caractérisés par une distribution de probabilité de la coordination k des sites en $P(k) \sim k^{-\lambda}$ en présence de désordre trempé ou recuit ainsi que sur graphe complet. Pour le modèle de Potts sur réseau invariant d'échelle, nous avons obtenu à l'aide d'une approche de champ moyen inhomogène l'ensemble des exposants critiques, des rapports d'amplitudes critiques et des fonctions d'échelle qui se révèlent dépendantes de l'exposant de décroissance λ. Dans ce sens, λ apparaît comme l'un des paramètres globaux qui déterminent la classe d'universalité. A côté de la méthode traditionnelle du champ moyen inhomogène pour traiter les systèmes sur réseau complexe, nous utilisons, pour la première fois dans ce contexte, les zéros de la fonction de partition dans le plan complexe. Un comportement inhabituel a été obtenu pour un certain nombre de grandeurs telles que l'angle de condensation φ des zéros de Fisher et l'exposant σ qui s'avèrent tous deux dépendants de λ. Nous observons également que le théorème du cercle de Lee et Yang est violé dans la région $3 < \lambda < 5$ pour le modèle d'Ising sur un réseau invariant d'échelle recuit.

PHASE TRANSITIONS ON COMPLEX NETWORKS

The thesis is devoted to the investigation of the critical behavior of spin models on a scale-free network with a power-law node-degree probability distribution $P(k) \sim k^{-\lambda}$, in presence of quenched or annealed disorder, and on a complete graph. For the Potts model on a scale-free network in terms of inhomogeneous mean-field approach we found the set of critical exponents, critical amplitude ratios and scaling functions, which appear to be dependent on the probability distribution decay exponent λ. In that sense λ is manifested to be one of the global parameters which define the universality class. Along with the traditional theory of complex networks by inhomogeneous mean-field method, we use for the first time the method of partition function zeros analysis in the complex plane. Unusual behavior was observed for a number of universal features, such as the angle of Fisher zeros condensation φ and the exponent σ which appear to be λ -dependent. We also observe that the Lee-Yang circle theorem is violated in the region $3 < \lambda < 5$ for the Ising model on an annealed scale-free network.

ФАЗОВІ ПЕРЕХОДИ НА СКЛАДНИХ МЕРЕЖАХ

Дисертаційна робота присвячена дослідженню критичної поведінки спінових моделей на безмасштабних мережах зі степенево-спадною функцією розподілу ступенів вузлів $P(k) \sim k^{-\lambda}$, при наявності замороженого чи відпаленого безладу, та на повному графі. Для моделі Поттса на безмасштабній мережі у наближенні неоднорідного середнього поля знайдено критичні показники, відношення амплітуд, скейлінгові функції, що виявляються залежними від показника загасання функції розподілу λ. Таким чином λ виявляється одним із глобальних параметрів, що визначає клас універсальності. Поряд із традиційним методом неоднорідного середнього поля вперше у теорії складних мереж використано метод аналізу нулів статистичної суми в комплексній площині. Виявлено незвичну поведінку ряду універсальних характеристик, а саме кут конденсації нулів Фішера φ та показник σ виявляються λ-залежними. Також ми спостерігаємо порушення теореми Лі-Янга про одиничне коло в діапазоні $3 < \lambda < 5$ для моделі Ізінга на відпаленій безмасштабній мережі.